Elucidating Key Proteins in the Internalization Pathway of Small Extracellular Vesicles

Nicholas Valentino

Thesis submitted to the University of Ottawa in partial

fulfillment of the requirements for the MSc degree in Cellular and Molecular Medicine

Department of Cellular and Molecular Medicine

Faculty of Medicine

University of Ottawa

Statement of Contributions

This M.Sc. thesis entitled “Elucidating Key Proteins in the Internalization of Small Extracellular Vesicles” was written by me. Dr. Derrick Gibbings and Yunping Xue were responsible for the conceptualization and design of the project at the early stages before I took the reins. I performed the experimentation, data collection, data analysis, and figure preparation except for the following:

James Taylor created and supplied the HEK293T cells expressing APEX-PTGFRN and HRP-PTGFRN.

Flow Cytometry experiments were performed and quantified by Yunping Xue using the BS LSR Fortessa

Funding was provided by an NSERC grant awarded to Derrick Gibbings, as well as both an Ontario Graduate Scholarship and a Canadian Graduate Scholarship, which I received.

Derrick Gibbings read and edited this thesis prior to submission.

Abstract

The delivery of oligonucleotide therapeutics, such as silencing RNAs (siRNA), into the cytoplasm of cells is the central plight of their use as a therapeutic. Our lab demonstrated that small extracellular vesicles (sEVs) are highly efficient delivery vehicles, capable of delivering 3-30% of the RNAs they contain into cells, and, importantly, traverse the blood–brain barrier, highlighting their promise as RNA carriers and making them a potent candidate for drug delivery in neurodegenerative diseases. The stark therapeutic potential of sEVs is contrasted heavily by the fact that the mechanism surrounding sEV internalization is relatively understudied. Our electron microscopy results reveal that sEVs can enter the cell through direct fusion with the cell membrane through a series of intermediates that deliver the sEV contents directly to the cytoplasm. Typical fusion mechanisms involve recruiting fusion proteins to decrease the free energy needed for a complete fusion event**.** Using mass spectrometry and gene ontology term analysis, the retromer complex was identified as a significantly enriched complex surrounding our sEVs as they enter into cells. Functional knock-down of core retromer subunits abolishes fusion-dependent lipid mixing and prevents siRNA-mediated gene silencing, implicating retromer as a previously unrecognized facilitator of vesicle fusion and cargo release.. Elucidating the mechanism of sEV internalization will fill the knowledge gap of a foundational pathway in cell biology, facilitating their use as therapeutic vehicles for various drugs and increasing our understanding of their use in neurodegenerative diseases.

Acknowledgments

I would like to express my deepest gratitude to my supervisor, Dr Derrick Gibbings, for their invaluable guidance, support, and patience throughout my years as a student. I will always be in awe of the insight you can provide, and the expertise and encouragement that you have shown toward me have been instrumental in shaping my understanding and development as a researcher. I would also like to thank the members of my thesis advisory committee, Dr. Dylan Burger and Dr. Vanessa DaCosta, for their insightful feedback and constructive suggestions, which significantly contributed to the improvement and direction of my work. The support you both have shown towards me has made the research process much more manageable.

I would like to extend a special thank you to my lab members, who made the research process more enjoyable and exciting. I am grateful for the many discussions, collaborations, and shared experiences that helped me through the most challenging times during this project. I would like to extend my sincere thanks to Yunping Xue, Ryan Reshke, Charlie Manser, and Kallol Dutta, who mentored me in the essential laboratory techniques necessary to ensure that I could create a scientifically profound thesis.

On a personal note, I want to express my heartfelt appreciation to my family and friends who have supported me over the years; it has not gone unnoticed. To my friends who had to listen to me talk about my project's nonsense, thank you for pretending to listen and care. Above all, I want to thank the many parents, Pat Valentino and Jackie Valentino, who have voiced their belief and encouragement in my pursuits, regardless of how daunting they may be. I thank you with all my heart. You are why I have had these opportunities, and I am forever grateful.

Table of Contents

List of Abbreviations

ONT	Oligonucleotide therapeutics
RNAi	RNA interference
RNAse	Ribonuclease
mRNA	Messenger RNA
FDA	Food and Drug Administration
ASO	Antisense Oligonucleotides
Nt	Nucleotide
LNA	Locked nucleic acid
PMO	Phosphorodiamidate morpholino oligomers
UTR	Untranslated region
miRNA	microRNA
AGO	Argonaute
siRNA	Short-interfering RNA
PEG	Polyethylene glycol
CNS	Central Nervous System
GalNAc	N-acetylgalactosamine
ASGPR	Asialoglycoprotein
sEV	Small Extracellular Vesicles
ILV	intraluminal vesicles
MVB	Multivesicular bodies
ESCRT	Endosome Sorting Complex Required for Transport
STAM	Signal transducing adaptor molecule
PI3P	phosphatidylinositol-3-phosphate
VPS28	vacuolar sorting protein 28
VPS37	vacuolar sorting protein 37
VPS36	vacuolar sorting protein 36
VPS22	vacuolar sorting protein 22
VPS25	vacuolar sorting protein 25
Alic	Alg-2 interacting protein X
VPS4	vacuolar sorting protein 4
PS	Phosphatidylserine
PE	Phosphatidyelthanolamine
PC	Phosphatidylcholine
PI	Phosphatidylinositol
LPC	lysophosphatidylcholine
HRS	Hepatocyte growth factor-regulated tyrosine kinase substrate
gDNA	genomic DNA
mtDNA	Mitochondrial DNA
ssDNA	single-stranded DNA
lncRNA	long noncoding RNA
RRM	RNA Recognition Motif
KH	k homology domain

ZnF	Zinc Finger domain
PAZ	piwi-argonaut-Zwille
TGN	trans-Golgi network
PIP	phosphatidylinositol phospholipid
GEF	Guanine-nucleotide exchange factors
GAP	GTPase-activating proteins
ER	endoplasmic Reticulum
BAR	Bin/Amphiphysin/Rvs
SNX	Sorting Nexin
VPS10	Vacuolar sorting protein 10
Bp	Base pair
TRBP	transactivation response element RNA-binding protein
MS	Mass spectrometry
APEX	Engineered Ascorbate Peroxidase
HRP	Horseradish Peroxidase
DMEM	Dulbecco's Modified Eagle media in high Glucose
FBS	fetal bovine serum
ABAM	Antibiotic-antimycotic solution
PEI	polyethylenimine
PES	polyethersulfone
SOC	Super-optimal Broth with Catabolic repression outgrowth media
LB	Lysogeny Broth
TFF	Tangential Flow Filtration
PBS	Phosphate buffer saline
NTA	Nanoparticle Tracking Analysis
SDS	Sodium dodecyl sulfate
TBST	Tris-buffered saline with 0.1% Tween detergent
ECL	Enhanced chemiluminescence
DAB	Diaminobenzidine
SILAC	stable isotope labelling by amino acid in cell culture
BP	Biotin-Phenol
PFA	Paraformaldehyde
F.A	Formic Acid
ACN	acetonitrile
TFA	Trifluoroacetic acid
R18	Rhodamine 18
GOTERM	gene ontology term
CSC	cargo-selective complex
PX	Phox

List of Figures

List of Tables

Introduction

1.1 Oligonucleotide Therapeutics

Oligonucleotide therapeutics (ONTs) target RNA or DNA to regulate protein expression.[1] ONTs can modulate gene expression through RNA interference (RNAi), Ribonuclease (RNAse) H-mediated degradation of messenger RNA (mRNAs), and modifying alternative splicing. As a result, they have therapeutic implications in silencing gene products associated with diseases.[2,3] The therapeutic application has been demonstrated in at least 24 United States Food and Drug Administration (FDA) approved RNA-based therapeutic products, with many participating in pre-clinical and clinical development as of December 2024, including drugs such as Patisiran, Givosiran, Lumasiran, and Inclisiran, treatments for Transthyretin amyloidosis, acute hepatic porphyria, primary hyperoxaluria, and atherosclerotic cardiovascular disease, respectively.[4-8] Oligonucleotide therapeutics can be split up into different categories: Antisense oligonucleotides (ASOs), RNAi oligonucleotides, mRNA therapeutics, and DNA-based oligonucleotides.[9,10]

1.1.1 Antisense Oligonucleotides

ASOs were one of the earliest studied ONTs, initially demonstrated by Zamecnik and Stephenson, who showed the inhibition of viral replication in vitro by adding a tridecamer complementary to the Rous sarcoma virus 35S RNA into chick embryo fibroblasts.[10] This discovery facilitated the development of the first oligonucleotide agent approved by the US FDA to treat cytomegalovirus-induced chorioretinitis.[11] ASOs are single-stranded oligonucleotides, typically 8-50 nucleotides (nt) in length and synthetic, such that the sequence for the ASO is complementary to the target mRNA sequence.[12,13] ASOs invoke their therapeutic effects through the direct binding of mRNA or the binding of pre-mRNA structures.[14] ASOs can be synthesized

using DNA or a DNA and RNA mixture. Using DNA allows endogenous RNase H to recognize the oligonucleotide, leading to its eventual degradation by exonucleases and decreasing the overall mRNA present for translation.[15,16] Alternatively, ASOs can be synthesized using only RNAs, in which the binding to the mRNA target sterically blocks ribosome recruitment, inhibiting translation and decreasing the amount of protein generated by the target mRNA.[15,17] ASOs can enter the cell's nucleus directly and bind to pre-mRNA at splicing sites.[18] The binding will lead to the generation of alternative splicing and may facilitate the elimination of specific variants of genes.[17-19] For example, in the *HTT* gene that encodes for the Huntington protein, there are 2842 nucleotide polymorphisms (different forms of nucleotides that account for the disease). However, 7% can only be targeted in the mature mRNA, ultimately forcing the use of targeting pre-mRNA targets, which will facilitate the targeting of 100% of the nucleotide polymorphisms.[17-19]

Challenges with early ASOs were their rapid degradation by endo- and exo-nucleases, which led to cleavage of the phosphodiester bond and decreased their therapeutic ability.[12,16] Chemical modifications were employed to ameliorate challenges with early ASOs and enhance their stability.[12,15,16] Replacing the phosphodiester linkage with a phosphorothioate backbone changes the oxygen atom with a sulphur atom, strengthening the resistance to nuclease degradation.[12,20,21] Moreover, adding the 2′-O-methyl or 2′-O-methoxyethyl at the 2′ position of the ribose sugar stabilizes the RNA-ASO duplex.[20-22] Another modification is the use of locked nucleic acids (LNAs). LNAs lock the ribose moiety into a specific orientation that is conformationally restricted by linking the 2′ oxygen and the 4′ carbon with a methyl bridge.[23,24] This variation results in increased thermal stability of the ASO-RNA duplex, thereby enhancing nuclease resistance.[23,24] The last modification is the use of phosphorodiamidate morpholino

oligomers (PMOs). PMOs introduce a morpholine ring as a replacement for the ribose sugar and a phosphorodiamidate linkage for the phosphodiester linkage, which are incredibly resistant to nucleases and are effective for splicing modulation.[25,26]

The advancements listed have been crucial in the clinical use of ASOs in neurological and muscular disorders. However, ASOs have several drawbacks that limit their efficacy, safety, and capacity to deliver to target tissues.[20] For delivery into the cytoplasm of cells, various biological barriers (endothelium and cellular membranes) must be overcome, which is not a strength for ASOs.[20] This delivery challenge is further compounded by the fact that ASOs often accumulate in non-target tissues such as the liver or kidney, which decreases therapeutic efficacy and increases off-target effects.[20,27,28] Therefore, despite the unique advantages ASOs provide, their drawbacks allow biotechnical advances that can improve characteristics such as bioavailability and off-target effects.

1.1.2 RNA Interference

RNAi is a conserved process that enables cells to regulate gene expression.[29,30] The method utilizes small noncoding RNAs to target and degrade mRNA, thereby preventing the expression of proteins. *Lee et al.* first discovered RNAi in 1993 while categorizing the *lin-4* gene in C. elegans.[31] They showcased that two separate lin-4 transcripts were generated from the *lin-4* gene; one was 22 nt in length, and the other was a stem-loop that was 61 nt in length.[31] These transcripts exhibited complementarity to repeated sequence elements in the 3' untranslated region (UTR) of the lin-14 mRNA, which, through translational repression, were able to downregulate the lin-14 mRNA and control lin-14 protein levels.[31,32] This study was the first to highlight a critical noncoding RNA involved in RNA interference, specifically microRNA (miRNA).

miRNAs are small noncoding RNA molecules ranging from 20 to 24 nucleotides.[33-35] Canonical miRNA biogenesis proceeds through a Drosha–Exportin‑5–Dicer pathway that ultimately loads a guide strand into Argonaute (AGO).[35,36] Initially, miRNA genes are transcribed by RNA polymerase II or III into primary miRNA transcripts, known as pri-miRNAs, which are present in an RNA stem-loop or hairpin structure.[37] From here, pri-miRNA is recognized by the RNase III enzyme Drosha and its cofactor DGCR8, in which a cleavage of 11 base pairs from the hairpin is removed.[38,39] This process yields a pre-miRNA that is approximately 65 nt long, which is exported from the nucleus to the cytoplasm by nuclear export protein Exportin-5 through a mechanism involving the hydrolysis of Ran-GTP in the cytoplasm.[40,41] Once in the cytoplasm, RNase III enzyme Dicer will cleave the loop of the hairpin, yielding a 22nt miRNA that will associate with the RNA-induced silencing complex consisting of four Argonaute (AGO) proteins, forming a ribonucleoprotein complex.[42] The duplex has two strands: a guide strand associated with the AGO proteins and a passenger strand cleaved.[43] This distinction is made based on thermodynamic asymmetry and structural features. In the context of thermodynamics, the strand that has its 5' end less tightly paired will bind with increased affinity to the AGO proteins.[44,45] Moreover, structural stability, such as the distribution of GC and AT nucleotides, will affect the ease of unwinding by the RISC complex.[44,45] The guide strand with RISC will then bind to complementary sequences in the 3' UTR of the mRNA.[33]

Subsequently, RNAi was also demonstrated by Fire et al. in 1998, showing that injecting exogenous RNA duplexes complementary to mRNAs can decrease gene expression by targeting the mRNA.[29,46] This study was the first to identify short-interfering RNA (siRNA).

siRNA is the second short noncoding RNA that acts similarly to miRNA but differs in the contexts of origin, structure, RISC associations, and mechanism of action. siRNA is typically

derived from exogenous double-stranded RNA sources, such as those resulting from viral infection or through the experimental introduction of synthetic RNA.[47] They can be found in endogenous sources like transposons or repetitive sequences to a lesser extent.[48] siRNAs are also cleaved to reach siRNA duplexes of approximately 22 nt in length with 2-nucleotide 3'overhangs.[48] siRNA structure differs because it contains perfect base pairs with the characteristic 2-nucleotide 3'overhangs, while miRNA has imperfect base pairing, including mismatches and bulges due to its hairpin precursors.[47] While miRNA can associate with all of the AGO proteins, siRNA is primarily associated with Ago2, which is hypothesized to have slicer activity.[49-52] The gene silencing mechanism also differs because siRNA binds to complementary sequences in the coding region and UTRs of the target mRNA, which, through direct cleavage of the mRNA strand, facilitates silencing.[53] The many structural and mechanistic changes between siRNA and other RNA therapeutics give it unique properties in its silencing capabilities; however, these changes make it a more powerful option than competitors like ASOs and microRNA. The molecular mechanisms of both miRNA and siRNA processes can be seen and contrasted in figure 1.

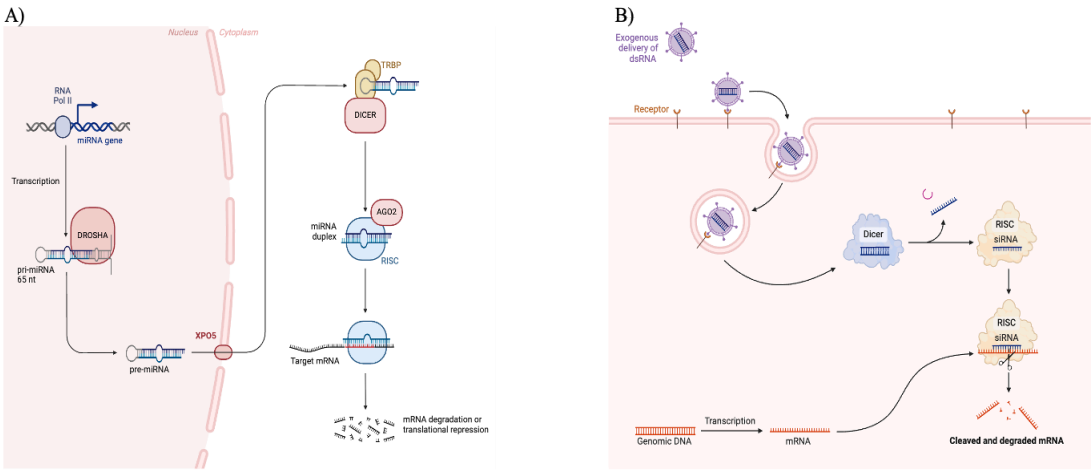

Figure 1: miRNA versus siRNA-mediated Gene silencing. A) Canonical miRNA biogenesis and Action. RNA Polymerase II transcribes pri-miRNA, which contains a hairpin loop structure. Drosha/DGCR8 cleaves pri-miRNA into a 65 nt pre-miRNA. This is exported into the cytoplasm, where Dicer cleaves the hairpin loop, yielding a 22 nt miRNA duplex that gets loaded into the RISC that binds to the 3' UTR of target mRNAs, leading to translational repression or mRNA destabilization. **B)** siRNA pathway for exogenous gene silencing. Exogenous dsRNA enters the cell and is taken into the cytoplasm, where DICER cleaves the dsRNA into 22nt siRNA duplexes. This siRNA is loaded into RISC, primarily Ago2, which pairs it with complementary target mRNA, leading to endonucleolytic cleavage and degradation of the transcript. Figure created with Biorender.

1.1.3 siRNA therapeutics

Antisense oligonucleotides (ASOs) and short-interfering RNAs (siRNAs) share the same ultimate goal of silencing disease-linked transcripts, but they achieve this with fundamentally different architectures and potencies. ASOs are single-stranded and rely on either RNase H recruitment or steric blockade, whereas siRNAs are double-stranded, 21- to 23-nt duplexes that harness the cell's endogenous RISC.[15] Fire et al.'s landmark 1998 study showed that duplex RNA triggers orders-of-magnitude stronger knockdown than single strands, because RISC's catalytic Ago2 can repeatedly cleave multiple copies of the target mRNA.[29] Although the field first translated ASOs into a drug (fomivirsen, FDA-approved in 1998), the subsequent approval of the inaugural siRNA therapeutic (patisiran, 2018) underscored how quickly the superior catalytic

and dose-sparing efficiency of RNAi could be brought to patients.[12] Thus, siRNAs now represent the most potent and sequence-specific class of oligonucleotide drugs.[15,54] As a result, this thesis will primarily focus on siRNAs. However, these physicochemical features also prevent them from passively crossing the plasma membrane.[55-57] Consequently, the future impact of RNA-interference drugs now hinges less on sequence design and more on delivery technology.

1.2 Delivery of siRNA

Efficient clinical use of siRNA hinges on solving a fundamental delivery problem: naked siRNAs are too large, highly anionic, and RNase-sensitive to cross the plasma membrane or survive long in the bloodstream.[58,59] Computational and in-cell titration studies suggest that hundreds to 10,000 intracellular copies of siRNA are needed to achieve a 50 % reduction in target-gene expression.[60-62] Even when endocytosed, the duplex must escape the endosome and reach the cytoplasm to engage RISC, steps that have repeatedly limited efficacy in clinical trials.[63,64] Consequently, the field has turned to delivery platforms that shield siRNA from nucleases, promote cellular uptake, and trigger endosomal release. Among the most advanced are lipid nanoparticles (LNPs), polymer–siRNA conjugates, and, more recently, small extracellular vesicles (sEVs), each offering distinct solutions to these barriers and forming the focus of the sections that follow.

1.2.1 Lipid nanoparticles

Lipid nanoparticles are composed of ionizable cationic lipids (lipids that are positively charged at acidic pH but neutral at physiological pH) together with phospholipids like distearoylphosphatidylcholine that aid with structural integrity, cholesterols that enhance membrane fluidity and stability in a temperature dependent manner, and covalently modified

polyethylene glycol (PEG) lipids that provide a hydrophilic shield that prevents aggregation and reduces opsonization (tagging by the immune system).[65-68] The components of the lipid nanoparticles self-assemble into lipid bilayers between 50-150nm in diameter that will surround negatively charged RNA.[66,69] The formulation of this structure facilitates the protection of the internal RNA from degradation by nucleases as well as enhances the cellular uptake and circulation time.[66,69] Studies have shown that LNPS can decrease therapeutic doses of siRNA in the liver by 100-fold, two orders of magnitude compared to the naked duplexes.[66] Moreover, the surface chemistry of the LNP can be altered to contain ligands that preferentially guide LNPs to different tissues, which can ameliorate biodistribution and uptake.[70,71] For example, adding retinol-binding proteins increases the uptake of LNPs in hepatic stellate cells, as they express the retinol-binding protein receptor.[72,73]

Despite these advantages, the use of LNPs for siRNA delivery is hindered by numerous barriers. Firstly, Ionizable cationic lipids can cause membrane disruption, leading to lipid-induced toxicity.[74,75] Secondly, immune activation caused by PEGylated lipids may trigger the complement system or elicit anti-PEG antibodies, leading to hypersensitivity reactions, cytokine release, and an accelerated blood clearance effect on repeat dosing.[76-78] Thirdly, nonspecific biodistribution can reduce therapeutic efficacy and increase side effects due to the limited targeted precision of LNPs. Lastly, there are challenges in targeting specific tissues, such as the central nervous system (CNS), due to the requirement of crossing the blood-brain barrier, which restricts treatments for neurological disorders.[79,80] Collectively, these limitations motivate exploration of alternative vectors, including polymer conjugates and small extracellular vesicles (sEVs) that can broaden tissue reach while minimizing immunotoxicity.

1.2.2 Covalent conjugates

The emergence of chemical modifications on siRNAs has enabled carrier-free delivery strategies that bypass the complexity of LNPs. These alterations in the chemical structure result in a range of functional benefits for the siRNA. For instance, incorporating 2'-O-methyl or 2'-fluoro ribose modifications shields siRNA from exo and endonucleases as well as dampens innate immunity.[81] Furthermore, the addition of phosphorothioate linkages (linkage of non-binding oxygen is replaced with sulphur) can enhance the binding of plasma proteins and increase resistance to nucleases, enabling siRNA to target and knock down specific genes for an extended period of up to six months.[81-83]

The ability to impart protection to siRNA without using LNPs sparked a significant increase in research towards the amelioration of naked siRNAs. One of the most prevalent modifications is the N-acetylgalactosamine (GalNAc) conjugation, which increases liver delivery.[84-86] Conjugating GalNAc to siRNAs leverages the natural binding affinity of GalNAc receptors on hepatocytes to facilitate tissue-specific siRNA delivery.[85-89] GalNAc is a monosaccharide derivative of galactose that contains an amine group with a biological role in cell recognition and signalling.[85-89] It has a ligand-receptor, Asialoglycoprotein (ASGPR), that is predominantly expressed on the surface of hepatocytes in the liver. ASGPR has an endogenous function relating to the endocytosis and clearance of binding glycoproteins with GalNAc residues.[85-89] As a result, when GalNAc is conjugated to siRNAs, it binds efficiently to ASGPR on hepatocytes, leading to internalization via clathrin-mediated endocytosis and, ultimately, reducing mRNA expression by 80% in human liver, which contributed to its FDA approval.[89]

Limitations and challenges persist in the use of GalNAc conjugates. The most telling is the tissue specificity. The fact that ASGPR is expressed primarily on hepatocytes restricts the

application of GalNac conjugates to hepatic diseases. Moreover, uptake can plateau as receptor sites saturate at high doses, and endogenous glycoproteins may compete under certain metabolic conditions.[89] Hence, while GalNAc revolutionized hepatocyte delivery, new conjugate chemistries or alternative vehicles are required to reach non-hepatic tissues, a gap that small extracellular vesicles may fill.

1.3 Small Extracellular Vesicles

Small extracellular vesicles (sEVs), operationally defined by the International Society for Extracellular Vesicles as cell-derived vesicles that are <200nm in diameter, have captured attention as a long-distance communication system capable of delivering RNA from one cell to another due to their longstanding implication in processes relating to mediating intercellular communication. [90-93] sEVs are a subset of all extracellular vesicles (EVs) released from the cell. EV subtypes are defined by factors such as size, biogenesis, biomarkers, and cellular origin.[88-104] Exosomes are endosomal-derived vesicles, typically between 30-150 nm in diameter, initially described by Johnstone et al. in 1983. This was achieved through an experiment that found labelled transferrin within reticulocytes transported by intraluminal vesicles (ILVs) within multivesicular bodies (MVBs) formed in endosomes.[95,96] In 1987, exosomes were formally defined as phospholipid-bilayer-enclosed vesicles formed within endosomes and fusing with the plasma membrane.[97] Microparticles are another type of EV that is formed through the outward blebbing of the plasma membrane using many cytoskeletal components, such as actin and myosin, which will rearrange the bilayer to generate membrane protrusion.[99] Among microparticles, the arrestin domain-containing protein 1-mediated microvesicles are a sEV (40-100 nm) that utilize ARRDC1 to bud from the plasma membrane.[99] They are typically

formed due to stress or apoptosis and sit in the size range of 100 nm to 1μm.[99-101] Apoptotic bodies are another vesicle type that have sizes significantly larger than 1–5 μm.[102] They are generated during the later stages of apoptosis and contain cellular debris, including organelles and nuclear fragments.[102-105] The purpose of these vesicles is to aid the role of phagocytes in clearing dying cells.[105] Blebbisomes are another EV type that reach sizes of 20 μm.[106] The term blebbisomes is derived from the blebbing process in which the membrane expands and contracts.[106] The blebbisome is unique in that it contains functional organelles such as mitochondria and endosomes; however, the lack of a nucleus distinguishes it from a cell.[106]

Recent data from the Gibbings lab has demonstrated that sEVs, specifically those of endosomal origin, are highly efficient delivery vehicles, capable of providing 50-100% of the RNAs they contain into cells.[94] These results suggest that sEVs are outperforming many synthetic delivery systems. The intrinsic transport capability combined with their biocompatible membrane and natural tropism positions sEVs as a promising alternative to LNPs or GalNAc conjugates for extra-hepatic siRNA delivery. The subsections that follow dissect the biogenesis, composition, uptake pathways, and fusion mechanics of these systems with an eye toward therapeutic engineering.

1.3.1 Exosome Biogenesis

Exosome biogenesis is accomplished through the inward budding of the endosomal membrane during the late endosomal phase, forming MVBs.[107-110] The budding event is typically initiated through the endosome sorting complex required for transport (ESCRT).[111] Through a series of protein-protein interactions, ESCRT facilitates the budding events, allowing for the pinching of the endosomal membrane and sorting of protein, nucleic acids, and lipid species into

ILVs.[112] Four ESCRT proteins, ESCRT-0, -I, -II, and -III, perform uniquely in forming sEVs and are critical drivers of sEV biogenesis. ESCRT-0 identifies proteins ubiquitinated within the endosomal membrane (cytoplasmic side).[112-114] Essential proteins in the ESCRT-0 complex include the signal-transducing adaptor molecule (STAM) that stabilizes cargo and helps localize ESCRT-0 to the membrane.[112,115] The ultimate goal of ESCRT-0 is to ensure that specific cargo enters endosomes enriched in phosphatidylinositol-3-phosphate (PI3P).[115] In contrast, cargo that is not destined for this location is excluded and does not make it into the forming vesicles.[112,116] ESCRT-I and ESCRT-II are responsible for surrounding identified cargo through their membrane-bending capabilities, forming ILVs.[116] Proteins such as vacuolar sorting protein 28 (VPS28) and vacuolar sorting protein 37 (VPS37) will contribute to membrane curvature, while vacuolar sorting protein 36 (VPS36) will recognize the ubiquitinated cargo.[117,118] Vacuolar sorting protein 22 (VPS22) and vacuolar sorting protein 25 (VPS25) are responsible for the stabilization of the membrane curvature complex.[117] At this point, cargo should be correctly sorted into budding membranes and prepared for the onset of ESCRT-III. ESCRT-III will perform membrane scission by pinching off the budding membrane, facilitating the release of ILVs into the lumen of the endosome. This process generates an MVB, which is then prepared for the exocytosis of sEVs into the extracellular space.[117,118] The ESCRT complex does not complete this process independently. It requires accessory proteins, such as Alg-2 interacting protein X (Alix), which facilitates the recruitment of ESCRT-III and interacts with syndecans.[119] Syndecans are proteins that bind to extracellular ligands and proteins to facilitate their endocytosis, and syntenins, which interact with syndecans and allow them to associate with the ESCRT-III, acting as an intracellular adaptor protein that connects syndecans to the ESCRT pathway through the mediation of Alix.[119] Vaculor sorting protein 4 (VPS4) is another important protein that is

essential for efficiently reusing ESCRT components.[117,118] VPS4 is an ATPase that disassembles ESCRT-III and recycles it after vesicle scission. Despite the importance of the ESCRT complex in sEV biogenesis, it has been found that when knocking down essential components of each of the four ESCRT complexes, vesicle output is found to be partially reduced.[112] As a result, another mechanism must be participating in this biogenesis process.

ESCRT-independent Pathways are pathways that involve complex lipids and other protein-related processes.[108-110] Lipids involved in ESCRT-independent pathways include ceramide, which can self-associate to form raft-like structures and contribute to developing the membrane curvature required for the inward pinching of the endosomal membrane.[108-110] Protein scaffold induced budding involves clustering of tetraspanin molecules (CD9/CD63/CD81) or syntenin-1 on the endosomal membrane, which causes curvature and recruits Alix even in the absence of ESCRT. [117-121]

Once formed, multivesicular bodies (MVBs) have two mutually exclusive fates: fusion with lysosomes for cargo degradation or fusion with the plasma membrane to release their ILVs as small extracellular vesicles into the extracellular milieu. Understanding how cells regulate these pathways is crucial for engineering exosomes to deliver therapeutic RNA.

1.3.2 Exosome composition

Exosomes are multifaceted vesicles that carry many proteins[122], lipids[123], and nucleic acids.[124-125] The aforementioned mechanism, which describes their biogenesis, facilitates the incorporation of many such macromolecules in a specific manner, thereby conferring a particular biomolecular identity on exosomes.[99]

Lipids in exosomes are often an underappreciated category of exosomal cargo. Lipids serve structural roles in vesicle membranes but also contribute to vesicle formation, stability, targeting, and cargo delivery.[100,127] Key classes of lipids include sphingolipids, phospholipids, cholesterol, and glycerophospholipids.[123,127] Spihngolipids come in the form of ceramides, which are lipids that aid in the ESCRT-independent pathway of exosome biogenesis through shaping the inward budding of the membrane. Sphingomyelin and glycosphingolipids both form membrane microdomains, also known as lipid rafts, which help cluster cargo for intracellular delivery.[128,129] Phospholipids such as phosphatidylserine (PS) are present on the exosomal surface and facilitate interactions with recipient cells and promote uptake via PS-receptors.[128,129] Phosphatidylethanolamine (PE), phosphatidylcholine (PC), and phosphatidylinositol (PI) are specific phospholipids that will contribute to membrane curvature and vesicle stability.[128,129] These phospholipids also influence immune regulation and migration signals due to their presence on the surface of the vesicle. Cholesterol in exosomes plays a crucial role in regulating the fluidity of the membrane. At high temperatures, cholesterol reduces fluidity by restricting the movement of phospholipid fatty acid chains through the insertion of these chains between phospholipid molecules, thereby limiting their movement and preventing the membrane from becoming overly fluid.[130] At low temperatures, cholesterol prevents the membrane from becoming too rigid by interfering with fatty acid interactions, which decreases the packing of the phospholipid tails, hindering the movement of the membrane.[130] Glycerophospholipids such as lysophosphatidylcholine (LPC) can modulate membrane curvature through their cone-shaped morphology. [129,131]

Exosomes contain a wide variety of unique proteins, each with its specific role. The first is tetraspanins (CD9, CD63, CD81, CD82), which serve as scaffolds for assembling multiprotein

complexes and are essential in membrane trafficking.[132] ESCRT machinery proteins, such as TSG101 and Alix, remain associated with exosomes as they are processed into the MVB.[133] Heat shock proteins such as HSP70 and HSP90 can be located on the exosomal surface and have been shown to play an essential role in immunomodulation by binding to antigen-presenting cells or promoting antitumor immune responses.[133] Integrins and cell adhesion molecules on exosomal membranes, such as ICAM-1 and VCAM-1, are found in exosomal membranes that aid cell adhesion and communication processes.[134] Moreover, cell-specific proteins and cargo-sorting adaptors like hepatocyte growth factor-regulated tyrosine kinase substrate (HRS) bind to ubiquitinated proteins during ILV formation, allowing for preferential sorting into endosomes.[135]

In the context of nucleic acids, much less is known regarding their composition in exosomes. Double-stranded genomic DNA (gDNA) and mitochondrial DNA (mtDNA) have been detected within exosomes.[136-139] mtDNA is released from tumours or stressed cells, which may affect immune recognition or metabolic functions within the recipient cell.[137] Studies have noted the presence of single-stranded DNA (ssDNA) and smaller DNA oligonucleotides. [137,138] The precise mechanisms by which DNA enters exosomes have yet to be elucidated. However, several hypotheses provide insight into this topic. For example, some studies suggest that nuclear envelope invaginations extend to late endosomes, potentially leading to the encapsulation of nuclear material, including nuclear debris.[139] Studies regarding DNA in exosomes have focused on diagnostic purposes and, as a result, still have much to decipher.[139]

Both long and small RNAs are present in exosomes. mRNAs can be packaged inside exosomes through the aid of RNA-binding proteins, such as hnRNPA2B1 and hnRNPU, which specifically bind to particular sequences or structural motifs on mRNAs, facilitating their selective loading into ILVs of MVBs.[140] EV-enriched transcripts are typically shorter, have a

higher exon density, and have fewer A/U-rich elements in their 3' UTRs.[140] RNA-seq data showed that 609 of the 10761 mRNAs and 72 of the 2393 long noncoding RNAs (lncRNAs) were enriched in exosomes relative to cells.[140] These RNAs can be delivered and translated into functional proteins, influencing gene expression and cell signalling pathways in recipient cells.[141,142] For example, lncRNAs can regulate gene expression post-transcriptionally, acting as sponges for miRNAs or scaffolds for protein complexes.[143,144] Moreover, packaging of particular RNA transcripts into exosomes has been hypothesized to play a role in RNA homeostasis, a way for cells to fine-tune their transcript pool by exporting surplus or regulatory RNAs.[145] Supporting this model, pharmacological or genetic blockade of sEV release causes the very transcripts typically loaded into vesicles to accumulate intracellularly, indicating that vesicle secretion functions as an active branch of RNA turnover.[145,146] For small RNAs, a subset of 200-500 miRNAs are consistently enriched in sEVs across different cell types. Other small RNAs, such as piRNAs, tRNAs, and snRNAs, have also been localized in sEVs at a much lower enrichment level when compared to cells.[146,147] The loading of miRNAs into sEVs is governed by a series of sequence motifs, secondary structures, and interactions with RNA-binding proteins (RBPs). Well-characterized examples include the GGAG “EXOmotif,” recognized by HNRNPA2B1; a UAG-rich motif bound by HNRNPA1, HNRNPA2B1, and RBM28; and GC-rich motifs that recruit RBM4, FUS, or RBM8A.[147] Not every RBP, however, relies on a short consensus sequence. For instance, YBX1 can chaperone selected miRNAs into vesicles under cellular stress without a strict motif requirement, probably by sensing RNA secondary structure or local nucleotide composition.[148,149] Whether they recognize defined motifs or broader structural cues, these RBPs share canonical RNA-binding domains that anchor them to miRNA cargo and the vesicle-sorting machinery.[150-154] These include the RNA Recognition Motif (RRM), a 90 amino

acid long that consists of two conserved sequences, an RNP1 octamer and RNP2 hexamer, which form a β-sheet structure that interactions with the miRNA backbone, the K homology domain (KH) that is 70 amino acids long with a βααβ fold that creates an RNA-binding groove that will interact with RNA via the GXXG loop motif, the Zinc Finger domain (ZnF) that is characterized by the presence of zinc-coordinated structural motif, and the PAZ (piwi-argonaute-Zwille) domain that is found in argonaute proteins forming an OB-fold structure that binds to the 3' end of miRNAs.[150-154] These modular domains enable RBPs to either read precise export signals (EXOmotifs) or bind more generically to structured miRNAs, ensuring that a diverse yet selective repertoire of small RNAs is packaged into sEVs.

1.3.3 sEV Endocytosis, Cell Signalling, and Cargo Delivery

After sEVs are released from their origin cell, they exhibit remarkable adaptability in navigating the extracellular space. Studies show that, in vivo, the navigation is not fixed, and sEVs can pursue both long-distance travels through body fluids or, importantly, engage in short-distance communication with neighbouring cells. Once the sEVs reach the plasma membrane of their recipient cell, a variety of mechanisms, each with its own unique characteristics, are employed to get to the cell's interior. These mechanisms include macropinocytosis, receptor-mediated endocytosis, phagocytosis, filopodia-mediated endocytosis, and surface-driven signalling.[155-160]

Macropinocytosis occurs when an invagination of the plasma membrane, driven by actin filaments, forms intracellular compartments called macropinosomes, facilitating the nonspecific uptake of extracellular fluid and small particles.[155] The macropinosome matures and can be degraded by the lysosome or recycled back to the plasma membrane. In the context of sEVs,

studies have shown that macropinocytosis is used for their uptake in HeLa cells, microglial cells, and to a lesser extent, epithelial cells.[155]

Receptor-mediated endocytosis requires the presence of a ligand to facilitate interaction between sEVs and the plasma membrane. This pathway is commonly referred to as clathrin-mediated endocytosis.[155] In this mechanism, clathrin and adaptor protein 2 coat the plasma membrane and accumulate, creating a positive feedback loop in which more clathrin is recruited from the cytosolic pool.[155] The assembly of these proteins allows for the invagination of the membrane, generating what is called a clathrin-coated pit. The membrane invagination is then cut by actin polymerization and scission proteins, facilitating its entry into the cell and allowing it to be trafficked further in the endosomal pathway.[155]

Phagocytosis is conventionally performed by macrophages or dendritic cells. However, it is also performed by γδ T cells. It has been shown to internalize sEVs through the engulfment of extracellular space via invaginations of the plasma membrane around the material to be internalized, similar to macropinocytosis.[156] The main difference between phagocytosis and macropinocytosis is the size of the material internalized, the former being used in the context of larger particles. However, studies show that phagocytosis has internalized particles as small as 85 nm in diameter, suggesting its involvement in the internalization of sEVs.[156]

sEV internalization has also been found to be mediated by filopodia. Filopodia are actin filament protrusions from the cell that scan the environment.[157,158] Due to the constant movement of the filopodia, these extensions increase the cell's surface area, ultimately making it a prime target for processes such as endocytosis. Studies have shown that sEVs could associate with filopodia extensions and move toward the plasma membrane.[158] These observations resembled a previously described process concerning viral particles associated with filopodia preceding viral

uptake, validating its applicability to sEVs.[159,160] Moreover, studies using artificial beads that bind to filopodia have been shown to associate with receptors from the integrin and cell adhesion molecule protein receptor families, which are implicated in sEV uptake, suggesting the use of filopodia as a mechanism of sEV internalization.[160]

sEVs can impart effects on the cells without entering the cell itself. Direct engagement of membrane-bound ligands on sEVs with receptors on a target cell can trigger downstream signalling.[110] Examples of this phenomenon include Notch1/Notch2-bearing sEVs that bind to Jagged/DII receptors on dendritic cells that, in turn, lead to an increase in Hes1 transcription, which plays a role in shaping excitatory synapse maturation.[161] Another example is found in cancer cell biology, where solid tumours secrete EphA2 sEVs that dock onto ephrin-A1-positive cancer cells and activate ERK1/2 via reverse Eph-ephrin signalling, which in turn propagates an invasive phenotype through the tumour mass.[162] These examples underscore that contact-dependent surface signalling is a cargo-independent axis of EV biology, operating in contexts such as neuronal plasticity and tumour progression alike.

Understanding which pathway predominates in the uptake of sEVs will be critical for engineering sEV surfaces or pre-conditioning recipient cells to maximize therapeutic siRNA delivery. A summary of biogenesis and internalization is shown in Figure 2.

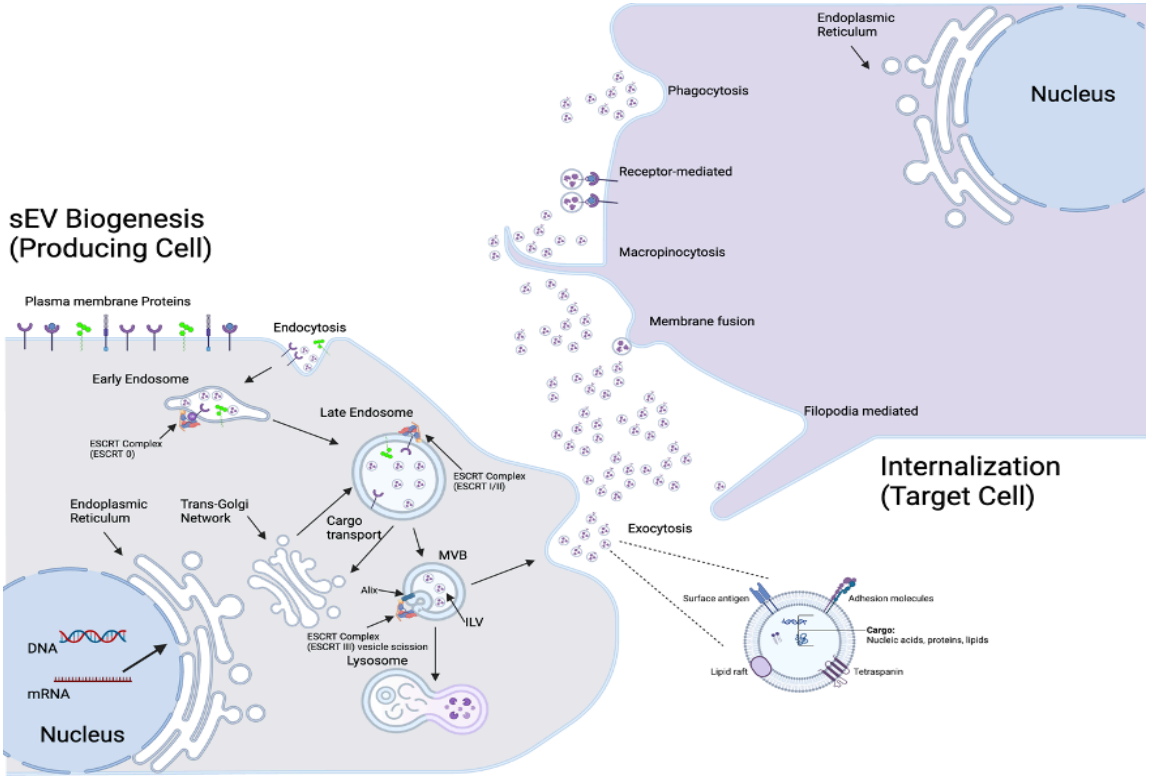

Figure 2. Biogenesis, sEV composition, and internalization of sEVs. Left (producing cell): Plasma-membrane proteins, cytosolic RNAs and other cargo are first internalized into early endosomes. Through sequential action of ESCRT-0, -I and -II, the selected cargo is concentrated; Alix then recruits ESCRT-III, driving inward budding and scission to form intraluminal vesicles (ILVs) inside multivesicular bodies (MVBs). Mature MVBs either fuse with lysosomes for degradation or with the plasma membrane to release their ILVs as small extracellular vesicles (sEVs). **Vesicle makeup:** Released sEVs display tetraspanins, lipid raft components, and surface antigens on their membrane and carry nucleic acids, proteins, and lipids in their lumen. **Right (target cell):** Extracellular sEVs reach recipient cells and can be internalized by several, partly overlapping mechanisms: macropinocytosis (large, actin-driven ruffles), clathrin-mediated receptor uptake, phagocytosis (primarily in professional phagocytes), filopodia-assisted "surfing," and, in some cases, direct membrane fusion. Once inside, sEV-containing vesicles may fuse with endosomal compartments, traffic to lysosomes, or, after fusion with the limiting endosomal membrane, release their cargo into the cytoplasm.

1.3.4 sEV fusion

In addition to endocytosis, fusion is another mechanism by which sEVs can deliver their cargo into the cell. sEV cell surface fusion is a process in which sEVs merge directly with the cell's plasma membrane.[163] Although only a handful of experiments have captured this pathway,

and most mechanistic details are extrapolated from viral and synaptic fusion studies, the biophysical sequences of events are well established. sEV fusion is initiated by direct contact of sEVs with the plasma membrane.[163-167] Since both membranes are hydrophobic, a point-like membrane protrusion is formed by one of the membranes that minimizes the energy of the hydration repulsion between the two plasma membranes.[163,164] This results in a hemifusion stalk with the proximal portions of the membranes fused. Following this, the stalk expands and produces a hemifusion diaphragm bilayer. This allows for the formation of a fusion pore, a connection between merging membranes involving both leaflets of the plasma membrane.[163-165] This fusion pore allows for the connection of the aqueous contents of each fusing body.[163-165]

While sEV fusion is a fascinating process, it has its challenges. It requires the cell to invest energy or employ energy-releasing processes to overcome the repulsive forces between the two lipid bilayers. These barriers arise from electrostatic repulsion, hydration layers, lipid rearrangements, bilayer bending (curvature), and ultimately, membrane merging (hemifusion, fusion pore formation).[163-170] The following paragraphs will explore the thermodynamic underpinnings and molecular mechanisms by which sEVs can overcome these barriers.

During the initial membrane approach phase, sEVs must overcome the electrostatic and hydration repulsion as the two membranes approach each other.[171] Lipid bilayers carry net negative surface charges due to phospholipid and negatively charged surface proteins, and the extracellular space contains water molecules that coat the membranes.[172] However, for the lipids of both lipid bilayers to intermix, they need to come into contact with each other, meaning that the water molecules that coat the membranes and the electrostatic interactions need to be removed from the interface.[172,173] Additionally, steric repulsion from glycolipids, glycans, or proteins on the membrane surface may contribute to further resistance to sEVs' fusion ability.[173]

To overcome this barrier, sEVs can employ protein-protein, protein-lipid, or ligand-receptor interactions. Particular surface proteins on sEVs have complementary receptors or lipids that bind to the target membrane.[173,174] These interactions provide an enthalpic gain through the strong non-covalent bonds between proteins and proteins/lipids, and displace water by bringing the proteins together favourably, thereby increasing entropy and leading to a more spontaneous reaction for fusion.[173,174] Furthermore, as described, sEVs have a particular lipid profile that can participate in membrane-membrane contacts. Cholesterol-rich domains can enhance membrane rigidity locally and promote lipid packing, which helps exclude water, thereby reducing the hydration barrier between two membranes.[174] For example, suppose there is PS on the external leaflet of sEVs; this can create favourable electrostatic interactions with positive patches on the recipient membrane, partially neutralizing the repulsive forces.[175,176]

Another energy barrier that needs to be overcome is the membrane's curving and the lipids' local deformation.[177] Deforming a flat membrane to initiate a fusion event with an sEV imposes an energetic cost by bringing proteins that generate curvature and stabilize the curved membrane.[176,177] sEVs preferentially binding to slightly curved membrane subdomains (membrane protrusions, endocytic pits) will overcome this energy barrier. These pre-existing localized curvatures reduce the energy cost of generating the curvature on the receiving membrane to accept a fusion event.[177] Active membrane remodelling, facilitated by protein assistance, is another way to overcome the energy barrier. Proteins or lipid microdomains at the site of contact between sEV and the plasma membrane can help reshape the membrane to fuse with the cell. By recruiting curvature-sensing proteins (like tetraspanins), the cell can locally deform the membrane to accommodate the sEV better.[178,179] This process can be partially ATP-dependent in the context of using the cytoskeleton, a network of protein filaments in the

cytoplasm, to rearrange the membrane through mechanical pulling or pushing, thereby offsetting the bending energy cost with chemical energy from ATP hydrolysis or the reorganization of the cytoskeleton. [180,181]

The next energy barrier that needs to be overcome is the generation of the hemifusion diaphragm. After the bilayers approach each other, the next step is to disrupt the lipid packing in each outer leaflet, bringing them into a single continuous leaflet. To overcome the barrier of disrupting the lipid barrier, the sEV lipid composition, which contains inverted-cone shapes such as PE and PS, can facilitate the formation of hemifusion by lowering the packing order at the fusion site.[182] Moreover, viral fusion peptides are known to be inserted directly into the host membrane to perturb local bilayer structure.[183,184] If sEVs deploy an analogous strategy, these proteins could insert their hydrophobic fusion loops into the outer leaflet of the target membrane, locally disrupting the tight, ordered packing of phospholipid head-groups.[179] This disordering increases the spacing between neighbouring lipids and softens the bilayer, conditions that lower the energetic cost of lipid flipping (the trans-bilayer movement of individual phospholipids from one leaflet to the other). Such rapid flip-flop helps mix the outer leaflets of the vesicle and plasma membranes, promotes formation of the hemifusion stalk, and ultimately drives expansion of the fusion pore.[185] Furthermore, sEVs have high curvature, often containing lipid packing defects. These defects are slight gaps or disruptions between lipid headgroups that can serve as points for hemifusion. In these areas, there is a lower energy requirement to disturb the packing.[185]

The final energy barrier that needs to be overcome is the formation of the fusion pore and the completion of the fusion process. In this step, the combined bilayer must traverse horizontally to allow the cargo to pass, which requires energy to overcome membrane edge

tension and stabilize the newly formed pore.[186] To overcome this barrier, particular membrane proteins, such as tetraspanins, can stabilize the initial fusion pore by surrounding and lining the nascent pore.[186,187] These proteins reduce the line tension that would otherwise cause the pore to return to the most energetically favourable conformation by closing.[186,187] Moreover, lipid geometry changes after the formation of the hemifusion stalk may occur, facilitating the movement of lipids that may stabilize pore formation at the fusion site, lowering the free energy of the process.[186,187] Figure 3 summarizes the free-energy profile of each stage, underscoring both the improbability of spontaneous fusion and the specialized molecular toolkit that makes sEV fusion thermodynamically feasible. This knowledge will be critical for engineering vesicles with enhanced delivery efficiency.

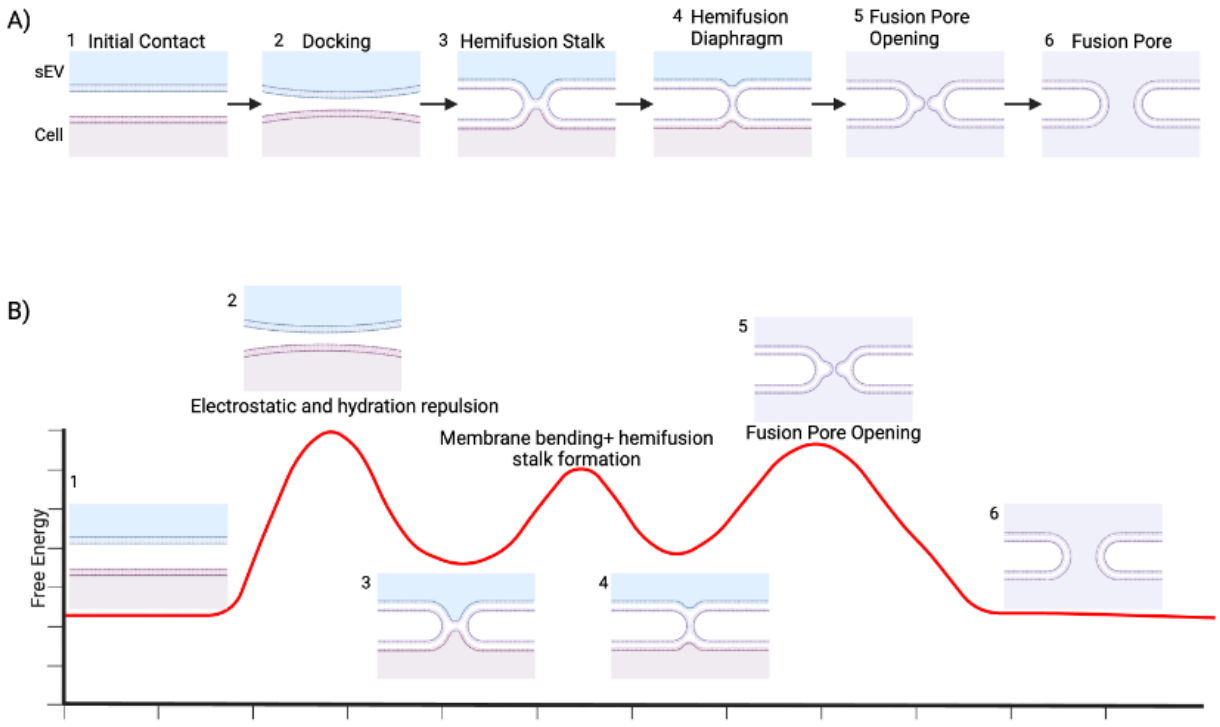

Figure 3: Mechanism and Energetics of sEV-Plasma Membrane Fusion: A) Depiction of the structural transformations of the membranes that must occur for a fusion event to occur from free sEV (left) to complete fusion pore formation (right). 1) sEVs approach the plasma membrane, displacing water molecules and partially neutralizing negative surface charges to allow for apposition to occur. 2) Adhesion molecules form noncovalent bonds that help bring membranes into closer contact and displace water molecules present between the membranes, allowing for tight docking. Local membrane bending occurs. 3) The outer leaflets of both membranes merge into a single bilayer, formally referred to as a stalk, generating a transient connection between the two compartments. 4) Stalk then leads to the formation of a hemifusion diaphragm. 5) Fusion pore begins to form, generating continuity between sEv and the cell interior. 6) Fusion power expands, and sEV cargo can then be released directly into the cytoplasm. **B)** Free energy graph depicting the free-energy profile correlating to the structural changes made in fusion. Peak 1 shows the overcoming of electrostatic and hydration repulsion, peak 2 reflects the energetic cost of membrane bending and hemifusion stalk formation, and peak 3 displays fusion pore opening and expansion. Figure created with Biorender.

1.3.5 Intracellular Signalling of sEVs

Once sEVs have been internalized, they typically travel through the endosomal pathway.[188] This pathway aims to facilitate the sorting and distribution of internalized cargoes to their proper destinations.[188] The cargo can be recycled back into the plasma membrane through the recycling endosome, sent to the trans-Golgi network (TGN) via retrograde trafficking, or sent to the lysosome through MVBs for degradation.[188,189] The regulation of the trafficking and sorting processes corresponding to sEV cargo is accomplished through control via physical attributes of vesicles as well as proteins recruited to these vesicles as they mature and reach their final destination [188,189]

As early endosomes mature into late endosomes, the lumen becomes increasingly acidic.[191,192] This phenomenon, known as endosomal acidification, is crucial in the sEV trafficking process. It results from the increase in hydrogen ions pumped through the action of a V-type vacuolar H+ ATPase, decreasing the pH of the lumen.[191,192] This change in pH promotes ligand-receptor dissociation, setting the stage for further maturation. Concomitant with the pH change, other mechanisms will adjust the membrane identity from early to late endosome. These mechanisms include the phosphatidylinositol phospholipid (PIP) composition and the Rab cascades [193-196]

PIP composition is different at each stage of the endosomal pathway, imparting specificity to the proteins recruited to the endosomal membrane compartment.[197,198] PIP will be differentially phosphorylated or dephosphorylated depending on the compartment it is associated with.[198,199] Evidence shows that PIP-specific lipid domains will bind lipids critical for the trafficking of sEVs through parts of the endocytosis pathway. For example, clathrin-mediated endocytosis components such as dynamin will bind to PI(4,5)P2 (PIP phosphorylated at positions

4 and 5), which is enriched at the plasma membrane.[198,199] However, in the early endosome, PI(3)P (PIP phosphorylated at position 3) is associated with the endosome and will bind to the FVYE and PC domains, recruiting proteins to trafficking through the early endosomal compartment.[198,199]

Rab proteins are critical in membrane trafficking and compartmentalization of the endomembrane system.[200] Rabs recruit sets of effector proteins to the surface of distinct membrane compartments, contributing to the structural and functional identity of the endosomal compartment.[200,201] The mechanism that allows Rabs to perform these functions involves using Rab GTPases. Rab GTPases will cycle between GDP and GTP-bound states through the catalyzing action of Guanine-nucleotide exchange factors (GEFs) (catalyzing the exchange of GDP to GTP) and GTPase-activating proteins (GAPs) (catalyzing the hydrolysis reaction of GTP to GDP).[200,201] When Rab GTPase is in the GTP-bound state (active), it will bind the Rab effector proteins, which, when bound to the vesicle in question, will act as markers that define the vesicle identity.[200,201] The associated Rab effector molecules will also facilitate vesicle formation, targeting, and fusion, dictating how the sEV is trafficked.[200,201] The Rab cascade is a proposed pathway that explains how vesicle identity changes, utilizing Rab, and ensures that trafficking has directionality.[200] In this pathway, a Rab that is associated with the vesicle (ex. Rab5 with the early endosome) will recruit a GEF, which will activate a subsequent Rab that would be present on a more mature endosome (ex. Rab7 with the late endosome). This recruitment of a downstream Rab will then recruit the GAP associated with the previous Rab, removing the previous Rab's presence on the vesicle and changing the vesicle identity entirely (in this case, the early endosome matured into the late endosome through the change of Rab5 into Rab7).[201] The PIP composition and Rab cascade explain how the endosome will change into its downstream

entities. Understanding how sEVs negotiate this itinerary will be essential for engineering vesicles that maximize functional RNA delivery while minimizing lysosomal loss.

1.3.6 sEV Cargo Sorting

sEV cargo being endocytosed enters the early endosome, where luminal pH and membrane identity determine onward trafficking.[192,193] As the sEV is internalized and formed into the early endosome, internalized ligand-receptor complexes will dissociate from the membrane based on the pH in the endosome and will then be trafficked subsequently.[201,202] For example, if the internalized receptor is dissociated in the early endosome at a pH of 6.5, the cargo will be recycled to the plasma membrane. Receptors that undergo this trafficking include transferrin and low-density lipoprotein receptors.[201,202] If a cargo of sEV is destined for the TGN, internalized transmembrane receptors will be released in the late endosome when the pH is approximately 5.5. The internalization of receptors will enable cargo to undergo retrograde transport, diverting it to the TGN, where it will be packaged and sent to the endoplasmic reticulum (ER) for subsequent processing.[201,202] Some signalling receptors will remain bound at low pHs of approximately 4.5. In this state, the bound proteins can participate in signalling from endosomal compartments until they are sorted into ILVs and sent for degradation in the lysosome.[201,202]

Other mechanisms of cargo trafficking and sorting include the recognition of ubiquitinated cargos by ESCRT-0, which allows the cargo to move directly into ILVs, facilitating their travel to lysosomes, where they will ultimately be degraded.[201] Moreover, sorting machinery (proteins involved in sorting cargo) can associate with particular sorting signals encoded within the amino acid sequence of cargo molecules, impacting the final destination of the

aforementioned cargo.[201] These interactions typically occur through endosomal membrane tubulation. Endosomal membrane tubulation is a process driven by proteins containing lipid-binding motifs.[201] An example of these proteins is Bin/Amphiphysin/Rvs (BAR) domain-containing proteins, which can induce membrane curvature.[202] Proteins interacting with the binding motif include sorting nexin family proteins (SNX).[202] SNX proteins were initially described as members of the yeast's evolutionarily conserved retromer complex. This retromer complex was essential in transporting the trans-Golgi sorting receptor, vacuolar sorting protein 10 (VPS10), from the endosome to TGN. Studies have shown that the retromer complex consists of two functionally distinct subcomplexes: the membrane recognition complex, which includes the BAR domain along with SNX, and the cargo-selective complex.[203] The complex is recruited to endosomes through SNX binding with PI(3)P or Rab8-positive late endosomes, conjugating to the cargo-selective complex.[205] This complex aims to rescue cargo receptors, such as CI-MPR or Wntless, that would have been dissociated due to pH changes, thereby rerouting the endosome to an alternative pathway, such as recycling to the plasma membrane or the trans-Golgi network.[205]

Although these pathways are well-characterized for transmembrane proteins, far less is known about how therapeutic RNA or protein cargo within sEVs escapes the endosomal lumen to reach the cytosol. Deciphering whether sEV-encoded siRNAs exploit retromer, back-fusion of ILVs, or other escape routes will be critical for engineering vesicles that maximize functional delivery rather than lysosomal loss.

1.3.7 Delivery of siRNA via sEVs

Small extracellular vesicles have captured attention as attractive carriers for therapeutic siRNA.[206] However, the efficient and non-disruptive loading of the siRNAs into sEVs remains a

challenge. Techniques such as electroporation [207,208] and hydrophobic modification by cholesterol conjugation [203] have been used to insert siRNA into vesicles. However, these techniques have flaws in that the phospholipid surface of the sEV may be compromised during the process, potentially leading to immunogenic considerations and a decreased ability to deliver their siRNA cargo.[208] A solution to this problem would be the alteration of the sEVs through co-opting the sEV's endogenous capabilities of packaging small RNAs such as miRNAs.

Reshke et al. found that by altering the producing cell, they can enrich siRNA endogenously in sEVs.[94] They did this by using miR-451, a highly enriched miRNA in sEVs. Two cleavage events of an RNA stem-loop, or hairpin structures, are essential to the canonical generation of miRNA.[94] First, RNase III endonuclease Drosha will participate in an 11-base pair (bp) cleavage from the base of the RNA transcript, generating a pre-miRNA consisting of approximately 65 nt. [94,209-214] Pre-miRNA will exit the nucleus and enter the cytoplasm, where RNase II endonuclease Dicer will cut 22 bp from the 3' overhang left by Drosha.[209-214] In the end, we are left with a 22-nt double-stranded RNA, removing any remnant of the loop. Here, Dicer and transactivation response element RNA-binding protein (TRBP) will associate the RNA duplex onto an AGO protein, where it will then proceed through the same downstream processing as miRNA as described previously in the introduction and figure 1.[210] However, miR-451 biogenesis undergoes a non-canonical pathway such that when the pre-miR-451 transcript is cleaved by Drosha, it produces a 42 nt hairpin as opposed to a 65 nt hairpin.[210-214] For subsequent processing by Dicer, a stem of a miRNA must be at least 19 nt long to bind and cleave the hairpin into the double-stranded form. The usually short hairpin structure of pre-miR-451 leaves a stem of only 17 nt long, inhibiting further processing by Dicer. As a result, the shorter hairpin is bound directly to Ago2.[210-215] This pathway ends in a final strand of

miR-451 that includes bases through the loop region cleaved in the canonical pathway. As a result, siRNA sequences can be inserted into the loop structure and remain intact inside the sEVs. Using these reprogrammed sEVs, the Gibbings lab has demonstrated the efficiency of sEVs as delivery vehicles for siRNAs, achieving functional cytoplasmic delivery of 3-30% of the RNAs they contain into cells.[94] Given the capacity of sEVs to deliver siRNA into tissues and induce a silencing effect in a nontoxic and non-immunogenic manner, sEVs packaged with siRNAs are a promising therapeutic. The miR-451 scaffold, therefore, provides proof of concept for harnessing endogenous sorting signals to load siRNA efficiently, a strategy that could be expanded to other miRNA backbones or combined with surface engineering to create next-generation sEV therapeutics.

1.4. Engineered Ascorbate Peroxidase Proximity labelling with Mass Spectrometry

Proximity labelling methods, in conjunction with mass spectrometry (MS), are tools for deciphering protein association networks in a spatially restricted area.[216-218] Proximity labelling uses an enzyme to generate reactive radicals that promote the local conjugation of functionalized biotin to surrounding proteins and RNAs. [216,217] The conjugated proteins can then be isolated for MS analysis, giving a high-throughput approach to analyzing the proteome of precise cellular locations.[216,217] The enzyme used can be fused to a protein of interest, allowing the identification of proteins that are in the vicinity of said protein.

Engineered Ascorbate Peroxidase (APEX) is one of the enzymes that will generate the aforementioned reactive radicals.[217] APEX can catalyze the oxidation of biotin-phenol to biotin-phenoxyl radical in the presence of H_2O_2.[218] Using APEX instead of other iterations of proximity labelling approaches such as BioID will allow for quick and efficient biotinylation of

protein species as it catalyzes labelling within one minute after H_2O_2.[218] APEX lacks disulphide bridges and calcium binding sites, meaning it can be expressed in the reducing cytosolic environment of cells without losing its enzymatic activity.[219] Therefore, APEX is used for extravesicular proximity labelling, which can be expressed outside vesicles to catalyze the biotinylation reaction.[219] APEX cannot be expressed in the lumen of sEVs due to the oxidizing environment, rendering APEX inactive as it misfolds in this environment.[219] However, plant horseradish peroxidase (HRP) can also identify intravesicular protein.[219] HRP is inactive in a reducing cytosolic environment because it is maintained with four disulphide bonds and two Ca^{2+} ion-binding sites.[219] As a result, it can exist in oxidizing environments. These tools facilitate the identification of protein products, thereby augmenting the existing arsenal of proteomic techniques. Together, the APEX2/HRP pair provides complementary coverage of extravesicular and intravesicular proteomes, offering a high-resolution strategy that this thesis will utilize to define the protein landscape governing the trafficking and fusion of siRNA-loaded sEVs.

1.5 Rationale and Hypothesis

sEVs combine innate biocompatibility, low immunogenicity, and the capacity to cross restrictive barriers such as the blood–brain barrier, positioning them as compelling carriers for therapeutic siRNA. Despite their potential to revolutionize targeted drug delivery, the mechanisms underlying the internalization of sEVs and cargo delivery remain elusive. Clarifying these pathways is crucial for fundamental cell biology and optimizing sEV-based therapeutics. **I hypothesize that tracking sEVs as they are internalized into the cell will reveal protein complexes that facilitate the internalization of sEVs and delivery of their cargo into cells.** Such mechanistic insights have two immediate benefits. First, they contribute to our foundational

understanding of intercellular communication, as the mode of sEV entry likely involves evolutionarily conserved membrane trafficking processes. Second, they provide a clear path forward for the bioengineering of sEVs to enhance cellular uptake, improve siRNA (or other cargo) delivery, and potentiate therapeutic outcomes. Defining the internalization mechanism will ultimately accelerate the development of sEV-based strategies for a wide range of diseases, particularly in neurodegenerative disorders, where targeted delivery across the blood-brain barrier remains a significant challenge.

Chapter 2: Materials and Methods

2.1 Cell lines

1. Human Embryonic Kidney cells (HEK293T) (ATCC; catalogue # CRL-3216)
2. HEK293T cells, APEX-PTGFRN. The techniques required to generate this cell will be described in more detail in subsequent sections. APEX-PTGFRN plasmid, PMD2.G and psPAX2 were briefly transfected into HEK293T cells. Lentiviral particles released by the cells were collected and precipitated and used to infect HEK293T cells. The cells were then selected using puromycin to produce a pure population of APEX-PTGFRN expressing cells. Expression was confirmed through DAB staining followed by light microscopy.
3. HEK293T cells, HRP-PTGFRN, HRP-PTGFRN. The techniques required to generate this cell will be described in more detail in subsequent sections. Briefly, HRP-PTGFRN plasmid, PMD2.G and psPAX2 were transfected into HEK293T cells. Lentiviral particles released by the cells were collected and precipitated and used to infect HEK293T cells. The cells were then selected using puromycin to produce a pure population of HRP-PTGFRN-expressing cells. Expression was confirmed through DAB staining followed by light microscopy.

2.2 Cell Culture

All cells listed in section 2.1 were kept in Dulbecco's Modified Eagle Media in high glucose (DMEM)(Millipore Sima, U.S.A) with heat-inactivated 10% fetal bovine serum (FBS)(Catalog#12484 Thermo Fisher Scientific), antibiotic-antimycotic solution

(ABAM)(Catalog#15240062 Thermo Fisher Scientific), and L-glutamine (catalog#25030149 Thermo Fisher Scientific) at 37˚C at 5% CO_2 prepared as described. Once cells reached confluence, they were lifted from the associated plate using Trypsin/EDTA (Wisent Bioproducts, 325-043-EL) for 10 minutes. After that, supplemented media was then added to neutralize the Trypsin/EDTA. For subsequent cell seeding for experimental and maintenance purposes, the cells were counted using a hemocytometer.

2.3 Production of HEK293 HRP/APEX cells

2.3.1 Lentiviral production of HEK293 HRP/APEX PTGFRN cells

HEK293T cells were seeded at 70% confluence on five 10cm plates. Two hours before transfection, the media was changed with 10 mL of fresh media containing 25 mM chloroquine. A mixture of plasmids psPAX2 (1.3 pmol), pMD2.G (0.72 pmol), and my transfer plasmid (APEX/HRP PTGFRN) (1.64 pmol) was combined and incubated for five minutes at room temperature. Subsequently, a ratio of 1:3 total DNA: polyethylenimine (PEI) was added to the same mixture and incubated for 15 minutes at room temperature. The transfection mixture was then added to each plate, supplemented with 5 ml of unsupplemented media. 24 hours after transfection, the media was replaced with 5 ml of supplemented media. Collections of the media were performed every 24 hours after the media change, for a total of three collections. The resulting media was subjected to a five-minute spin at 2000 rpm. The supernatant was collected and filtered through a 0.45 μm polyethersulfone (PES) filter. The virus was precipitated from the media using the Benchmark Bio Virus Precipitation Kit (catalogue # P100), as instructed by the manufacturer.

2.3.2 Lentiviral Transduction, Infection, and Population Selection

HEK293 cells were seeded at 50% confluence the day before lentiviral infection in a 6-well dish. The transduction day started with preparing a batch of non-supplemented DMEM with 10 µg/mL polybrene. Lentivirus was thawed immediately before use and aliquoted in various dilutions, allowing the cells to be subjected to varying concentrations of the virus. The dilutions are listed in Table 1. A single viral dilution was added to each well at a volume of 0.5 mL. The cells were incubated with the virus for 48 hours, and the media was replaced with 1.5 ml of non-supplemented DMEM containing 2 µg/ml puromycin. The selection process continued until a polyclonal population of resistant cells had proliferated, and individual wells had become confluent. At this point, the cells were lifted from the plate according to the protocol outlined in Section 2.2, then seeded into larger plates and frozen to prepare cell stocks. Expression was confirmed via DAB staining and light microscopy.

Table 1: List of Dilutions used for Lentiviral Transduction

Dilution	Volume of Lentivirus (µL)	Volume of DMEM (µL)
0	0	500
1:5	300	200
1:10	150	350
1:50	30	370
1:100	15	486
1:500	3	497

2.4 Transformation and inoculation of HRP/APEX-PTGFRN plasmids into Stbl3 cells

The HRP/APEX-PTGFRN plasmids were then transformed into chemically competent Stbl3™ cells (Thermo Fisher Scientific). 3µL of the HRP/APEX-PTGFRN plasmid is combined with 30µL of Stbl3 TM cells, placed on ice for 30 minutes, heat shocked at 42℃ for 45 seconds, and moved back to ice for 2 minutes. The cell suspension was then added to 500µL of Super-optimal Broth with Catabolic repression outgrowth media (SOC) (Catalogue #B9020S N.E.B) and was subsequently incubated at 250 rpm at 37℃. To increase transfection efficiency, cells were spun at 200g for 5 minutes, and 400µL of media was removed. Cells were then resuspended, and 100 µL of the cell suspension was plated on Lysogeny broth (LB) agar plates containing 50 µg/mL ampicillin and incubated at 37°C overnight. After incubation, two colonies were selected and transferred to a culture tube containing 3 mL of LB broth (Catalogue #SD7002, BioBasic) and 1x ampicillin. The culture was then incubated overnight at 37℃ and 250 rpm.

2.5 Minipreparation and sequencing of plasmid DNA

HRP/APEX-PTGFRN plasmids were then isolated using "*EZ-10 Spin Column Plasmid DNA Minipreps Kit"* (Catalogue #BS413, BioBasic, CA) as per the protocol listed by the manufacturers. To ensure isolation was successful, the DNA was sent to Plasmidsaurus for full plasmid sequencing.

2.6 Isolation of sEVs from media

Cells were grown to 70–80% confluence to produce sEVs. sEVs were collected from cells grown in DMEM F12 (Wisent Bioproducts; catalogue no. 319–015-CL; 4.5 g l−1 glucose)

with 5% Insulin-Transferrin-Selenium-Ethanolamine (Thermofisher, catalogue no.51500056). sEVs were produced using two methods: differential ultracentrifugation or tangential flow filtration.

2.6.1 Differential Ultracentrifugation

The sEV-containing media collected from the cells was first spun at 300g for 10 minutes. The supernatant was collected and spun at 2000g for 10 min,10,000g for 30 min (SW32Ti rotor, Beckman-Coulter Life Sciences; polycarbonate tubes, catalogue no. 355631, Beckman-Coulter Life Sciences) and 100,000g for 2 h (SW-32Ti rotor). From here, the formation of an sEV pellet will have been completed at the bottom of the tube. The pellet was first resuspended in 1 ml of 1x PBS (Wisent Bioproducts; catalogue no. 311–010-CL) and centrifuged at 100,000g for 30 min (TLA-100.3, Beckman-Coulter Life Sciences; polypropylene microfuge tubes, catalogue no. 357448, Beckman-Coulter Life Sciences). The protocol was performed as described in Théry et al.[220]

2.6.2 Tangential Flow Filtration

For tangential flow filtration (TFF), sEVs would be collected 3 times from 10 15cm plates. sEVs-conditioned media were spun at 300g for 10 min, and supernatants were subsequently spun at 2,000g for 10 min. Supernatants were passed through a 0.22 μm filter (Thermo-Scientific, catalogue no. 09–741–04) and concentrated to a final volume of 15 ml using the KR2i tangential flow filtration system (Spectrum Labs) with a 75 cm2 modified polyethersulfone hollow fibre column with 500 kDa cut-off (Spectrum, D02-E500- 10-S) at a flow rate of 120 ml min−1 and transmembrane pressure 3 psi to

achieve a shear rate of 2,000 s^{-1}. The concentrated media underwent 10× buffer exchange in Plasmalyte.

2.7 Nanoparticle Tracking Analysis

Nanoparticle tracking analysis (NTA) was performed on a ZetaView PMX-110 (ParticleMetrix). Calibration of the ZetaView Nanoparticle tracking analysis was performed prior to each experimental run. 100 nm polystyrene beads (Microtrac, catalogue no. 900383) were injected into the machine to optimize the focusing and alignment of the machine. Subsequently, dilution of the final TFF product or the final ultracentrifugation product was performed in phosphate-buffered saline (PBS) at a ratio of 1:10000 to 1:1000000. Approximately 1 mL of the diluted product was then injected into the machine. Once the particle drift sensor determines that the sample is at acceptable levels and the concentration falls within the acceptable reading concentration range, the machine will then perform video acquisition and analysis of the undiluted concentration and median size. The acceptable measurement range was determined using serial dilutions of 100 nm polystyrene beads of known concentration (5.0 × 10^12 particles/mL). Table 2 displays parameters that the NTA was set at for video acquisition and analysis.

Table 2: NTA settings used for sEV measurements

Pre-Acquisition Parameters	
Sensitivity	85
Shutter speed	40
Frame Rate (fps)	30
Resolution	Highest
Camera Gain	770
Positions Measured	11
Post-Acquisition Parameters	
Minimum Brightness	15
Minimum Size (pixels)	10
Maximum Size (pixels)	500

2.8 Optiprep Density Gradient

Optiprep gradients were performed as described in Dolley et al.[221]. In an ultracentrifuge tube (#331372, Beckman-Coulter Life Sciences), 1 mL of TFF product was mixed with 3 mL of 60% iodixanol solution (#D1556-250ML, Millipore Sigma) at the bottom. Homogenization buffer (250 mM sucrose, 1 mM EDTA, 10 mM Tris-HCl, pH 7.4) was used to dilute OptiPrep, generating less dense solutions that allowed for the creation of a gradient. The following solutions of Optiprep in homogenization buffer were layered onto the initial sEV mixture in the ultracentrifuge tube from most to least dense: 30% (3 mL), 23% (2 mL), and 18% (2 mL). Lastly, 1 ml of PBS was added to the top of the ultracentrifuge tube. Gradients were spun at 150,000 x g for 16h at 4°C in a SW-41Ti rotor (Beckman-Coulter Life Sciences). 950µL fractions were

collected from the top of the spun gradient, and densities were measured with a refractometer (#16046, ERMA).

2.9 Western blotting

Protein samples were mixed with 5x sodium dodecyl sulfate (SDS) loading buffer (60 mM Tris HCl pH 6.8, 10% glycerol, 2% SDS, 0.01% Bromophenol Blue, 10% β-mercaptoethanol (Bio-Rad, 1610710)) and heated for 10 minutes at 95°C. The resulting samples were separated using 10% SDS-PAGE at 100V for 10 mins and 150V for 1 hour and 15 mins. Samples were transferred onto a positively charged nylon membrane (Roche, 1417240) for 1 hour and 15 minutes at 100 V. The membranes were then washed with 1× Tris-buffered saline with 0.1% Tween detergent (TBST) (three times, 5 minutes each) and blocked with 1× TBST plus 5% milk for 1 hour. The membrane was subsequently probed overnight at 4°C with the following antibodies and then incubated for 1 h with a secondary antibody at a dilution of 1:7500 in PBST at room temperature. Finally, membranes were washed 3 times (10 minutes each) in TBST and incubated with enhanced chemiluminescence (ECL) Western HRP Chemiluminescence Substrates Crescendo (Fisher Scientific, catalogue no WBLUR0500). The chemiluminescence signal was recorded using a GE ImageQuant LAS4010 system. The membrane was stripped using 0.2M NaOH for 30 minutes when necessary. Antibodies are listed in Table 3.

Table 3: List of Antibodies used for Western blotting

Antibody Name	Producer	Catalog #	Dilution
APEX	Cell Signalling Technology	74728T	1:1000
CD63	Santa Cruz Biotechnology	sc-5275	1:5000
TSG101	Genetex	GTX70255	1:1000
Alix	Cell Signalling Technology	2171S	1:1000
Syntenin-1	Abcam	ab133267	1:1000
Tomm20	Thermo Fisher Scientific	ab133267	1:1000
Calnexin	Cell Signalling Technology	2679S	1:1000

2.10 Diaminobenzidine Staining and Electron Microscopy

HEK293 cells were treated with small extracellular vesicles (sEVs) derived from cells that stably express HRP-PTGFRN at a density of 10000 sEVs per cell for 30 minutes. Cells were fixed in 0.1M Sodium cacodylate (6131-99-3, Fisher Scientific) with 2% glutaraldehyde (G7776, Millipore Sigma) for 60 minutes on ice. Cells were washed in a 0.1 M Sodium cacodylate buffer with 2 mM $CaCl_2$. Cells were blocked with 2 mM CaCl2 and 2 mM glycine in a 0.1 M solution of Sodium cacodylate. 0.5 mg/mL Diaminobenzidine (DAB) (catalogue #12385, Millipore Sigma) was added to the cells in a 0.1 M Sodium cacodylate solution. Rinsed in buffer, post-fixed in 1% osmium tetroxide in buffer for 90 min, dehydrated in a graded ethanol series (50%,70%,90% and 100%, 20 minutes each step) followed by two propylene oxide changes for 30 min, and embedded in Quetol-Spurr resin. Blocks were cured overnight in the oven at 60 °C. Sections 70nm thick were cut on a Leica EM UC7 ultramicrotome, stained with uranyl acetate

and lead citrate. Sections were then imaged on the JEM-1400 Flash TEM at 100 kv. Images were taken using a 16MP digital camera (GATAN OneView).[226]

2.11 SILAC labelling and sample preparation for MS

For 100% stable isotope labelling by amino acid in cell culture (SILAC) labelling, HEK293 Cells were incubated in DMEM consisting of 13C6 15N2 L-Lysine-2HCl and 13C6 15N4 L542 Arginine-HCl (catalogue #A33972, Thermofisher) and passaged for five doubling events, and the incorporation of heavy amino acids was tested using mass spectrometry analysis. Protocols involving the incorporation of heavy amino acids were performed as instructed by the manufacturer.[222]

2.12 In-vitro APEX2 proximately labelling of cells treated with APEX-PTGFRN sEVs

SILAC-labelled HEK293 cells seeded at 90% confluence in 10cm plates were treated with sEVs derived from cells that stably express APEX-PTGFRN at a density of 10000 sEVs per cell for 10 mins, 30 mins, and 1 hour. To initiate APEX2 labelling, DMEM containing 500 nM Biotin-Phenol (BP) was added to the cells for 2 hours at 37°C under 5% CO2. Subsequently, 1 mM H2O2 was added to the cells for 1 minute and then immediately removed. After removal of H_2O_2, the APEX2 reaction was quenched by replacing the medium with an equal volume of quenching buffer (5 mM Trolox, 10 mM sodium ascorbate and 10 mM sodium azide in DPBS). Cells were washed in cold PBS (2x). RIPA lysis buffer (10mM Tris-HCl, pH 8.0, 1mM EDTA, 0.5mM EGTA, 1% Triton X-100, 0.1% Sodium Deoxycholate, 0.1% SDS, 140mM NaCl) was put on the cells, and the cells were scraped with cell lifers and transferred to a 1.5 ml Eppendorf tube. Cells were sonicated and pelleted by centrifugation at 300g for five minutes at 4°C, and

then stored at -80°C for further experiments. Protocols for APEX2 proximity labelling were based on protocols generated from Benedict et al.[223]

2.13 Immunofluorescence

HEK293 cells were treated with small extracellular vesicles (sEVs) derived from cells stably expressing APEX-PTGFRN at a density of 10,000 sEVs per cell for 10 minutes or 30 minutes. Cells were fixed in 4% Paraformaldehyde (PFA) (Catalogue #15714, Electron Microscopy Sciences) for 20 minutes at room temperature. Cells were permeabilized using 0.1% Triton X-100 (catalogue #T878) (Millipore Sigma) and 2 mM ammonium chloride in PBS. Cells were blocked with 3% Bovine Serum albumin (Millipore Sigma Catalogue # A4737) for 60 minutes. The primary antibody was added in PBS with 3% Bovine Serum albumin and incubated overnight at 4 °C, followed by incubation with the secondary antibody delivered in PBS at room temperature for 60 minutes. Antibodies and concentrations are listed in Table 4. Images were obtained using an Opera Phenix (Revvity, formerly PerkinElmer), an automated confocal microscope, or manually via the LSM800, a confocal microscope. A 63x oil immersion objective/1.4 NA was used. Images were captured using a sCMOS camera, the Photometrics Prime BSI (1966 x 1966).

Table 4: List of Antibodies used for Immunofluorescence

Antibody Name	Producer	Catalog #	Dilution
FLAG	Millipore Sigma	F1804	1:500
Rab5	Cell Signalling Technology	C8B1	1:200
Rab7	Cell Signalling Technology	D95F2	1:200
Rab11	Cell Signalling Technology	D45F	1:50
GALNT	Millipore Sigma	HPA009035	1:200
Lamp1	Cell Signalling Technology	D2D11	1:200
VPS35	Abcam	ab10099	1:50

2.14 Fluorescence Image Analysis

Co-localization was measured using CellProfiler. The precise pipeline can be found under the Colocalization pipeline present on the CellProfiler website.[224] At the end of the pipeline, fluorescence coefficients such as the Manders and Pearson coefficients were calculated.

2.15 Streptavidin purification of APEX biotinylated proteins

Biotinylated proteins in the supernatant were incubated with Dynabeads MyOne Streptavidin C1 (Invitrogen, cat. no. 65001, 65002) and washed according to the manufacturer's protocol.[223]

2.16 Mass Spectrometry Sample Preparation

Biotin-streptavidin pulldown samples were prepared for mass spectrometry analysis with an on-bead digestion method. Briefly, a magnetic stand was used to remove liquid from the beads. The beads were resuspended in 9 µL of 20 mM Tris-HCl (pH 8) with 1.6 µL of 25 mM DTT and then incubated at room temperature for 30 minutes. After adding 1.2 µL of 50mM iodoacetamide and incubating for 10 minutes, 10 µL of 100 ng/µL mass-spec grade trypsin was then added to achieve a final concentration of 45 ng/µL. The mixture was then incubated on the rotator at 37 °C overnight. The next day, the beads were removed using a magnetic stand, and an additional 500 ng of trypsin was added for 4 hours of incubation at 37 °C with gentle vortexing. Digestion was stopped with formic acid (F.A.) at a final concentration of 2%. For desalting, Sep-Pak tc18 1cc cartridges were conditioned in 900 µL of 100% acetonitrile (ACN) followed by 300 µL of 50% ACN and 0.5% acetic acid (HAcO). Cartridges were then equilibrated with 900 µL of 0.1% trifluoroacetic acid (TFA). Samples were adjusted to a final concentration of 0.4% TFA, passed through the cartridges, desalted with 900 µL of 0.1% TFA, and washed with 90 µL of 0.5% HAcO. They were then eluted with 500 µL of 50% ACN, 0.5% HAcO.

2.17 Mass Spectrometry Analysis

For LC-MS analysis, the Eksigent 2D+ nanoLC system (Dublin, CA) was hooked up with a Q-Exactive mass spectrometer (Thermo Electron, Waltham, MA), equipped with a nanoelectrospray interface operated in positive ion mode. The solvent system consists of buffer A of 0.1% F.A. in water and buffer B of 0.1% F.A. in 80% ACN. Dried-down protein digests were acidified with 0.5% (v/v) formic acid and loaded on a 75 µm I.D. × 150 mm fused silica analytical column packed in-house with 1.9µm ReproSil-Pur C18 beads (100 Å; Dr. Maisch

GmbH) at a flow rate of 500 nL/min for 15 min. The flow rate was then adjusted to 200 nL/min to perform the peptide separation using a 1-hour method with a gradient elution set at 5–35% buffer B over 45 minutes. The spray voltage was set to 2.0 kV, and the heated capillary temperature was 300 °C. The instrument method consisted of one full M.S. scan from 300 to 1800 m/z followed by a data-dependent MS/MS scan of the 12 most intense ions, a dynamic exclusion repeat count of 1 in 30, and an exclusion duration of 30. The full mass was scanned in an Orbitrap analyzer with R = 70,000 (defined at m/z 400) for MS1 and 17,500 for MS2. To improve the mass accuracy, all the measurements in the Orbitrap mass analyzer were performed with a real-time internal calibration by the lock mass of background ion 445.120025. The charge state rejection function was enabled, and charge states with unknown and single charge states were excluded for subsequent MS/MS analysis. All data were recorded using Xcalibur software (ThermoFisher Scientific).

2.18 Rhodamine 18 labelling of sEVs

Fluorescent labelling of sEVs for live imaging studies, sEVs were labelled with Octadecyl Rhodamine B Chloride (R18) (Thermofisher, catalogue no.0246). sEVs were incubated with 10 μg ml-1 R18 in a total volume of 1 mL 1× PBS at room temperature on a rotator for 30 min. sEVs were then centrifuged at 100,000g for 30 min (TLA-100.3 rotor) and resuspended in 100 μl of PBS (1×). Negative controls involved PBS (1x) treated with the same concentration of dye and centrifuged and resuspended identically to sEVs.[225]

2.19 siRNA Transfection

HEK293 cells were plated at 70% confluence. Subsequently, silencer siRNAs (ThermoFisher Scientific) against candidate proteins, or scrambled siRNA, were transfected into the cells using Lipofectamine RNAiMax transfection reagent (ThermoFisher, catalogue no. 13778150) according to the manufacturer's instructions to a final siRNA concentration of 10 nM. Table 5 contains silencer siRNA assay IDs used in experiments throughout this thesis. After 72 hours, cells were subjected to flow cytometry or RNA isolation.

Table 5: Silencer siRNAs used for delivery assays

Gene Name	Assay ID (ThermoFisher Scientific)
VPS35	s31374
VPS26A	137817
SNX27	131016
SNX9	134899
Negative Control	AM4635

2.20 Flow Cytometry of R18 Treated sEVs

Cells were seeded in a 96-well U-bottom dish and treated with siRNA as described in Section 2.18. sEVs incubated with R18 were placed onto cells for 10 mins, 30 mins, or 1 hour. After the incubation time, sEVs were aspirated from the well and washed 2x with PBS. Cells were fixed with 4% Paraformaldehyde (Catalogue #15714, Electron Microscopy Sciences) (PFA) for 20 minutes at room temperature. R18 was detected through the BD LSRFortessa - 16 - colour Analyzer 561 nm laser. Approximately 3000-10000 events were collected, and the gate was placed on R18-positive cells.

2.21 Transfection of pDEST-eGFP-C1-VPS35 plasmid

Cells were plated at 40% confluency with HEK293 cells one day before transfection. 1µg of pDEST-eGFP-C1-VPS35 (Addgene 163622) was combined with warm OptiMEM (Catalogue #31985, Thermo Fisher Scientific). 10 µl of enhanced polyethylenimine (ePEI) (catalogue #R01, University of Ottawa Biobar) was added to the mixture and mixed thoroughly, followed by quick centrifugation. The resulting mixture was incubated at room temperature for 30 minutes. HEK293 cells were then transfected with the pDEST-eGFP-C1-VPS35 plasmid. Cell media was replaced 5 hours post-transfection for cellular recovery. Cells were incubated for 48 hours and then proceeded with sEV treatment and imaging.

2.22 Live Cell Imaging

Cells were seeded on µ-Slide 8-well chambered polymer coverslips at 50% confluence per well and transfected with pDEST-eGFP-C1-VPS35 (Addgene 163622). After 48 hours, a live imaging chamber maintained at 5% CO2 and 37°C was used on a Quorum spinning disk confocal microscope (Leica DMI6000B inverted model). Once GFP-positive cells were localized, R18 sEVs were added to the cells at a concentration of 10000 particles per cell. Multiple cells in the field of view were selected for imaging, and phenol-free DMEM medium was added. GFP signals (490 nm laser) and mCherry signals (561 nm laser, with a Cy3 emission filter set at 605/52 nm) were used. A 63x oil immersion objective/1.4 NA was used. Images were captured using a sCMOS camera: Photometrics Prime 569 BSI (1966 x 1966).

2.23 RNA Extraction and cDNA Synthesis

Cell pellets were resuspended in 1 ml of cold TRIzolTM (Catalogue #15596026, Thermo Fisher Scientific) and lysed. TRIzolTM solution was incubated at room temperature for 5 minutes. 200 µL of chloroform (Catalogue #67-66-3, Millipore Sigma) was added to the TRIzol solution. The resulting mixture was shaken and incubated at room temperature for 2 minutes. The samples were then centrifuged for 15 minutes at 20,000 g at 4 °C. The aqueous phase of the mixture was removed, and 500µl 100% isopropanol (Catalogue #A416 Thermo Fisher Scientific) was added. To allow for RNA precipitation, the solution was incubated for 10 minutes at room temperature. Subsequently, the samples were centrifuged at 4˚C for 10 minutes at 20000g, yielding an RNA pellet. 1 ml of 75% ethanol (Commercial Alcohols) was added to the resulting pellet. The solution was centrifuged again at 4˚C for 5 minutes at 15000g. The RNA pellet was air-dried for 5 minutes, resuspended in RNase-free water, and then placed in a heat block at 55˚C for 10 minutes. Samples were stored at 4˚C. Complementary DNA (cDNA) was synthesized through the use of Maxima H. Minus First Strand cDNA Synthesis Kit (Catalogue #K1651, Thermo Fisher Scientific) as per instructions listed by the manufacturer.

2.24 RT-qPCR

qPCR reaction was performed by adding 1µg of cDNA to 5µM qPCR primer concentration (2.5 forward and reverse primers), and 5µl of 2x Green2Go Master mix (BioBasic, Catalogue #QPCR004-S) for a total of 10µl. The following protocol was then applied to the qPCR reaction: 10 minutes at 95˚C, followed by 40 cycles of 95˚C for 15 seconds and 60˚C for 60 seconds. Fluorescent intensity was captured after every cycle. Cycle threshold (Ct) values

were used to determine expression changes of the genes in question through the delta-delta CT method.

Table 6: RT-qPCR Primers

Primer Name	Sequence 5'-3'	Experimental use
HPRT-FWD	CCTGGCGTCGTGATTAGTGA	sEV cargo delivery assay Figure 11b
HPRT-REV	CGAGCAAGACGTTCAGTCCT	
GAPDH-FWD	TCGGAGTGAACGGATTTGGC	sEV cargo delivery assay Figure 11b
GAPDH-REV	TTCCCGTTCTCAGCCTTGAC	

2.25 Statistical analyses

GraphPad Prism was used to perform all statistical analyses shown in this study. When appropriate, a One- or Two-way ANOVA followed by a Tukey post-hoc analysis for multiple comparisons was performed. Figure captions will include the particular statistical test used and the sample size.

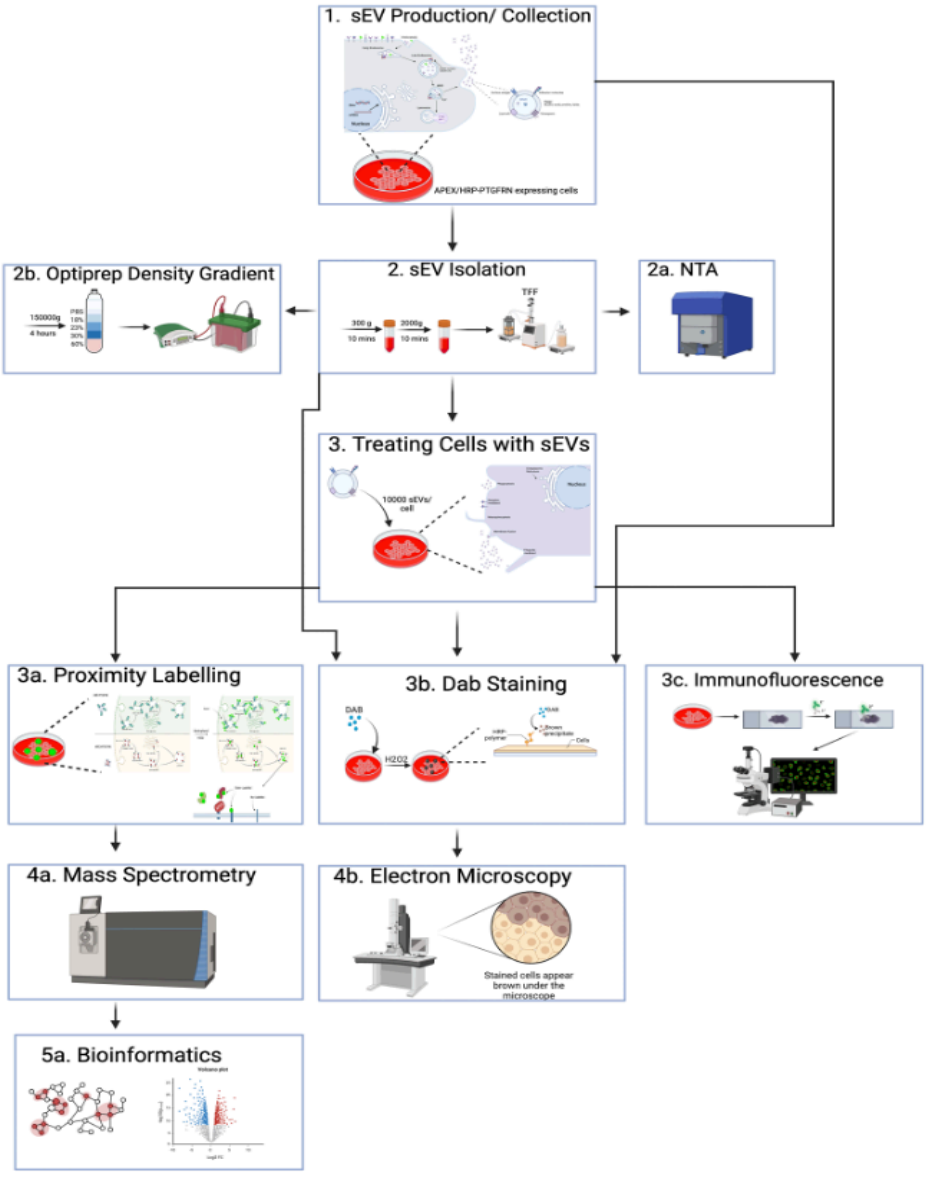

Figure 4. Experimental Flowthrough for sEV production, labelling, and analysis. 1. Cells expressing APEX or HRP-PTGFRN were cultured to generate sEVs in the media. **2.** sEVs were isolated from the media using TFF. **2a**. NTA was used to assess the size distribution and concentration of the isolated sEVs, and **2b**. Optiprep gradient and western blotting were used to co-localize markers with PTGFRN. **3**. sEVs isolated from TFF were used to treat cells at about 10000 sEVs per cell. **3a**. HRP or APEX2 on the sEVs will react with biotin phenol and H_2O_2 to label nearby proteins in the recipient cells. **4a.** MS identifies biotinylated proteins, and bioinformatics allows the identification of key pathways, protein interactions, and functional insights. **3b.** DAB staining allows for the formation of a brown precipitate at locations with HRP, which EM. 3c can visualize**.** Immunofluorescence enables the co-localization of sEVs with various protein markers, including endosomal markers. Image made with Biorender.

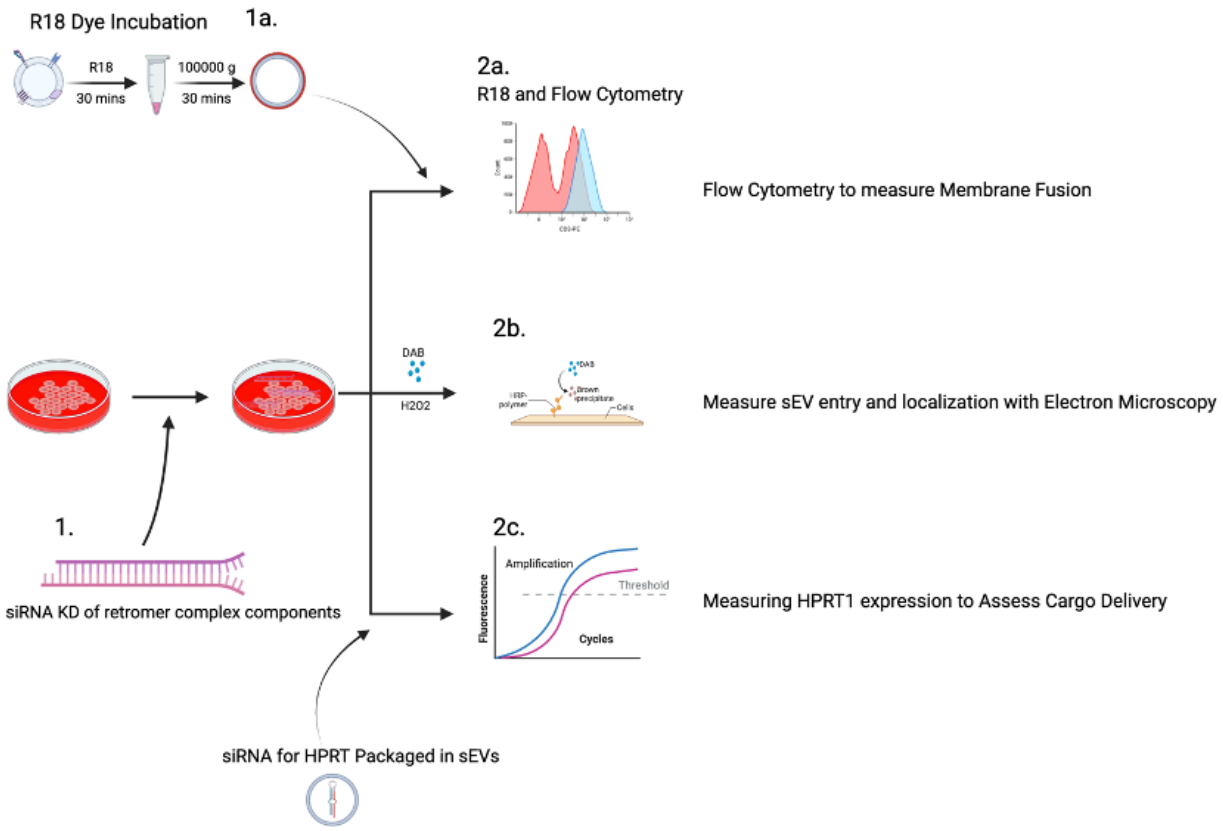

Figure 5. Downstream assays for assessing sEV membrane fusion and cargo delivery. 1a. HEK293 cells will be treated with siRNA for retromer complex components.**.** In tandem, sEVs will be incubated with the lipophilic dye R18. **2a.** Treatment with sEVs containing R18 lipophilic dye will occur on siRNA-treated cells, and flow cytometry is used to detect membrane fusion events via fluorescence dequenching. **2b.** siRNA-treated cells will be DAB-stained, generating a brown precipitate, which will enable EM visualization of sEV entry and localization within cells. **2c.** Treatment with sEVs derived from cells stably expressing siRNA for HPRT1 in a pre-miR451 backbone will occur on siRNA-treated cells. RNA will be isolated after treatment and converted into cDNA, in which the mRNA expression of HPRT1 will be assessed using qPCR. Image made with Biorender.

3. Results

3.1 Peroxidase Enzymes are Expressed on the Correct sEV Population and are Enzymatically Active

Reshke et al. demonstrated that the abundance of both the pre-miR-451 backbone and siRNA for GFP peaked in sEV-containing fractions at a density of 1.10-1.18 g/ml after a sucrose density gradient.[94] This data displays that siRNA is packaged in the pre-miR-451 backbone, which is selectively enriched in sEVs. Given that the isolated product from TFF is a heterogeneous population, we verified that the PTGFRN-peroxidase fusion protein co-partitions with the sEV population of interest, as the following experiments aim to track sEV endocytosis, not all EV endocytosis.

sEVs were isolated from HEK293 cells using media subjected to TFF. Subsequently, an optiprep density gradient was performed on the TFF product to separate the heterogeneous population of EVs into different density fractions. The densities of each fraction were acquired through refractometry. Each fraction was analyzed by Western blot and probed for various sEV markers (Syntenin-1, CD63, TSG101, and Alix) and APEX. The blot shows that APEX abundance peaked in sEV marker-containing fractions at a density of 1.10-1.18 g/ml (figure 6a), indicating that the peroxidase enzyme is preferentially localized to sEV populations.

To ensure that the APEX enzymes on our sEVs were enzymatically active, I performed DAB staining. The peroxidase enzyme catalyzes the reaction between DAB and H_2O_2, generating a black precipitate (an electron-dense DAB precipitate) at the site of the enzyme.[226] This black precipitate can be visualized by electron microscopy (figure 6b). Performing DAB staining on isolated sEVs containing the PTGFRN fusion protein with H_2O_2 showcases the black precipitate form on sEVs of approximately 100 nm in size, further reinforcing the fact that the

peroxidase enzyme is present on the correct sEV population. When comparing the formation of DAB precipitates in the $+H_2O_2$ condition to the negative control ($-H_2O_2$), a noticeable decrease in DAB formation is visualized. This showcases that the precipitate is generated due to the presence of the peroxidase enzyme. To corroborate that the size of sEVs is consistent with the electron microscopy calculation, I performed NTA (figure 6c). The analysis reveals that most particles containing DAB precipitate are approximately 100 nm in size, consistent with the findings from electron microscopy. Moreover, compared to the negative control ($-H_2O_2$), there is no difference in size and number of particles tracked when the peroxidase enzyme is added, indicating that expression of PTGFRN-peroxidase does not alter vesicle yield or size distribution (figure 6C).

To further validate that we are tracking the correct sEV population, I performed DAB staining on sEV-producing cells. This step is essential as it verifies the generation of MVBs containing our sEVs. Since MVBs are a crucial component in the sEV biogenesis process, forming MVBs containing our DAB precipitate will give us further confidence that we are tracking an sEV population. When performing DAB staining on sEV-producing HEK293 cells, a black precipitate is present in the MVBs, suggesting an enzymatically active peroxidase on the sEVs is prepared for exocytosis (figure 6D), which is consistent with correct sorting of PTGFRN-tagged sEVs before secretion. Together, these data verify that the PTGFRN–peroxidase fusion protein is (i) restricted to canonical sEV fractions, (ii) catalytically competent on the vesicle surface, and (iii) does not perturb vesicle biogenesis, thereby providing a validated tool for the subsequent tracking of sEV uptake and intracellular trafficking.

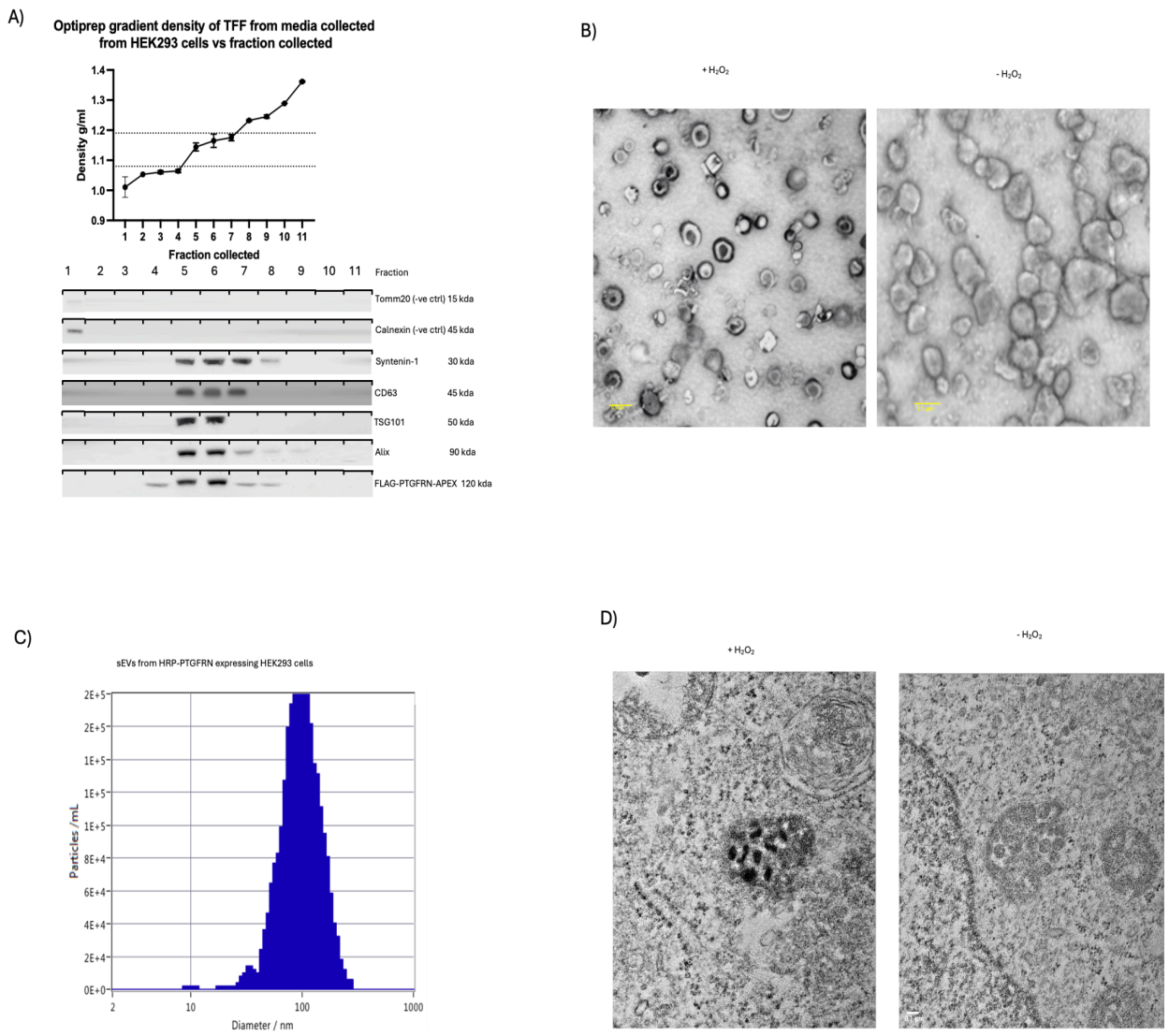

Figure 6: Peroxidase enzymes are conjugated to vesicles of approximately 100 nm and are enzymatically active in HEK293 cells. (A) Western blotting of TFF product after Optiprep density gradient. sEV markers Cd63, Syntenin-1, Alix, and Tsg101 were probed for, as well as APEX-PTGFRN, which is conjugated to our scaffold protein PTGFRN. **(B)** Electron microscopy images of the TFF product after DAB staining with H_2O_2 and without H_2O_2. Vesicles were imaged at 50000x magnification at a voltage of 100KeV. Scale bars of 100nm were added to the bottom left corner using ImageJ. **C)** Nanoparticle tracking analysis of sEVs containing the HRP-PTGFRN construct. Representative plot of particle number (y-axis) versus diameter in nm (x-axis) of sEV preparations from HEK293 cells. **D)** Electron microscopy images of cells producing sEVs with APEX-PTGFRN tag on them, with H_2O_2 and without H_2O_2. Images were taken at 25000x magnification at a voltage of 100KeV.

3.1.1. sEVs enter and deliver their cargo through fusion events with the target cells

For siRNAs from sEVs to elicit effects in the target cell, the siRNAs must enter the cytoplasm and associate with the RISC.[227] As discussed, this can occur through the endosomal escape of the siRNA or the fusion of sEVs with the cell membrane, releasing their contents into the cell's cytoplasm.[227] Using powerful imaging techniques such as electron microscopy in conjugation with DAB staining will allow the visualization of ultrastructural details of cells and vesicles that our sEVs are interacting with or in proximity to, ultimately providing direct evidence of the mechanisms by which sEVs interact with cellular membranes and organelles and insight into how content is delivered from sEVs.

DAB staining of HEK293 treated with sEVs containing the PTGFRN-HRP fusion protein reveals DAB precipitation on the plasma membrane, within endosomes and endosomal membranes. Localizing the DAB precipitate at these sites may suggest potential entry mechanisms such as fusion and endocytosis. DAB precipitates are continuously found on the plasma membrane and are fully integrated with it. This observation may indicate a completed fusion event, as the vesicle membrane has now become a part of the plasma membrane (figure 7A). Moreover, dab-stained vesicles can also be found inside endosomes, suggesting internalization through a conventional endocytosis pathway (figure 7A,7C). Lastly, the same integrated membrane patches on the plasma membrane can also be located on endosomal membranes (figure 7A). This integration can also signify a fusion event, however, one that occurs from the endosomal lumen to the cytoplasm, still maintaining the ability to impart change by associating with the RISC.

Furthermore, vesicles containing the DAB precipitate can also be seen abutting the plasma membrane in a configuration resembling a widening fusion pore (figure 7b). This fusion

event is crucial as it enables sEVs to deliver their cargo, including siRNAs, into the cytoplasm, where they can associate with the RISC and exert their silencing capabilities. Moreover, the initial approach of the vesicle to the plasma membrane can be observed in the bottom image of figure 7b, where a DAB-stained vesicle is positioned near the membrane, resulting in a slight indentation of the membrane directly in front of the vesicle. These images corroborate that sEVs may enter through a fusion event to elicit their silencing capabilities by delivering siRNAs into the cytoplasm.

Electron micrographs further reveal that sEVs may prefer particular locales on the plasma membrane more than others. Images showcase that sEVs can associate with membrane protrusions that extend tens of micrometres from the cell surface (figure 7C-E). Although the identity of the structures has not been objectively confirmed, the general morphology of the extensions and the fact that the cells being imaged are HEK293 cells suggest that they may be filopodia searching for sEVs.[157] The association with the length of the filaments may suggest that sEVs are undergoing "surfing" on the filopodia to reach the cell body and potentially locate particular plasma membrane locales that are superior for internalization. This preference could have significant implications for the targeted delivery of sEVs and their cargo, potentially enhancing their efficiency in gene regulation.

Quantification of dab staining on both plasma membrane and cytoplasm reveals that dab precipitates are significantly more abundant in sEV and H_2O_2-treated samples compared to H_2O_2-only or sEV-only treated samples. This indicates that the visible dab precipitate is derived from the reaction between H_2O_2 and the peroxidase enzyme, rather than a background effect (Figure 7H).

To corroborate electron microscopy findings suggesting fusion, sEVs were incubated with R18, a lipophilic self-quenching dye, and then placed onto HEK293 cells. Discrete, transient bursts of red fluorescence, indicative of dye de-quenching upon dilution into the plasma membrane, were observed on one sector of the cell surface and within the cortical cytoplasm (figure 7I). These bursts coincide spatially with the membrane regions that accumulate DAB puncta.

Taken together, DAB electron microscopy and R18 fluorescence de-quenching support a model in which PTGFRN-bearing sEVs deliver their cargo through a combination of direct fusion at preferred plasma-membrane microdomains and classical endocytic uptake. Quantitative dissection of the relative contributions of these pathways will be addressed in subsequent experiments.

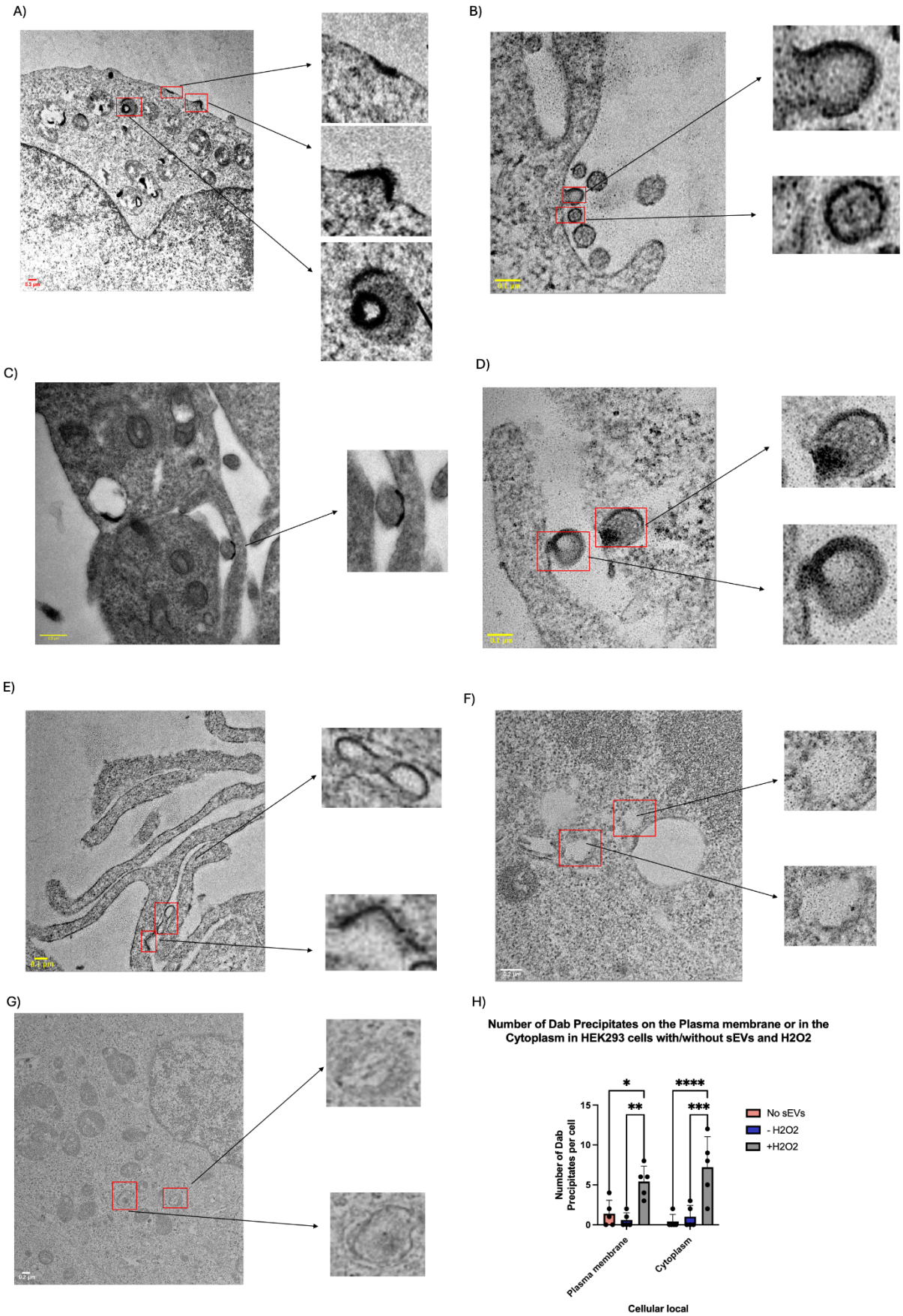
A)
B)
C)
D)
E)
F)
G)
H)
Number of Dab Precipitates on the Plasma membrane or in the Cytoplasm in HEK293 cells with/without sEVs and H2O2
Number of Dab Precipitates per cell
15
10
5
0
*
**
****
***
No sEVs
- H2O2
+H2O2
Plasma membrane
Cytoplasm
Cellular local

I)

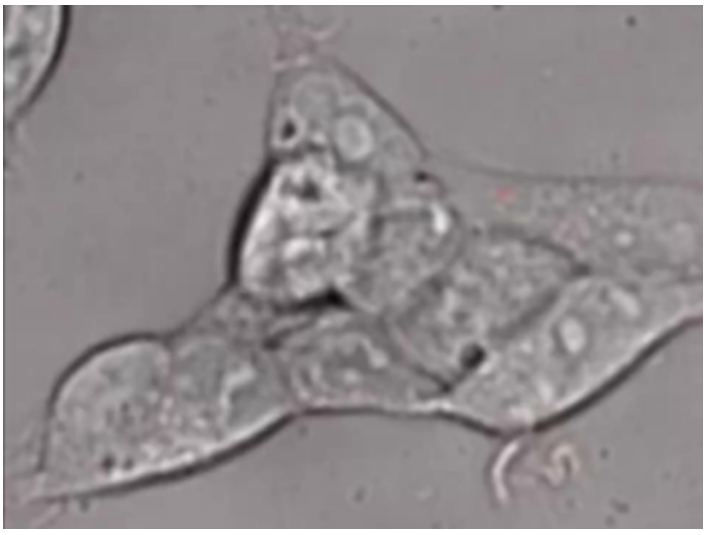

Figure 7: sEVs fuse with the cell membrane to deliver their cargo. (A-G) Electron Microscopy images of HEK293 cells treated with HRP-PTGFRN sEVs for 30 mins after DAB staining with H2O2 (A-E), without H_2O_2, and DAB stain (F,G). Cells were imaged at 3000-20000x magnification at a voltage of 100KeV. Scale bars of 200nm were added to the bottom right corner using ImageJ, including images of fusion at different stages and endosomes (with sEVs fused or with sEVs intact inside). H) Quantification of the number of vesicles with dab precipitate on the endosome or plasma membrane for each condition. Quantifying DAB precipitates was accomplished by counting vesicles with DAB precipitate inside the cytoplasm and on the plasma membrane. Five images per condition were assessed. I) HEK293 cells were treated and imaged for 5 minutes, and sEVs were incubated with R18 dye. 7I is a video that can be found conjugated to this thesis; the current image placed in 7I's position is a picture of the aforementioned video. Images were captured using the LSM880 microscope at 64x magnification with the brightfield light setting and a 564 nm wavelength.

3.2 Proximity labelling of sEVs to delineate intracellular trafficking

The increasing evidence suggesting fusion as a means to deliver sEV cargo raises the question of how the fusion event occurs. As described, fusion proteins are typically recruited to decrease the free energy of the fusion event.[183,185] To elucidate the proteins that may be facilitating membrane fusion, I employed proximity labelling in combination with the PTGFRN-APEX system to determine proteins that sEVs interact with as they are trafficked through the endocytic pathway to narrow down organelles, membrane domains, and endosomal compartments that sEVs interact with (figure 8A). HEK293 cells cultured in SILAC media were treated with sEVs containing APEX-PTGFRN fusion protein (approximately 10000 per cell) for different durations and labelled with BP for 30 minutes +/- H_2O_2 for 1 minute (figure 8A). SILAC media contains regular and heavy isotope amino acids, which, when used to culture cells, metabolically label the proteins. This enables proteins from the recipient cells to be distinguished through MS.

3.2.1 Validation of the Proximity Labelling Workflow

Streptavidin pull-down of cell lysates and subsequent HRP-streptavidin blotting confirmed robust biotinylation only in samples that received both sEVs and H_2O_2 (figure 8C). As treatment time increases, the complexity and intensity of labelled bands increase, consistent with vesicles traversing sequential endocytic compartments and sampling distinct proteomes. This observation validates the experimental theory, providing reassurance about the reliability of our research.

Confocal microscopy of the biotinylated proteins was also performed to corroborate trafficking dynamics identified in the western blotting data. This experiment aims to validate that

the biotinylation reaction colocalizes to various compartments in the endocytic pathway, or organelles, which will aid in deciphering the pathway of sEV cargo trafficking (figure 8B). Figure 8b and 8d demonstrate that sEVs colocalize more with early endocytic markers, such as Rab5, at the 10-minute time point. However, as the incubation time increases to 1 hour, colocalization with various endocytic markers and organelles can be observed. Rab7 (late endosome),[228] Rab11 (recycling endosome),[228] and Lamp1 (lysosome)[228] have increased colocalization at the 1-hour time point compared to Rab5. Together, these data demonstrate that the APEX–PTGFRN construct faithfully reports the changing micro-environment of internalized sEVs and enables subsequent proteomic identification of candidate fusion and trafficking mediators.

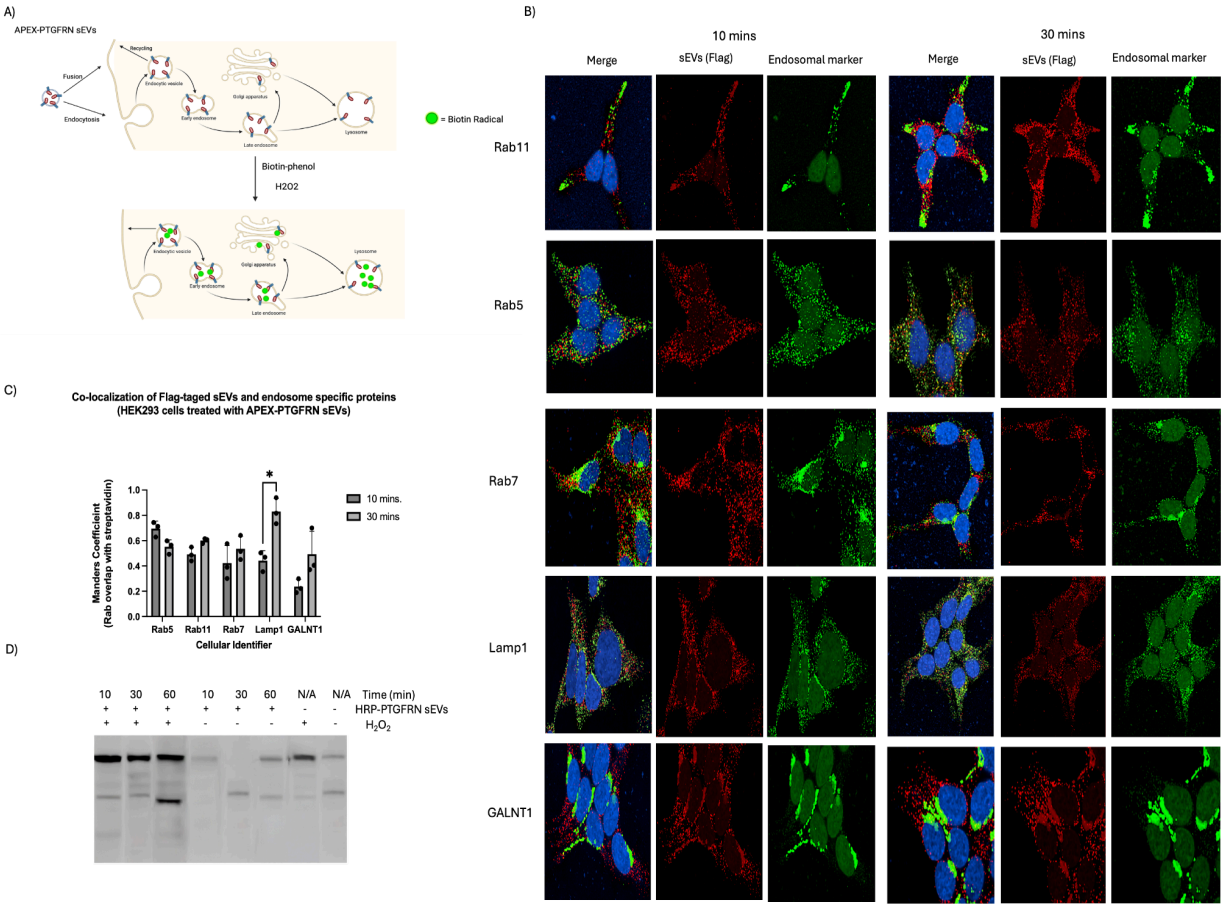

Figure 8: Biotinylated Proteins Localize with Endosomal Markers and intracellular trafficking complexes in vitro. A) Schematic representation of proximity labelling of sEVs using APEX-PTGFRN expressing sEVs. **B)** Confocal microscopy images displaying co-localization between FLAG (green) and Rab5, Rab11, Rab7, Lamp1, and GALNT1 (Red). Images are taken at 63x magnification. Bar graph displaying the Manders co-localization coefficient between FLAG and various endosomal markers during 10- or 30-minute sEV incubation. **C)** Quantification of images. Three images per endosomal marker and time point were quantified using a pipeline in CellProfiler to identify co-localization. Data is presented as mean +/- SEM of 3 biological replicates. Statistical analysis was performed by two-way ANOVA. **D)** Western blotting of proteins derived from HEK293 cells after treatment with sEVs with PTGFRN-HRP fusion protein for 0 min, 30 min, and 1 hour. After incubation with sEV, biotin was added for 30 minutes, and H2O2 was either added (+) or not added (-) after the 30-minute incubation. Proteins were pulled down with streptavidin beads, eluted in a biotin-containing buffer, and blotted on a 10% SDS-PAGE gel.

3.2.2 Proximity Labelling Reveals Important Complexes Involved in the Process of sEV Internalization

Biotinylated proteins were subjected to MS to identify proteins surrounding our sEV cargo. Proteins derived from the MS were first triaged by excluding any proteins that showed a log_2fold change that was not statistically significant compared to the -H_2O_2 negative control, as these would be considered background. Moreover, proteins that did not contain any heavy labelling would also be excluded, as they would be derived from sEVs and would not be informative about the cell's workings. The final protein list was then subjected to Gene Ontology Term (GOTERM) analysis to identify cellular components, molecular functions, and biological processes associated with each time point.[229]

The GOTERM analysis unveils distinct endosomal compartments and processes that may play a significant role in sEV fusion and cargo delivery (figure 9a). Each time point showcases associations with endosomal compartments; for example, at 10 minutes, we see early endosomes, cellular projections, and lysosomes; at 30 minutes, we see late endosomes and lytic vesicles; and at 1 hour, we see more late endosomes and recycling endosomes. These datasets provide us with confidence in our experimental method, which has been meticulously designed and executed, as they demonstrate that we are tracking a clear progression of intracellular vesicles that has been well-defined in the literature.

This proteomic analysis also gives insight into particular mechanisms that may be involved in the intracellular trafficking of sEVs. Actin-related categories, including “ARP2/3 complex” and “actin filament bundle”, scored highly, suggesting a role for cortical actin remodelling in sEV entry or trafficking. Moreover, the retromer complex was found to have an

enriched role in the GOTERM analysis, suggesting that the interaction between the two complexes may have a role in the trafficking of sEV-specific cargo.

To prioritize individual effectors, I calculated the $\log_2$fold change of all proteins in the heavy condition compared to the light condition at each time point. I calculated the p-value of all proteins from the $+H_2O_2$ condition compared to the $-H_2O_2$ condition (figure 9B). Using this data, I generated volcano plots displaying proteins taken from the cell (heavy) and proteins significantly enriched compared to the $-H_2O_2$ condition. Among these proteins, multiple components of the retromer network exceed the significance threshold: the core subunit VPS35 and cargo-selective VPS26A, together with sorting nexins SNX9, SNX27, SNX3, SNX5, and SNX12, which link retromer to the actin or tubulation machinery. These proteins were absent or below threshold in $-H_2O_2$ controls, confirming that their detection depends on APEX-mediated proximity labelling. Conversely, proteins such as ANXA1, VAMP8, VPS28, and FCRL3 are found in the light-labelled (enriched in sEVs) fraction and have been validated in proteomic datasets from sEVs, demonstrating the sensitivity of the workflow. Collectively, the enrichment of retromer subunits, actin nucleation factors, and membrane-remodelling SNX adaptors points to a model in which incoming sEVs intersect the retromer pathway, possibly to recycle entry receptors or facilitate back-fusion of intraluminal vesicles. These findings nominate the retromer complex as a high-confidence candidate for regulating cytosolic delivery of sEV cargo, providing a mechanistic foothold for targeted functional experiments.

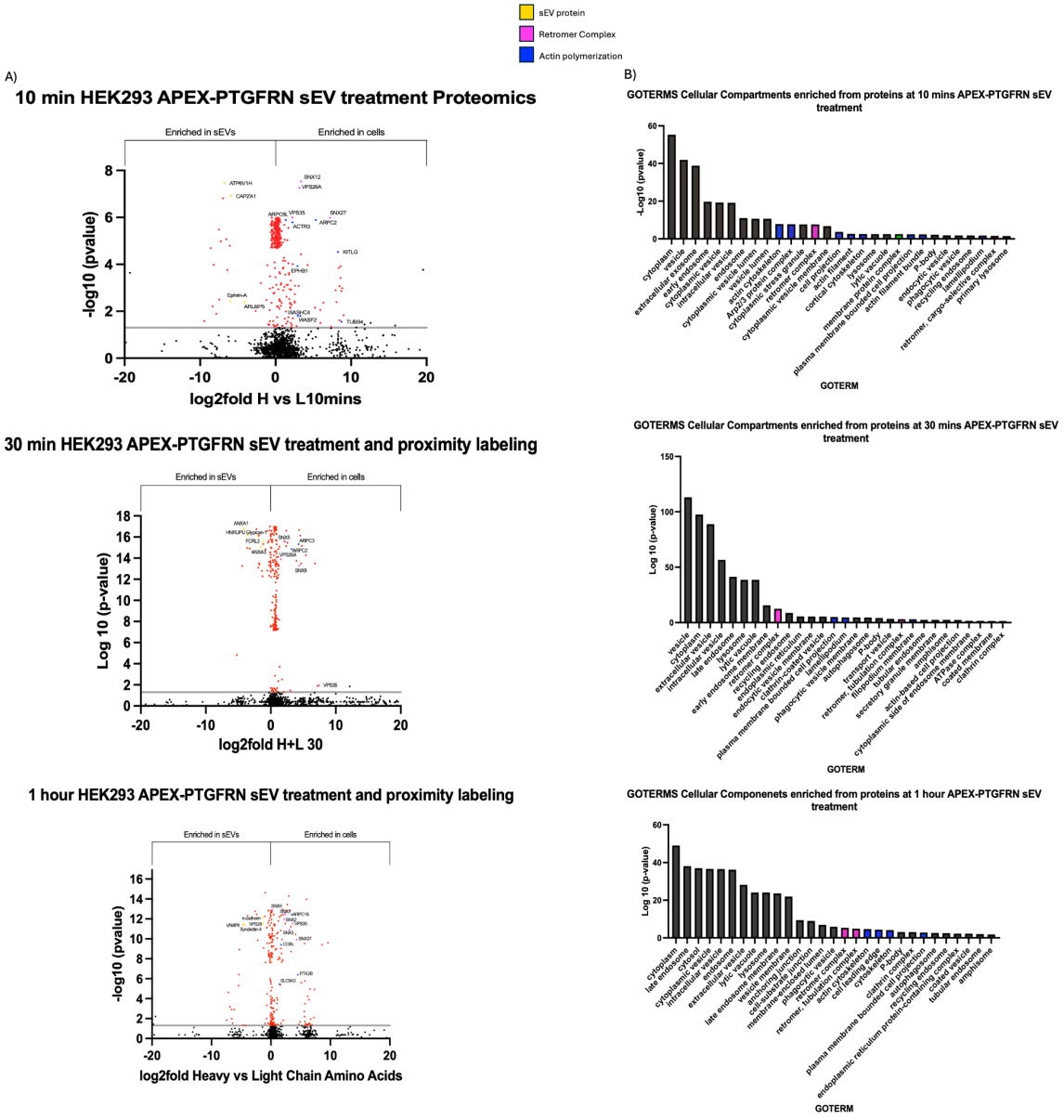

Figure 9: Proteomic Analysis of biotinylated proteins reveal complexes and interactions that might facilitate the sEV internalization. Biotinylated proteins were pulled down and subjected to MS to identify the protein species involved with sEVs as they entered the cell. **A)** Volcano plots of proteins derived from cells treated with APEX-PTGFRN sEVs from Hek293 cells for 10 mins, 30 mins, or 1 hour. Log_2Fold change of Heavy to Light expression was calculated (y-axis), and the p-value of + vs – H_2O_2 was calculated and graphed (x-axis). **B)** Proteins in the negative control (no H_2O_2) and proteins not containing heavy labelling were excluded, and all remaining proteins pulled down were subjected to GOTERM analysis. Graphs of GOTERMS display the $–Log_{10}$ of the p-values for each GOTERM at each time point. The legend is present at the top of the figure, showcasing that the coloured dots in the volcano plot represent a protein from an essential complex identified in GOTERM.

3.2.3 Network Analysis Identifies Putative sEV Interactors with Actin-Polymerization and Retromer Machinery

Although identifying complexes through GOTERM helps decipher more about the mechanism of fusion between sEV and the plasma membrane, analyzing the cellular and sEV proteins identified in the proximity labelling experiment might give insight into how the free energy barrier is lowered. To map physical links between vesicle-borne proteins and host factors, I submitted the union of significantly biotinylated sEV-derived (light-labelled) and cell-derived (heavy-labelled) proteins to the STRING v11.5 database, restricting edges to high-confidence scores (>0.7) and visualizing clusters using Markov clustering (inflation = 2).[229,230] The resulting network (figure 10) is segregated into 17 functional modules, several of which corroborate the GOTERM analysis. Notably, an actin-polymerization cluster containing the ARP2/3 core (ACTR2/3, ARPC1B, ARPC2) connected to multiple vesicle proteins, including ANXA1, CAPZA2, HNRNPU, MYH10, TAOK1, VAT1 and VAMP8 (red-circled nodes), suggesting that incoming sEVs encounter or possibly recruit actin-remodelling factors at the cortex. A second prominent module corresponded to the retromer pathway, anchored by VPS35, VPS26A and SNX27, and linked to sEV-associated VAMP8, IGF1R and GGA1. The presence of both core components and cargo-selective sorting nexins supports our MS-based inference that retromer participates in post-entry sorting of sEV membranes. Annexin1, identified on sEVs, has been found in a complex of other annexins found in the cellular dataset, potentially playing a role in strengthening the binding between sEVs and the membrane through phospholipid binding.

Overall, STRING network topology reinforces two mechanistic themes: (i) actin dynamics, potentially driven by ARP2/3 and its adaptors, and (ii) retromer-mediated membrane recycling, both of which may lower energetic barriers to fusion or facilitate endosomal escape of

sEV cargo. These interactomes provide a focused candidate list for forthcoming loss-of-function studies aimed at dissecting the molecular determinants of efficient siRNA delivery.

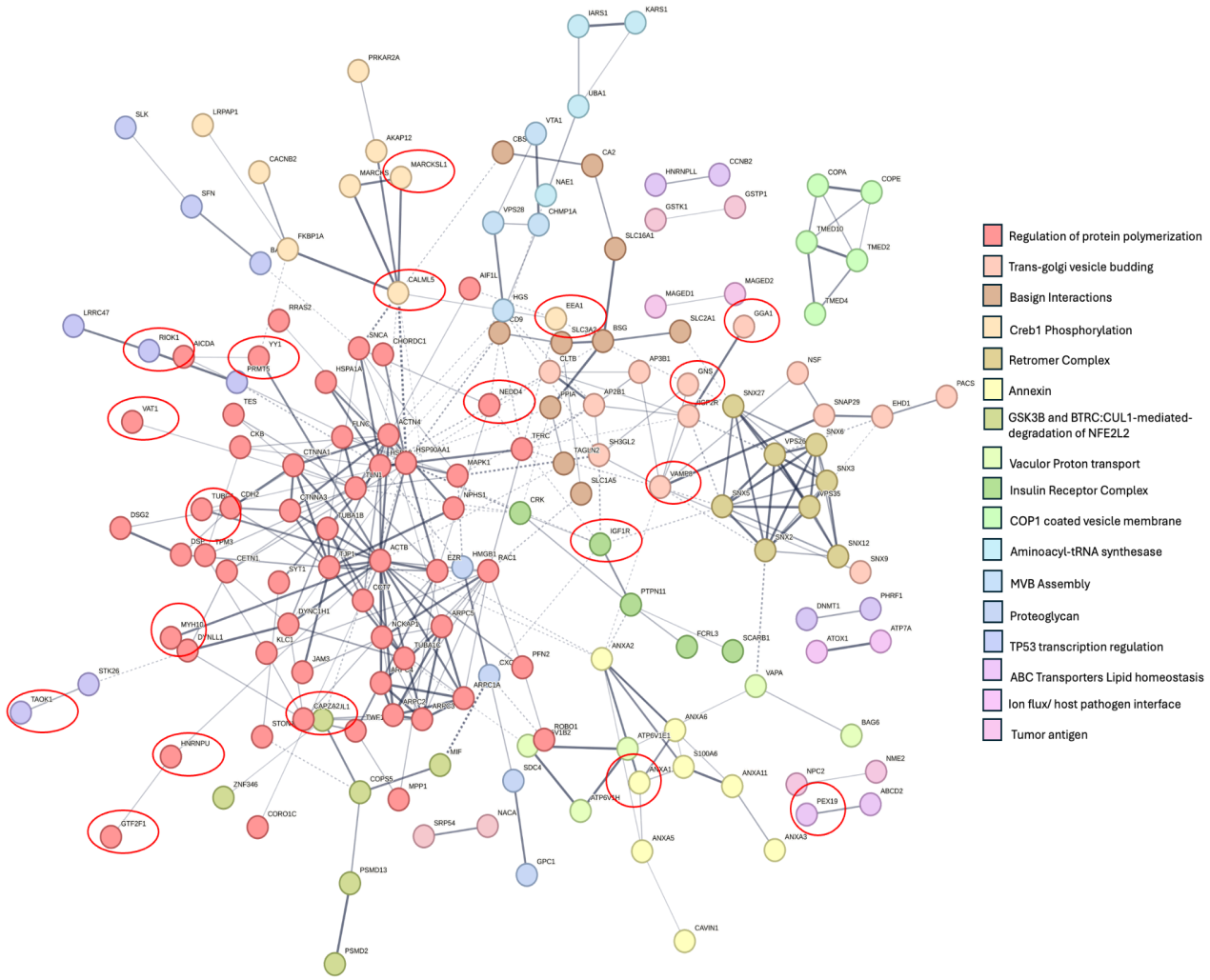

Figure 10. String proteomic analysis reveals physical connections between sEVs and the plasma membrane. To decipher the connections between sEV proteins and cellular proteins, proteins derived from both cells and sEVs, which were significantly enriched in the biotinylated samples, were subjected to string proteomic analysis, identifying physical links between proteins. I also applied Markov clustering analysis with an inflation parameter of 2, which provided 17 enrichment categories based on colour. Circled proteins are proteins derived from sEVs and allow the visualization of connections between sEVs and various complexes identified in the cell.

.

3.3 The Retromer complex is an essential component in trafficking sEV-related cargo

Proteomic and network analyses (Sections 3.2.2–3.2.3) highlighted the core retromer scaffold (VPS35–VPS29–VPS26A) and its SNX27 adaptor as recurrent interactors of internalized sEVs. Validation of the retromer complex's role in the endocytic processing of sEV cargo, specifically the trafficking of packaged siRNA in sEVs, is a natural next step to assess its role in sEV cargo delivery.

3.3.1 RT-qPCR to assess delivery of siRNA packaged into sEVs after Retromer complex knockdown

Retromer complex compartments (VPS35, VPS26, SNX9, SNX27) were silenced using siRNA, and inhibited HEK293 cells were treated with sEVs isolated from cells stably expressing siHPRT using the miR-451 backbone. RNA was isolated from these cells and subjected to qPCR analysis of HPRT expression (figure 11b). HPRT expression was significantly increased when VPS35, VPS26, and SNX27 were silenced compared to the scrambled treatment, indicating that siHPRT was not delivered. This suggests that the retromer complex is involved in the trafficking of sEV cargo. These findings underscore the necessity of retromer components for the effective intracellular delivery of sEV-packaged siRNAs, highlighting their critical role in facilitating gene silencing.

3.3.2 Flow Cytometry of R18 dye incubated sEVs in HEK293 cells

To distinguish whether retromer acts at the point of fusion or a later trafficking step, we quantified sEV membrane fusion using self-quenching R18 dye. Retromer complex compartments (VPS35, VPS26, SNX9, SNX27) were silenced using siRNA, and HEK293 cells

were treated with sEVs incubated with R18 lipophilic dye (figure 11a). Cells were treated for 10 minutes, 30 mins, or 1 hour, fixed, and the presence of R18 dye was assessed through flow cytometry at a wavelength of 541 nm of light. It is shown that at the 10 min and 30 min time points, the presence of R18 was lower in VPS26, SNX27 and VPS35 conditions compared to the scrambled control (figure 11a). However, SNX9 did not display this decrease in fluorescence. Moreover, at the 1-hour time point, there is no apparent difference between the scrambled and treated conditions. This suggests that retromer primarily facilitates an early fusion or post-fusion disassembly step. SNX9 knockdown, which does not target core retromer, showed no effect on R18 de-quenching, consistent with the proteomic data and sEV cargo delivery data.

3.3.3 Fluorescent imaging of R18 dye incubated sEVs in HEK293 cells

Understanding the behaviours of the retromer complex as sEVs enter the cell may give us insight into the role this complex plays in sEV entry. HEK293 cells transfected with VPS35-GFP and treated with sEVs incubated with R18 lipophilic dye showed sEV fusion over time and VPS35 co-localization with sEV fusion events (figure 11C). Co-localization events occur both at the membrane and within the cell, implicating the retromer complex in internalization at the plasma membrane and continued association as sEVs are endocytosed. This spatial coupling supports a model in which retromer is recruited to sEV fusion sites and remains associated during early endosomal maturation.

Furthermore, HEK293 cells were transfected with VPS35-GFP (figure 11D, E) and treated with APEX-PTGFRN-FLAG sEVs for 10 mins. They were then fixed and stained for FLAG to identify if the treatment of sEVs affects the localization of the retromer complex in the cell and to corroborate data suggesting that the retromer complex is associated with sEV entry.

VPS35-GFP images showcase a large number of sEVs and retromer present on the outer membranes and extensions of the cells themself when compared to the negative controls, with some presence found internally. These imaging results provide direct visual evidence that retromer components, such as VPS35, actively co-localize with sEVs during their entry, underscoring the pivotal involvement of the retromer complex in sEV trafficking.

3.3.4 Electron microscopy of retromer-inhibited cells reveals unique morphological characteristics

When electron microscopy was performed on HEK293 cells treated with siRNA for SNX27 and VPS35, treated with sEVs containing HRP-PTGFRN, and DAB stained, DAB staining patterns were significantly different compared to Scrambled siRNA-treated samples (figure 11F). In SNX27 siRNA-treated samples, little to no dab precipitate was found inside the cell. However, more DAB was found on the plasma membrane in either the form of an intact vesicle or associated with the plasma membrane itself (figure 11F, G). Moreover, in VPS35-siRNA-inhibited samples, DAB staining is incredibly diffuse in the cytoplasm, as opposed to being on top of or adjacent to endosomes and fusing with the plasma membrane itself, as seen in the scrambled control (Figure 11F, G). Electron microscopy of HEK293 cells with retromer complex components inhibited revealed that the ability of sEVs to interact with cell membranes and potentially deliver their cargo successfully is decreased in the absence of the retromer complex. Therefore, the altered morphological patterns resulting from retromer inhibition highlight the essential role of retromer in coordinating both the initial membrane fusion steps and the subsequent intracellular processing of sEVs.

Taken together, loss-of-function assays, fusion kinetics, live imaging, and EM converge on the conclusion that the retromer core and its SNX27 adaptor are essential for productive sEV fusion and/or rapid post-fusion uncoating, thereby enabling timely release of siRNA cargo to the RISC pathway. These findings position retromer as a critical node in the molecular machinery that underpins sEV-mediated gene silencing.

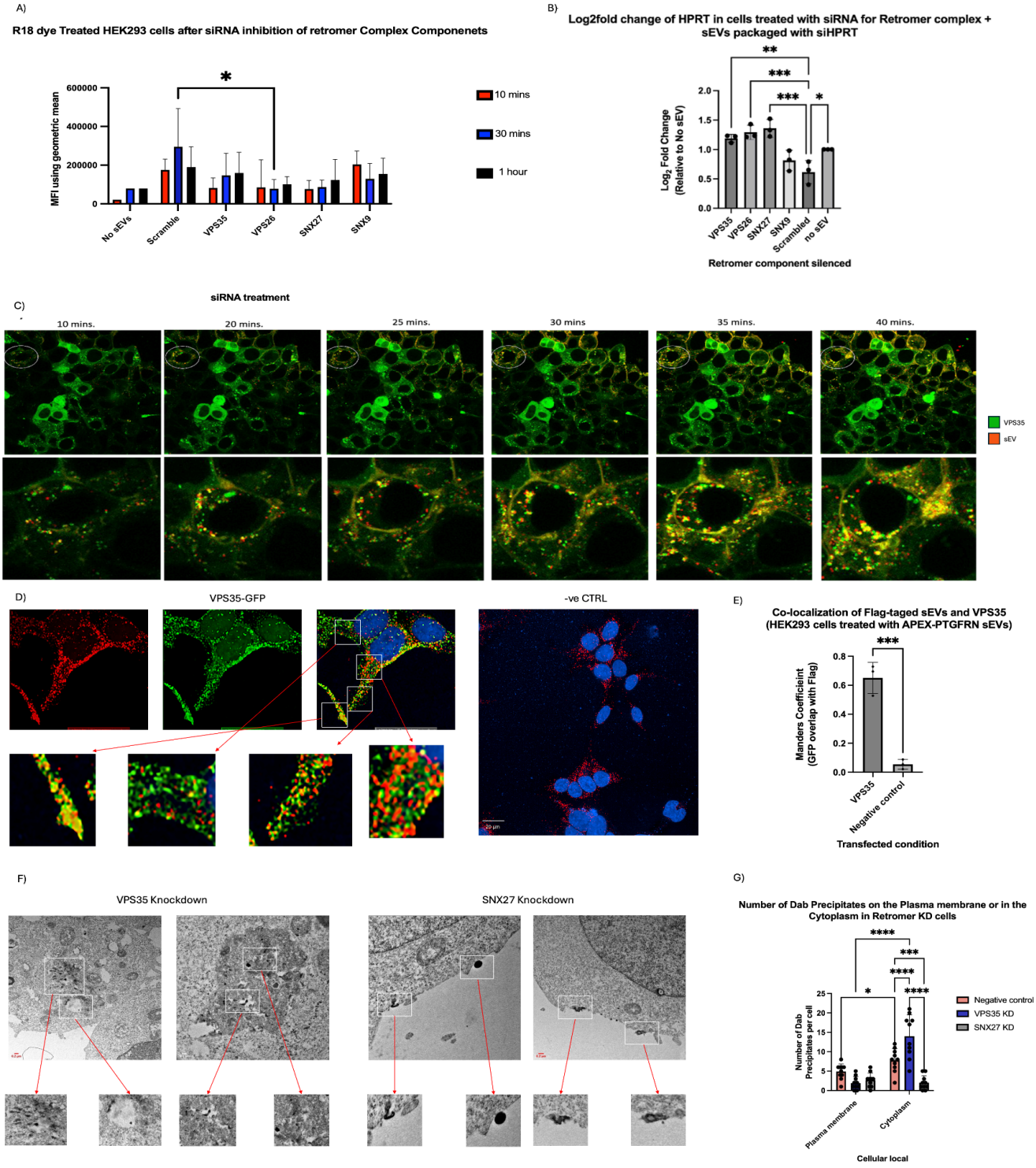
A)
R18 dye Treated HEK293 cells after siRNA inhibition of retromer Complex Componenets
MFI using geometric mean
600000
400000
200000
0
*
No sEVs
Scramble
VPS35
VPS26
SNX27
SNX9
10 mins
30 mins
1 hour
B)
Log2fold change of HPRT in cells treated with siRNA for Retromer complex + sEVs packaged with siHPRT
Log2 Fold Change (Relative to No sEV)
2.0
1.5
1.0
0.5
0.0
**
***
***
*
VPS35
VPS26
SNX27
SNX9
Scrambled
no sEV
Retromer component silenced
C)
siRNA treatment
10 mins.
20 mins.
25 mins.
30 mins
35 mins.
40 mins.
VPS35
sEV
D)
VPS35-GFP
-ve CTRL
E)
Co-localization of Flag-taged sEVs and VPS35 (HEK293 cells treated with APEX-PTGFRN sEVs)
Manders Coefficieint (GFP overlap with Flag)
0.8
0.6
0.4
0.2
0.0
***
VPS35
Negative control
Transfected condition
F)
VPS35 Knockdown
SNX27 Knockdown
G)
Number of Dab Precipitates on the Plasma membrane or in the Cytoplasm in Retromer KD cells
Number of Dab Precipitates per cell
25
20
15
10
5
0
****
***
****
*
****
Plasma membrane
Cytoplasm
Cellular local
Negative control
VPS35 KD
SNX27 KD

Figure 11: The retromer complex plays a role in sEV cargo delivery and fusion. A) Measurement of 514 nm light of cells treated with siRNA for VPS35, VPS26, SNX27, SNX9 and Scrambled, as well as R18 dye for 10 mins, 30 mins, and 1 hr. **B)** Quantified mRNA expression of HPRT in HEK293 cells treated with siRNA for VPS35, VPS26, SNX27, SNX9 and Scrambled, and sEVs packaged with siRNA for HPRT. Quantification relative to the Scrambled control. mRNA levels were normalized to Gapdh. Data is presented as mean +/- SEM of 3 biological replicates. **C)** Confocal microscopy images of HEK293 cells transfected with the VPS35-GFP plasmid. Subsequently, they were treated with sEVs that had been incubated with R18 dye for 1 hour, with images taken sporadically during the incubation period. Images were taken at 63x magnification. **D)** Confocal microscopy images of HEK293 cells transfected with VPS35-GFP plasmid and subsequently treated with sEVs containing HRP-PTGFRN-Flag for 10 minutes. Images were taken at 63x magnification. **(E)** Three images per time point were quantified using a pipeline in CellProfiler to identify co-localization. Data is presented as mean +/- SEM of 3 biological replicates. Statistical analysis was performed by one-way ANOVA. **F)** Electron microscopy images of HEK293 cells treated with siRNA for VPS35 or SNX27 and treated with HRP-PTGFRN sEVs for 30 mins, and DAB stained in the presence of H_2O_2 and without H_2O_2, and with and without DAB stain. Cells were imaged at 3000-20000x magnification at a voltage of 100 keV. ImageJ added scale bars of 200nm to the bottom right corner**. G)** Quantification of the number of DAB precipitates present on membranes and endosomes. Measurements of DAB were performed by counting the continuous DAB precipitates in ImageJ.

4. Discussion

The findings presented in this thesis identify a critical mechanism underpinning the internalization and cytoplasmic delivery of sEV cargo, with the retromer complex playing a central and previously unappreciated role. We have demonstrated that sEVs, which have long shown promise as natural, biocompatible delivery vehicles for therapeutic RNAs, enter cells through endocytic pathways and via a direct fusion event at the plasma membrane. This fusion, supported by our electron microscopy and mass spectrometry analyses, suggests a coordinated recruitment of fusion machinery that includes the retromer complex. By leveraging this mechanism, sEVs can efficiently bypass many intracellular trafficking barriers that plague other RNA delivery systems, achieving an unparalleled level of cytoplasmic RNA release. Recognizing and characterizing the importance of the retromer complex in sEV internalization not only enhances our foundational understanding of sEV biology but also opens avenues for manipulating this pathway to improve the therapeutic potential of sEV-based drug delivery, particularly for neurological diseases where the ability to cross the blood-brain barrier is crucial. Throughout this discussion, I will explain a theoretical mechanism of fusion that utilizes the retromer complex and other complexes identified in my proteomics dataset to facilitate sEV fusion.

4.1 Heterogeneous sEV Populations Affect PTGRN-APEX Enrichment in the Density Gradient

TFF is a size-based method that utilizes media-containing EVs through a membrane with a specific molecular weight cutoff, which facilitates the concentration of EVs and removes impurities of lower molecular weight more efficiently.[221] Despite the positives associated with

the isolation technique, TFF is not a perfect fractionation method when attempting to achieve a pure sEV population because it separates particles using the reasoning of size as opposed to density or the biogenesis pathway, which are the main discerning characteristics of EV populations.[97,221] As a result, many different vesicle types will enter the TFF product in addition to the desired sEV population. Another discriminating step is required to differentiate further our sample, which is precisely why I performed an OptiPrep gradient.[220] This gradient will separate the EVs based on their buoyant density. Due to the lipid and protein composition, the acceptable buoyant density of sEVs is 1.10-1.18 g/mL.[231]

Interestingly, the findings show that fractions containing APEX-PTGFRN overlap with fractions that do not include all sEV markers. For example, fraction 4 shows no sEV markers enriching with the fusion protein, fraction 7 is devoid of TSG101, and fraction 8 omits both TSG101 and CD63. The presence of particular sEV markers and the lack of others in specific fractions is explained by the fact that sEVs are highly heterogeneous.[231] Therefore, in the case of fraction 8, this may represent an sEV population that is simply tetrapanin-poor but contains other sEV-associated machinery, including Alix or Syntenin. However, PTGFRN is known to interact closely with tetraspanins to form tetraspanin-enriched microdomains.[233] PTGFRN is a single-pass membrane protein of the EWI family that forms stoichiometric complexes with CD9 and CD81 in tetraspanin-enriched microdomains;[234] nevertheless, the present data suggest that a proportion of PTGFRN-positive vesicles also exist in tetraspanin-poor subpopulations. Recognizing this heterogeneity is essential for interpreting downstream proximity-labelling results, as different vesicle subsets may recruit distinct host factors during fusion and trafficking.

4.1.1 Molecular Interactions Governing PTGFRN Localization

Mutational scanning of PTGFRN revealed that its Ig-like C-loops contain a conserved EWI/WEI tri-peptide; substitution of this motif abolishes co-immunoprecipitation with the large extracellular loop (EC2) of CD9 and CD81, indicating that PTGFRN is recruited into tetraspanin microdomains through direct side-chain contacts between these regions.[235] One would therefore expect PTGFRN to partition predominantly with tetraspanin-rich vesicles. Yet, our density-gradient data show a co-fractionation of PTGFRN in the fraction that is comparatively poor in CD63. To explain this, PTGFRN may interact with alternative interactors, such as ESCRT-associated complexes or other scaffolding proteins, like integrins, which could drive its incorporation into subpopulations of EVs where tetraspanins are less abundant but ESCRT-related proteins are prevalent.[234.235]

EWI-2, another member of the EWI family, has been shown to bind to integrin α4β1 and modulate cell spreading and ruffling.[236] Given the structural homology between PTGFRN and EWI-2, this raises the possibility that PTGFRN engages integrins present on sEVs. Integrins are found in sEVs and can be trafficked via ESCRT or ESCRT-independent pathways.[236] As a result, if an interaction exists between PTGFRN and integrins, PTGFRN may be recruited into integrin-bearing vesicles, which do not require the presence of tetraspanins, explaining its presence in fraction 8.

Other interactions may include interactions with ESCRT-associated proteins. Syntenin-1 and Alix, proteins found to be co-enriched with PTGFRN in fraction eight without tetraspanins, are central to many ESCRT-dependent pathways. They participate in binding to specific motifs, such as LYPXnL motifs for Alix.[120] Although PTGFRN lacks the canonical YPX□L motif recognized by Alix, it could be tethered indirectly: syntenin's PDZ domains bind the C-terminal

EFYA motif of syndecans,[237] which in turn interact with Alix. PTGFRN may therefore participate in a multimeric complex → syndecan → syntenin → Alix that substitutes for direct tetraspanin contact and steers a subset of PTGFRN-positive vesicles toward ESCRT-dependent budding or cargo sorting. Elucidating these alternative binding routes will be essential for understanding how PTGFRN marks molecularly distinct sEV subtypes and how each subtype engages the retromer-actin machinery characterized in this study.

4.1.2 Impact of the APEX Fusion Tag on PTGFRN Behaviour

Another crucial aspect to consider is the potential of the APEX tag to alter PTGFRN's natural conformation. The conjugation of APEX to PTGFRN results in a significant increase in its molecular weight, potentially altering its membrane affinity.[238] The addition of APEX-PTGFRN fusion protein can disrupt the natural conformation of PTGFRN, potentially blocking binding epitopes crucial for tetraspanin association.[239] Alternatively, the added surface area of APEX2 may create novel contact sites that favour interaction with ESCRT-associated scaffolds, thereby routing PTGFRN into tetraspanin-deficient vesicles. Furthermore, the introduction of fusion proteins can sometimes lead to partial aggregation or a slight shift in buoyant density, which could be observed as a wider distribution of PTGFRN presence on the western blot.

Ultimately, the strongest PTGFRN-APEX signals overlap substantially with classical sEV markers in their recognized density range, and negative controls such as calnexin/Tomm20 (ER and mitochondrial markers) remain in other fractions, confirming that a substantial subset of PTGFRN-APEX is indeed associated with the sEV population we intend to track.

4.2 Endosomal Trafficking of sEVs: Pathways and Functional Implications

Confocal imaging of biotinylated proteins (figure 8B) revealed that PTGFRN-containing membranes intersect a succession of endocytic compartments. Ten minutes after vesicle addition, the label co-localized chiefly with Rab5-positive early endosomes, consistent with the classical uptake pathway visualized by DAB-EM (figure 7A). By 30–60 min, the overlap shifted to Rab7-positive late endosomes and Lamp1 lysosomes, indicating onward maturation.[240]

Unexpectedly, a significant signal also appeared in Rab11 recycling endosomes and in GALNT1-positive Golgi cisternae. Because APEX2 reports only proteins within ~20 nm of the PTGFRN cytoplasmic tail, these observations most likely reflect post-fusion sorting of the sEV-derived membrane rather than direct transport of luminal cargo to these organelles. To address the co-localization with the Golgi apparatus and recycling endosomes, it is essential to note that we are tracking the trafficking pathway of PTGFRN, not that of all sEV cargo. As a result, after a fusion event, the membrane of the sEV remains intact but merges with the recipient cell's plasma membrane. Over time, these membrane proteins will be internalized through endocytosis and further trafficked along the endocytosis pathway. Thus, the observation that Rab11 and GALNT1 become biotinylated does not necessarily indicate that sEVs traffic directly to these compartments but rather that the PTGFRN-containing membrane is processed through intracellular sorting pathways post-fusion.

Rab11 is a marker of recycling endosomes, suggesting that some PTGFRN-containing membranes are retrieved and returned to the plasma membrane, implying an active process that brings sEV-derived membrane components into the recipient cell's plasma membrane through recycling pathways.[242] This process may have a functional implication, as reintegrating sEV-derived membrane components could alter the lipid composition at specific membrane sites,

thereby increasing the likelihood of future fusion events. PTGFRN and potentially other membrane components brought to the plasma membrane may prime the plasma membrane to be more receptive to fusion.[241,242] This increase in fusion may result from restoring the lipid environment to recruit essential fusion material; for example, increasing the presence of negatively charged lipids at the plasma membrane may facilitate the tethering of sEVs.[241,242] By actively recycling these components via Rab11-positive recycling endosomes, the cell effectively "primes" the plasma membrane, ensuring that the molecular constituents necessary for efficient membrane merging are present at the right place and time. This priming could lower the energetic barrier for subsequent fusion events, thereby increasing the likelihood of further sEV uptake.

Co-localization in Golgi-associated regions suggests that some sEV-derived membrane proteins undergo post-fusion modifications and sorting. The reason why this may occur could be due to the post-translational modification.[243] PTGFRN consists of glycosylation sites and may be directed to the Golgi for these purposes.[243] These modifications can affect the stability, conformation, and functionality of these proteins. Moreover, they could play a critical role in modulating the fusion competency of membrane components. Glycosylation can affect how proteins interact with other cellular factors, potentially altering the local lipid environment or clustering essential proteins that may be used for fusion. Whether the Golgi passage is obligatory for all PTGFRN-positive membranes or represents a specialized quality-control route remains to be determined.

These findings suggest that post-fusion maneuvers enhance the fusogenic potential of membranes. However, further experimentation is necessary to fully understand the fundamental

role of protein recycling in membrane fusion. The potential impact of this research on future studies in the field is promising, offering new avenues for exploration and discovery.

4.3 sEVs use filopodia, ARP2/3, and WASH complex to facilitate fusion into cells

Data from EM (figure 7C-E) suggest that sEVs are aligned along thin membrane protrusions whose calibre and ultrastructure resemble filopodia. Proteomic evidence of enrichment of the ARP2/3 and the WASH complex (figure 9), together with a STRING module centred on actin-polymerizing proteins (figure 10), suggests that sEVs exploit a specialized actin network to reach fusion-competent plasma-membrane domains.

4.3.1 Filopodia "surfing" brings sEVs to areas of fusion

The actual association with filopodia from sEVs is not a novel discovery. Many virology and cell biology reports show that pathogens exploit the mechanism of "surfing" on filopodia to approach the cell body.[157-160] In this process, polymerization of actin monomers at the distal end of the filopodium drives filopodial extension; simultaneously, older actin subunits depolymerize at the proximal pointed ends of the filaments near the base, creating a continuous conveyor belt-like process known as treadmilling.[157-160] This process generates a net flow inward from the tip toward the cell body. As a result, any particle, receptor, or vesicle associated with these filaments is carried inward as the filaments move. The DAB-stained sEVs captured at intermediate positions along filopodia (figure 7B–E) mirror those observations. In several cases, two converging actin bundles frame a vesicle at the moment of membrane merger (figure 7B). This geometry is consistent with a model in which continuous actin treadmilling delivers sEVs to discrete plasma-membrane nanodomains that are enriched in fusogenic lipids or receptors. These

findings align with previous studies and suggest a potential mechanism for sEV docking and internalization.

4.3.2 Candidate Molecular Tethers Revealed by STRING Analysis

Insights from our String proteomic analysis indicate that sEVs leverage a coordinated network of actin-regulating proteins to bind and navigate along filopodial structures. In particular, CAPZA2, MYH10 and ANXA1 stand out among the actin-polymerization-related factors identified (figure 10), suggesting these proteins may act as specialized binding partners that anchor sEVs to filopodia and facilitate their eventual fusion or internalization.

CAPZA2 is the alpha subunit of the capping protein complex that binds to the barbed end of actin filaments, preventing further polymerization at the end and ultimately regulating the actin filament length and organization. Through this action, CAPZA2 ensures that the growth of actin filaments remains organized.[244] Although CAPZA2 is not a "classic" vesicle marker, actin-modulating proteins and many cytoskeletal regulators, including capping proteins and cofilin, are often detected in proteomic analysis.[233] CAPZA2 is found in sEVs because sEVs can bud from regions of the plasma membrane or MVBs where actin remodelling is active. CAPZA2 might then become enriched in sEVs during these processes. Due to the targeting of actin filaments, if CAPZA2 is present on the sEV membrane, it would recognize the barbed end of actin filaments at filopodial tips or shafts, most specifically in areas where new actin polymerization is being formed.[244,245] CAPZA2 would be able to lock the sEV into proximity to the cell membrane through this binding action. The binding would act as a physical tether, thereby reducing the distance the sEV membrane must traverse and lowering the energy cost of fusion.

MYH10 is a non-muscle myosin that interacts with actin filaments to generate force to help regulate cell shape and tension in the cortical cytoskeleton and organize stress fibres.[246] It also participates in cell motility, cytokinesis, and adhesion.[246] Although myosins are not classical vesicle markers, cytoskeletal components do sporadically co-purify with sEVs,[233] and MYH10 is indeed detected in our proteomic dataset.[233] Due to the contractile forces that MYH10 is canonically known to produce, if the motor were displayed on the vesicle surface in the correct orientation, it could grip cortical actin and "reel" the vesicle toward the plasma membrane, shortening the gap the two bilayers must bridge and thereby lowering the energetic barrier to fusion.[246] Force production by myosin II requires activation of its regulatory light chain: Ca^{2+} binds calmodulin, which then stimulates a myosin-light-chain kinase (MLCK) to phosphorylate the motor.[246,247] This is somewhat plausible due to calcium microdomains near the plasma membrane, which contain Ca2+ concentrations of 1-2 mM, and the fact that a calmodulin-like protein, CAML5, is found to be enriched on sEVs in our proteomic dataset.[248] However, subsequent steps require the use of a kinase that will phosphorylate MYO10 to generate the contractile force. Although kinases like RIOK1 are found in our proteomic datasets to be enriched on sEVs, RIOK1 does not have well-defined biological functions phosphorylating MYH10.[247] While the presence of MYH10 on sEVs and local calcium microdomains raises the intriguing possibility that contractile force generated from MYH10 might overcome fusion barriers, current knowledge cannot give confidence in the ability of MYH10 to be phosphorylated in the extracellular space.

ANXA1 is part of the annexin protein family and is a phospholipid-binding protein that binds to negatively charged phospholipids.[250] Annexins promote membrane curvature and fusion, and they are among the most frequently reported proteins in sEV proteomes, likely because

vesicles bud from highly curved membrane domains where annexins already concentrate.[243,250] Filopodial membranes are rich in acidic lipids like phosphatidylserine and phosphoinositides and contain micro-domains where extracellular Ca^{2+} can reach 1–2 mM.[249,250] Therefore, as an sEV bearing ANXA1 encounters such a Ca^{2+} pocket, Ca^{2+} binding triggers a conformational switch that exposes hydrophobic loops; these loops insert into the outer leaflet and tighten electrostatic contacts with the negatively charged surface. The result is a molecular bridge that tethers the vesicle to the plasma membrane, neutralizes inter-bilayer repulsion and lowers the energy barrier to fusion. The Ca^{2+} sensor CALML5, also enriched in our vesicle dataset, might guide sEVs toward these high-Ca^{2+} zones, further facilitating ANXA1 activation, though this auxiliary role remains to be tested.

It is important to note that bulk LC-MS cannot assign these proteins to the luminal versus cytosolic leaflet of sEVs; follow-up surface-protease shaving or proximity-biotinylation on intact vesicles will be required to confirm their topology. Nevertheless, the co-occurrence of CAPZA2, ANXA1, and MYH10 with ARP2/3 and WASH adaptors strengthens the concept of an actin-centric entry route.

The co-presentation of CAPZA2 and ANXA1 on sEVs synergistically promotes docking and fusion. CAPZA2 organizes and caps actin filaments, ensuring that ordered filopodia deliver the vesicle to the membrane efficiently and with minimal steric hindrance, while ANXA1 provides strong membrane anchoring, bridging phospholipid domains in a Ca^{2+}-dependent manner that locks the sEV close to the filopodial surface. These proteins reduce the electrostatic, hydration, and structural obstacles that typically keep bilayers from merging, lowering the energy threshold required for sEV-membrane fusion and ensuring the sEV's cargo is delivered into the cells.

4.3.3 The Wash Complex and the ARP2/3 complex may apply mechanical force on sEVs

Actin filaments, as dynamic structures, play a crucial role in intracellular trafficking, membrane remodelling, and force generation for locomotion.[252] Their typical localization and association with endosomal sorting highlight, alongside the proteomic enrichment of the ARP2/3 complex and its activator WASH (figure 9), together with STRING clustering (figure 10), suggest that incoming sEVs intersect an actin-nucleation platform at the cell surface.

Once an sEV is tethered to the cell surface, a branched actin network nucleated by the ARP2/3 complex can generate a mechanical push. ARP2/3 attaches to an existing mother filament in the cortex or along the filopodial shaft and sprouts a daughter filament whose barbed (+) end grows toward the vesicle or the adjacent plasma membrane. Each actin monomer added to this barbed end lengthens the filament by a few nanometers,[252,253,] exerting a minute but real displacement. Repeated polymerization events accumulate, producing a cumulative force that can press the membrane against the vesicle or drive the vesicle toward the membrane, thereby facilitating the close apposition required for fusion between the two bilayers. From here, there are two different options to consider. One pushes the membrane towards the sEV, and the second pushes the sEV towards the membrane. The former is more straightforward to conceptualize, as it simply requires anchoring the sEV to the membrane and polymerizing the filament, which pushes the plasma membrane outward and pins the sEV between the bulging membrane and the initial filament. This process is illustrated in figure 7b, where an outward protrusion closes the gap between sEV and the plasma membrane. The latter, however, requires a physical linkage between the sEV and the cytoskeleton. Mechanical forces cannot be transmitted across empty spaces and require a continuous physical path. If the sEV wants to be pushed towards the plasma membrane via actin polymerization, a pathway must convey that force outward from the

cytoplasm to the sEV membrane. Based on our current proteomic data, a complete ladder of proteins connecting the sEV to the actin cytoskeleton has not been elucidated; however, candidates mentioned previously, such as ANXA1 and CAPZA2, can connect to actin and may facilitate the transmission of force that pushes sEVs to the plasma membrane. Direct evidence for this linkage is presently lacking and will require surface-proximity biotinylation or cross-linking assays. Typically, it is a combination of both in which there is a dynamic interplay where the plasma membrane can move while the sEV can also move. Either way, actin polymerization helps overcome hydration and electrostatic repulsion and pre-bends the bilayers, lowering the energy barrier for hemifusion.

The WASH complex, an activator of the ARP2/3 complex, plays a key role in directing actin growth.[254,255] It has established roles in endosomal cargo sorting, but recent data suggest its operation near the plasma membrane and filopodial bases.[254,255] WASH's activation of the ARP2/3 complex and its control over the growth of branched actin filaments provide crucial directional information.[254-257] This information determines the cell's ability to efficiently push or pull on the vesicle, thereby facilitating the coordination of the branches to exert maximum force on the sEV or plasma membranes [254,257]

In addition to the roles WASH has in directed actin growth, the WASH complex is known to generate or stabilize tubular extensions through branched actin in the context of endosomal sorting.[256,257] An equivalent activity at the plasma membrane would push outward on the bilayer, holding it in a curved configuration that would otherwise spring flat, as the flat configuration is more thermodynamically stable.[256-258] Mechanistically, each actin filament that the WASH complex governs to be polymerized exerts a mechanical force against the membrane.[257] Actin networks beneath the curved membranes can act like a scaffold and resist attempts at

flattening.[258] As a result, the energy from ATP hydrolysis is used for actin polymerization, which offsets the cost of bending the membrane, allowing it to adopt a higher curvature state than it would spontaneously. But why is curvature essential for membrane fusion? Membrane merger proceeds through highly curved intermediates, most notably the hemifusion stalk, where the outer leaflets of the sEV and the plasma membrane bend sharply toward one another.[164] Under normal conditions, lipid bilayers are flat; as a result, forcing them into a curved state would cost energy.[164,165] If WASH-driven actin polymerization has already pre-bent the membrane, the system starts mid-way up the energy barrier, so less additional work is required to reach the hemifusion state.[164] From the thermodynamics perspective, the energy required is much less, as you have a membrane in which energy has already been invested.[164,165] Moreover, the actin scaffold acts like a brace, preventing the curved diaphragm from relaxing back into two separate bilayers while the fusion pore is forming. In this way, the mechanical work supplied by ATP-driven actin polymerization is effectively stored as curvature energy and spent to keep the fusion pathway moving forward.

In addition to its role as a guide for actin, the WASH complex also serves as a molecular scaffold, binding to protein complexes that target curved membranes. The retromer complex is one of these complexes bound by WASH via the FAM21 subunit and is highly enriched in proteomics datasets, suggesting its role in the internalization of sEVs.[259,260] The WASH complex collaborates with the retromer complex to facilitate endosomal protein sorting, either from the endosome to the Golgi or from the endosome to the plasma membrane.[260,261] In the context of endosomal tubulation and cargo sorting, the WASH complex binds to VPS35, a retromer complex's cargo-selective complex (CSC) member, which will attach to endosomal membranes (specialized microdomains defined as assemblies of cargo proteins, lipids, and peripherally

associated proteins) to demarcate them into a particular sorting fate.[260] Given that both the retromer complex and the WASH complex were present in the proteomic datasets, examining how the retromer-WASH partnership may extend beyond endosomal sorting may reveal another layer of regulation that ensures the successful internalization and trafficking of sEV contents. To test whether WASH is simply permissive for curvature or an active "gatekeeper" that hands sEV membranes over to retromer, we propose an acute optogenetic shutdown: photoinactivate WASH in live cells and use live microscopy to track R18-labelled fusion events in real time. A rapid loss of successful pore opening after WASH inactivation would argue that the WASH–retromer module is essential for the final steps of sEV cargo release.

4.4 The Retromer complex stabilizes the fusion of sEVs

Loss-of-function data (figure 11) show that depletion of VPS35, VPS26A or SNX27 reduces R18 de-quenching and prevents siRNA knock-down, suggesting that retromer activity is required at, or shortly after, the point where sEVs release cargo. While the retromer complex's classical role in endosomal cargo sorting is well-established, its involvement in membrane fusion is a novel discovery. Retromer lacks the hallmark fusogenic domains found in SNAREs or multisubunit tethering complexes, so it is unlikely to initiate bilayer merger. Instead, loss-of-function experiments demonstrate that retromer is required after vesicle docking: knocking down VPS35 or SNX27 leaves sEVs bound or internalized yet unable to discharge siRNA into the cytosol. These findings, together with the curvature-sensing BAR domains of retromer-associated SNX dimers, suggest a structural role in stabilizing the highly curved rim of the hemifusion diaphragm and promoting pore expansion (figure 12). In my proposed model,

retromer acts not as a fusogen but as a membrane-remodelling clamp that lowers the energy barrier for the last and most critical step of cargo release.

4.4.1 Hypothetical Mechanism of Retromer Complex Fusion Stabilization

SNX proteins in the retromer complex typically induce a curvature of the membrane toward the plasma membrane (positive curvature). The curvature induction is due to the shape of the BAR domain, which is typically that of a crescent.[261] If SNX proteins were to bind on the cytoplasmic side in a place of fusion, this curvature would increase the energy needed, bringing the plasma membrane further away from the sEV membrane. As we see in figure 7b, curvature towards the sEV membrane (outwards to the extracellular space) is typically visualized, meaning that the mechanism by which the retromer complex induces fusion would not be through direct binding and stabilization of membranes at the early stages of fusion.

However, when generating the latter fusion intermediates, such as the hemifusion stalk and the hemifusion diaphragm, a localized curvature induced by the SNX proteins may facilitate the necessary bending, making the fusion process more energetically favourable. During the hemifusion stalk, the outer leaflets of the two membranes are combined and generate a lipid stalk that is highly curved on both sides of the stalk.[164,165] The outer leaflets move laterally from the stalk to the diaphragm, allowing the inner leaflets' lipids to interact with each other. I propose that SNX-BAR dimers, with their intrinsic crescent shape, clamp onto the rim of the growing diaphragm.[261,262] By adding additional positive curvature, they pull the diaphragm’s edges away from the central stalk, encouraging the inner leaflets to meet and lowering the energy required for pore opening (figure 12, panel 3). Once bound, the SNX coat would continue to hold the rim in its curved conformation, preventing the diaphragm from snapping back to a flatter,

lower-energy state. In this way, SNX-BAR proteins act much like an actin brace, stabilizing the membrane geometry long enough for the fusion pore to expand and complete cargo release.

This hypothetical model suggests that the SNX proteins would initially avoid binding to the initial site of curvature and would be delayed until a hemifusion diaphragm has formed. The later recruitment of SNX proteins is plausible because SNX proteins will prefer pre-stabilized curvature. If the retromer complex were to enter a fusion site, the curvature towards the extracellular matrix would be inconsistent with the curvature of the BAR domain, making it unfavourable for binding. The lateral portions of the hemifusion diaphragm or stalk have mild curvature in the same direction as the SNX proteins, allowing the BAR domain to bind energetically favourably. Therefore, the model itself is supported by biophysical principles.

In summary, while the retromer complex is unlikely to initiate membrane merger, its membrane-remodelling properties and observed requirement for efficient siRNA delivery point to a previously unappreciated role in stabilizing or enlarging the fusion pore through which sEV cargo gains access to the cytoplasm.

4.4.2 Differences in SNX protein's ability to affect fusion and cargo delivery

Figure 11B shows that knock-down of SNX27, but not SNX9, abolishes HPRT1 silencing, even though both proteins appear in our proteomic dataset. The functional divergence can be rationalized by their distinct domain architectures and cellular roles. SNX27 has a PDX domain that allows the binding of specific cargo containing the PDZ-binding motif and the PX domain targeting certain phosphoinositides [262,263]

SNX27 combines a PDZ domain (which recognizes C-terminal PDZ-binding motifs on cargo), a PX domain (phosphoinositide binding) and a short FERM-like linker that tethers it to

the VPS35 core of retromer.[262,263] In epithelial cells, SNX27 localizes to the plasma membrane and early endosomes, where it captures cargo and recruits retromer for rapid retrieval.[263] SNX9, by contrast, contains an SH3–PX–BAR module and functions primarily as an accessory factor in clathrin- and dynamin-mediated endocytosis; it does not interact directly with the VPS35/29/26A scaffold. As shown in figure 11, the absence of an SH3-containing SNX (SNX9) has a minimal impact on sEV fusion or siRNA release. This may be because other BAR-domain paralogues, such as SNX18 or SNX33, can compensate for membrane curvature and dynamin recruitment.[263]

In SNX27-depleted cells, electron microscopy shows DAB-labelled vesicles stalled at the cell surface with negligible cytoplasmic signal (figure 11F–G). I therefore propose that SNX27 acts at a late docking step: its PDZ domain binds a yet-to-be-identified motif on the PTGFRN-containing vesicle or a cooperating receptor, thereby positioning the retromer coat at the fusion rim. Loss of SNX27 would decouple retromer from the membrane, preventing the curvature-stabilizing “clamp” hypothesized in Section 4.4.1 and ultimately blocking complete fusion-pore expansion and siRNA release. Testing this model will require mapping PDZ-binding sequences on vesicle or host proteins and assessing whether a PDZ-null SNX27 mutant phenocopies the knockdown.

4.4.3 Retromer Complex Localization to the Plasma Membrane via Cargo Accumulation

Given the retromer complexes' known role in recycling and the importance of the SNX27 protein in membrane fusion and cargo delivery (figure 11B), it is possible that specific cargo proteins cluster at fusion hotspots, allowing the retromer complex to be naturally recruited to these sites as a part of its cargo-sorting function.[260,264] Membrane proteins, such as TFRC and SLC2A1, are known retromer complex cargo that are recycled to the plasma membrane and have

also appeared to be heavily labelled in the proteomic dataset.[264,265] If these proteins accumulate at or near fusion hotspots, they may serve as active recruitment signals for retromer subunits and the associated SNX-BAR domains.

Both TFRC and SLC2A1 are recognized by the retromer complex's SNX-BAR domains through short cytoplasmic motifs in their intracellular domains.[264,265] More specifically, TFRC is recognized by SNX17, whereas SLC2A1 carries a C-terminal DTQF motif bound by the PDZ domain of SNX27.[264,265] Once bound, the cargo is isolated from the rest of the endosome and is trafficked to the plasma membrane, allowing for the maintenance of critical surface levels of TFRC or SLC2A1 for iron uptake or glucose transport respectively. In the context of fusion, this trafficking can lead to the retromer complex remaining at or accumulating on the membrane as it continuously retrieves the membrane proteins, potentially creating a local pool of retromer/SNX subunits that can independently participate in the fusion of sEVs. The repeated trafficking by the retromer complex could transform these sites into recycling hubs enriched in curvature-sensing proteins and scaffold factors, which are essential for membrane fusion. For example, the retromer complex recruits actin regulators, such as the WASH complex, which can act as a cortical scaffold beneath the membrane and maintain the curvature required for fusion. This consistent retrieval accomplished by the retromer complex could provide sufficient reasoning as to why it remains spatially and temporally poised to promote the later stages of membrane fusion. Therefore, as opposed to the current view of the retromer complex suggesting that it merely cycles through different endosomal compartments, the occupation of the plasma membrane by the retromer complex can occur for enough time to support the energetically demanding events of sEV fusion.

This scenario leads to two testable predictions: (i) acute antibody cross-linking of TFRC or SLC2A1 should trap retromer at the surface and enhance sEV fusion efficiency, whereas (ii) CRISPR removal of the PDZ-binding motif from SLC2A1 should delay fusion or reduce siRNA delivery without affecting vesicle binding. Testing these predictions will determine whether retromer's presence at fusion hot spots is an epiphenomenon of bulk recycling or a dedicated mechanism that couples membrane turnover to the energetically demanding final steps of sEV entry.

4.4.4 VPS35 KD allows Internalization of sEVs; however, the Delivery Capacity of siRNA is Lost

In figure 11b, we see that VPS35 KD does not allow the delivery of functional siRNA into the cell; however, when visualizing EM data of VPS35 KD HEK293 cells in figures 11F and 11G, it is shown that the dab precipitates are found in the cytoplasm, suggesting that the entry of sEV into the cell is maintained. Unlike the membrane-associated puncta seen in control cells, the label appears diffuse within the cytoplasm or loosely associated with amorphous vesicles, suggesting that vesicle membranes either fail to tether to defined endosomal sub-domains or disintegrate without releasing cargo into productive compartments.

VPS35 coordinates the retrieval of cargo-loaded tubules and has been implicated in back-fusion of intraluminal vesicles with the limiting membrane.[265] Its loss is therefore expected to disrupt the micro-environment, including the lipid composition, curvature, and actin/WASH coat, which are components required for pore enlargement and siRNA escape. I propose that, in the absence of VPS35, incoming sEVs are internalized by classical endocytosis (as suggested by the Rab5→Rab7→Lamp1 itinerary in wild-type cells; figure 8B–C), but their membranes are

mis-sorted, preventing the formation or stabilization of a fusion pore that would normally discharge the siRNA into the cytosol. Future experiments combining live pH-sensitive cargo reporters with acute VPS35 degradation (e.g., auxin-inducible degron) should establish whether the block occurs at the back-fusion step or at an earlier retromer-dependent membrane-remodelling event.

4.5 Integrated Working Model of sEV Fusion

I propose a six-step model that combines imaging, proximity labelling, and loss-of-function data with published mechanisms of actin-driven membrane remodelling (Figure 12).

1. **Initial encounter and loose tethering:** Brownian motion brings sEVs into transient contact with filopodial tips. Vesicle-associated annexins, activated by extracellular Ca^{2+}, may bind negatively charged lipids on the filopodial membrane. The putative presence of actin-capping protein CAPZA2 and other cytoskeletal adaptors on the vesicle surface remains hypothetical and will require topological validation.
2. **Retrograde surfing and membrane deformation:** Actin treadmilling carries the vesicle toward the cell body. Near the base of the filopodia, the WASH complex activates ARP2/3, producing a branched actin network that pushes the plasma membrane outward and presses it against the docked vesicle, initiating local curvature.
3. **Hemifusion stalk formation:** Membrane crowding plus annexin-mediated bridging overcome hydration repulsion, allowing the outer leaflets of the two bilayers to merge into a hemifusion stalk.

4. **Stabilization of the hemifusion diaphragm:** Retromer complex arrives together with curvature-sensing SNX-BAR dimers. Their crescent BAR domains bind to the positively curved rim of the nascent diaphragm, lowering line tension; SNX27, via its PDZ domain, may tether specific cargo (eg, SLC2A1) to the same site, helping to position the coat.
5. **Fusion-pore opening and enlargement:** Continued actin polymerization, plus the mechanical clamp provided by the SNX-BAR coat, drive radial expansion of the pore until it becomes large enough for siRNA to dissipate into the cytosol.
6. **Post-fusion recycling:** Residual vesicle membrane, now part of the plasma membrane, is internalized via Rab5-positive endocytosis. Retromer/WASH subsequently segregates PTGFRN and associated lipids into Rab11 recycling tubules, possibly priming new fusion hot spots.

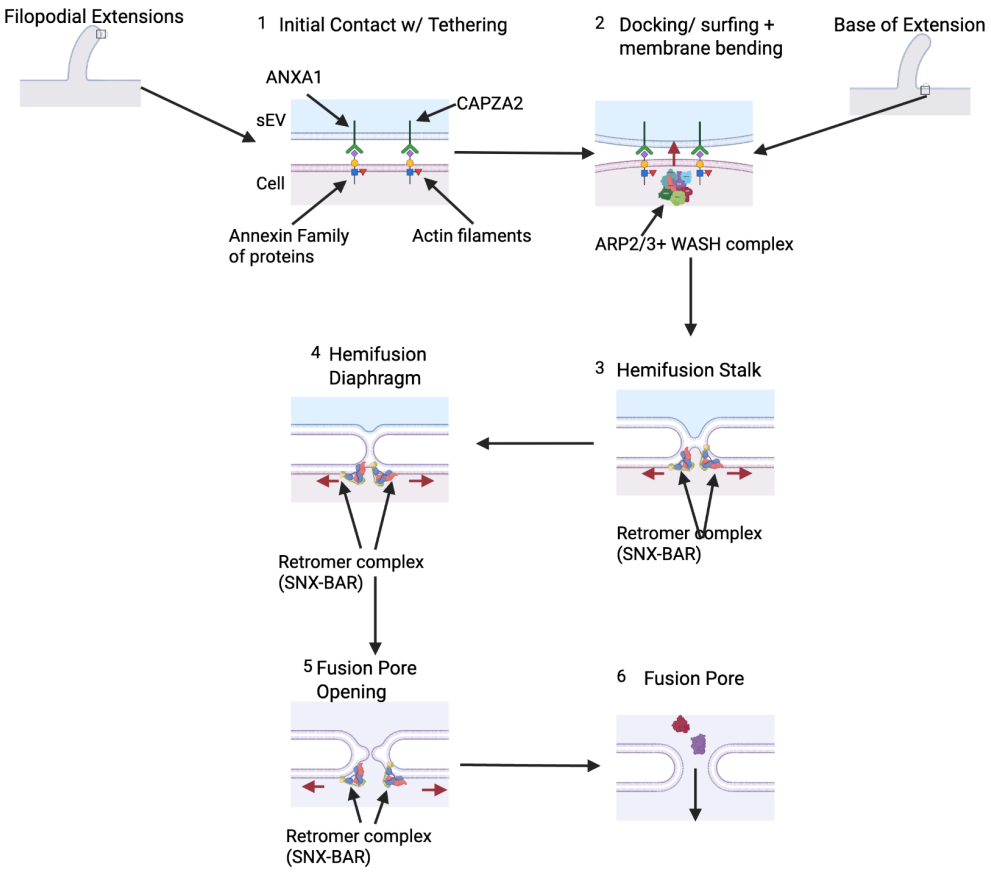

Figure 12: Proposed Stepwise Model of sEV Fusion. 1) Initial contact is facilitated through attachment of the sEV with proteins such as ANXA1 and CAPZA2 that help tether the sEV to actin filaments at the membrane. **2)** sEVs surf along the filopodia toward the cell body, guided by ARP2/3 and WASH complexes that regulate actin polymerization and retrograde flow toward the cell body. Actin polymerization generates mechanical forces that push upon the cell membrane, pushing it towards the sEV to overcome repulsion forces. Red arrows indicate the direction of forces applied to the membrane. **3)** Hemifusion stalk is stabilized and expanded by the retromer complex (shown at the site of membrane curvature. **4)** The merging of the outer leaflets is stabilized by the retromer complex (notably SNX BAR domains) to maintain the bent membrane configuration supporting progression to complete fusion. **5)** Efforts of actin and retromer-driven forces facilitate a curvature of the membrane that leads to pore formation, allowing particle exchange between sEV and the cytoplasm. **6)** A fully established pore enables direct cargo release from the sEV into the cytoplasm. Red arrows illustrate membrane movement or curvature changes at each stage, reflecting how protein interactions and actin dynamics collectively overcome energy barriers to promote efficient sEV fusion.

4.6 Future Directions

This study has provided new insights into the mechanisms of sEV fusion, highlighting roles for cytoskeletal dynamics, the retromer complex, and associated proteins. Future studies could begin by optimizing the systems used.

4.6.1 Minimizing Proximity-Labelling Bias

While experimental data using proximity labelling provides compelling insights on sEV trafficking and potential players involved in fusion, biases inherently exist in this experiment that need to be addressed. Labelling bias may be a possible limiting factor with the proximity labelling of APEX-PTGFRN. APEX proximity labelling depends on reaction kinetics and may preferentially label more stable proteins that are not all in interaction. This might introduce a bias towards more stable interactions rather than transient or dynamic interactions, which may be essential in the fusion process. Consequently, the resulting data might present an incomplete picture of the interaction landscape, skewing interpretations toward more persistent associations. It is challenging to address this concern entirely because other biotin ligases, such as BioID or TurboID, are significantly slower. Chemical crosslinking is used to freeze transient interactions and capture weak, short-lived interactions that might be underrepresented in the APEX proximity method. Combining a crosslinking experiment to freeze protein-protein interactions by forming covalent bonds between proteins near sEVs could further validate and extend the list of interacting proteins, allowing for the analysis of fleeting protein interactions. To do this, I propose coupling millisecond diazirine photo-cross-linking to an APEX pulse–chase protocol: a 1-s APEX labelling pulse records stable neighbours, the culture is quickly quenched, and

diazirine activation freezes transient contacts for a second MS run.[266] Overlap and divergence between the two datasets will benchmark the interactome's temporal hierarchy.

4.6.2 Surfaceome-focused CRISPR screen for Fusion Receptors

The use of GOTERM analysis relies on existing annotations and curated databases, meaning the identification of proteins is biased toward those with previously established roles in processes like fusion or trafficking. Therefore, proteins that participate in sEV fusion or endocytosis pathways but have not been previously characterized in these contexts will be overlooked, masking the discovery of novel or unconventional proteins that are integral to sEV dynamics but remain unannotated in current databases. Future studies could include a unique CRISPR library knockout of all membrane proteins to address this knowledge gap.[267] This innovative method will then assess sEV internalization and fusion using the R18 assays used in this thesis. To determine efficient siRNA cargo delivery, you can treat HEK293 GFP/RFP cells with membrane protein knockout using sEVs containing siRNA for GFP, and then assess the GFP signal using qPCR and flow cytometry as readouts. Cells positive for sEV fusion and internalization could then be subjected to sequencing to identify the membrane proteins participating in sEV fusion and internalization.

4.6.3 Ligand Validation on Vesicle Membranes

Although putative sEV ligands (e.g., ANXA1, CAPZA2) have been elucidated, further validation of the role of these ligands in facilitating the entrance of sEVs is paramount. By forming interactions with proteins or other molecules on the plasma membrane, these ligands play a crucial role in either reducing the free energy required for fusion or maintaining the sEV

bound until receptor endocytosis occurs. To validate the importance of these ligands in sEV cargo delivery, knocking out the proteins in sEV-producing cells and treating HEK293 cells with the resultant sEVs from the knocked-down cells is required. This approach allows us to directly assess the role of these ligands in sEV cargo delivery. Proximity ligation assays (PLA) will confirm whether the sEV and the membrane protein are in close proximity, validating the binding for the precise determination of protein interactions. Probing for both the ligand and the membrane protein to ensure accuracy.

4.6.4 Real-time Visualization of Retromer at the Fusion Rim

The most crucial aspect that needs to be addressed in this dataset is the role of the retromer in the fusion process. Although I have postulated a potential mechanism, this needs to be empirically determined. The most direct way to elucidate this is using Correlative Cryo-electron microscopy. Visualizing sEVs as they enter the cell using high-resolution imaging techniques will enable the categorization of the mechanism of sEV fusion and determine the role of the retromer complex in this process. Correlative cryo-TEM is a technique that facilitates the generation of high-resolution images of specific interactions. By using antibodies against VPS35 or other SNX proteins that are hypothesized to participate in the fusion process, we can identify them at these fusion interphases. Using R18, the locations of fusion can be identified, where pressure-freezing the sample captures the native and most morphologically accurate state of the sample, thereby avoiding the problems that glutaraldehyde fixation and DAB precipitation have on cellular membranes. The samples can then be imaged in a cryogenic transmission electron microscope, which will enable the co-localization of retromer components with fusion compartments and may facilitate their precise localization at the site of fusion.

4.6.5 Disease Relevance: VPS35-D620N in Parkinson's Models

Beyond ameliorations to the current experiments, studies building on the findings of this research might address the retromer complex in neurodegenerative diseases. The presence of retromer complex components in the proteomic dataset and mutations of the VPS35 gene (D620N) in PD patients could indicate a mechanism of PD pathogenesis involving the mis-sorting of a-syn by sEVs during endocytosis, facilitating its aggregation in the cytoplasm. Multiple preliminary studies would need to be accomplished, such as verifying the presence of a-syn inside sEVs and ensuring that it can be trafficked into neurons with and without the retromer complex.[268] Pursuing these directions will convert the descriptive model proposed here (figure 12) into a quantitative, molecular movie of sEV fusion, bridging basic membrane biophysics with neurodegenerative disease mechanisms.

5. Conclusion

Expanding on the work of the Gibbings lab that showcased that sEVs were capable of delivering siRNAs into mouse models and facilitating silencing events in the liver, kidney, and small intestine, I sought to determine the mechanism that sEVs employ to enter the cell and deliver their cargo to illicit the silencing effect. This data would address my hypothesis of deciphering the mechanism of sEV fusion through tracking sEV. I found that sEVs can enter the cell through a fusion event with both the plasma membrane and the endosome of cells. I deciphered that three host machineries emerge as key players at the site of fusion: the actin-nucleating ARP2/3–WASH network, which generates curvature and mechanical force, and the retromer coat (VPS35–VPS26A–SNX27 plus SNX-BAR dimers), which appears to stabilize late fusion intermediates. I validated the role of the retromer complex through the depletion of core retromer components, which in turn abolishes R18 de-quenching, disrupts ultrastructural fusion signatures, and prevents siRNA-mediated HPRT1 knockdown, underscoring the functional importance of retromer.

By clarifying the entry route of sEVs, this work addresses a central bottleneck in the development of vesicle-based oligonucleotide therapeutics, A mechanistic blueprint now exists for rational engineering: enhancing annexin or SNX27 engagement, modulating cortical actin, or pharmacologically boosting retromer activity could expand delivery beyond the liver to tissues such as brain and muscle. More broadly, the findings highlight an unexpected intersection between membrane-remodelling coats and extracellular vesicle biology, opening new avenues in both fundamental cell trafficking and translational medicine.

References:

1. **Khvorova, A., Watts, J.** (2017) The chemical evolution of oligonucleotide therapies of clinical utility. *Nat Biotechnol* **35**, 238–248
2. **Dana H, Chalbatani GM, Mahmoodzadeh H, et al.** (2017) Molecular Mechanisms and Biological Functions of siRNA. *Int J Biomed Sci*. **13** 48-57.
3. **Kole, R., Krainer, A. & Altman, S.** (2012) RNA therapeutics: beyond RNA interference and antisense oligonucleotides. *Nat Rev Drug Discov* **11**, 125–140.
4. U.S. Food & Drug Administration. 2025. "Approved Cellular and Gene Therapy Products." Accessed January 22, 2025. https://www.fda.gov/vaccines-blood-biologics/cellular-gene-therapy-products/approved-cellular-and-gene-therapy-products.
5. **Zogg, H., Singh, R. & Ro, S.** (2022) Current Advances in RNA Therapeutics for Human Diseases. *Int J Mol Sci* **23**
6. **Kulkarni, J.A. et al.** (2021) The current landscape of nucleic acid therapeutics. *Nat Nanotechnol* **16**, 630-643
7. **Alnylam Pharmaceuticals.** "Pipeline." *Alnylam*, https://www.alnylam.com/pipeline. Accessed 22 Jan. 2025.
8. **Ionis Pharmaceuticals.** "Pipeline." *Ionis Pharmaceuticals*, https://ionispharma.com/pipeline/. Accessed 22 Jan. 2025.
9. **Rinaldi C, Wood MJA. (**2018) Antisense oligonucleotides: the next frontier for treatment of neurological disorders. *Nat Rev Neurol*, **1**, 9-13.
10. **Zamecnik PC, Stephenson ML.** (1978) Inhibition of Rous sarcoma virus replication and cell transformation by a specific oligodeoxynucleotide. *Proc Natl Acad Sci U S A* **75** 280-284.
11. **De Smet MD, Meenken CJ, van den Horn GJ.** (1999) Fomivirsen - a phosphorothioate oligonucleotide for the treatment of CMV retinitis. Ocul Immunol Inflamm. **4**, 189-98.
12. **Bennett CF, Swayze EE.** (2010) RNA targeting therapeutics: molecular mechanisms of antisense oligonucleotides as a therapeutic platform. *Annu Rev Pharmacol Toxicol.* **50**, 259-93
13. **Wu H, Lima WF, Crooke ST.** (1999) Properties of cloned and expressed human RNase H1. *J Biol Chem.*28270-8.
14. **Kulkarni, J.A. et al.** (2021) The current landscape of nucleic acid therapeutics. *Nat Nanotechnol* 16, 630-643 .
15. **Crooke ST, Vickers TA, Lima WF, Wu H, Bennett CF**. (2021) Molecular mechanisms of antisense oligonucleotides. *Nucleic Acids Res.* 6953-6970.
16. **Bennett CF, Krainer AR, Cleveland DW.** (2019) Antisense oligonucleotide therapies for neurodegenerative diseases. *Annu Rev Neurosci.* 385-406.
17. **Shen X, Corey DR.** (2018) Chemistry, mechanism and clinical status of antisense oligonucleotides and duplex RNAs. *Nucleic Acids Res.* 1584-1600.
18. **Muntoni, F. & Wood, M.J.** (2011) Targeting RNA to treat neuromuscular disease. *Nat Rev Drug Discov*. 621-637
19. **Fields E, Vaughan E, Tripu D, Lim I, Shrout K, Conway J, Salib N, Lee Y, Dhamsania A, Jacobsen M, Woo A, Xue H, Cao K.** (2021) Gene targeting techniques for Huntington's disease. *Ageing Res Rev.* 101385.

20. **Rinaldi, C. & Wood, M.J.A.** (2018) Antisense oligonucleotides: the next frontier for treatment of neurological disorders. *Nat Rev Neurol* 9-21
21. **Gagliardi, M. & Ashizawa, A.T.** (2021) The Challenges and Strategies of Antisense Oligonucleotide Drug Delivery. *Biomedicines* 9
22. **Inoue H, Hayase Y, Iwai S, et al.** (1987) Synthesis and hybridization studies on two complementary nona(2′-O-methyl) ribonucleotides. *Nucleic Acids Res.* 6131-6148.
23. **Obika S, Nanbu D, Hari Y, Andoh J, Morio K, Doi T, Imanishi T.** (1998) Stability and structural features of the RNA duplex of locked nucleic acids (LNA). *Nucleic Acids Res.* 3403-3410.
24. **Braasch DA, Corey DR.** (2001) Locked nucleic acid (LNA): fine-tuning the recognition of DNA and RNA. *Chem Biol.* 1-7.
25. **Summerton J, Weller D.** (1997) Morpholino antisense oligomers: design, preparation, and properties. *Antisense Nucleic Acid Drug Dev.* 187-195.
26. **Gebski BL, Mann CJ, Fletcher S, Wilton SD.** (2003) Morpholino antisense oligonucleotide induced exon skipping of the CFTR gene in vitro: application to the treatment of cystic fibrosis. *J Cell Mol Med.* 223-234.
27. **Van Poelgeest, E.P. et al.** (2015) Antisense-mediated reduction of proprotein convertase subtilisin/kexin type 9 (PCSK9): a first-in-human randomized, placebo-controlled trial. *Br J Clin Pharmacol* 1350-1361.
28. **Frazier, K.S. & Obert, L.A.** (2018) Drug-induced Glomerulonephritis: The Spectre of Biotherapeutic and Antisense Oligonucleotide Immune Activation in the Kidney. *Toxicol Pathol*, 904-917
29. **Fire A, Xu S, Montgomery MK, Kostas SA, Driver SE, Mello CC.** (1998) Potent and specific genetic interference by double-stranded RNA in *Caenorhabditis elegans*. *Nature.* 806-811.
30. **Hannon GJ.** RNA interference. (2002) *Nature.* 244-251.
31. **Lee RC, Feinbaum RL, Ambros V.** (1993) The *C. elegans* heterochronic gene lin-4 encodes small RNAs with antisense complementarity to lin-14. *Cell.* 843-854.
32. **Wightman B, Ha I, Ruvkun G.** (1993) Posttranscriptional regulation of the heterochronic gene lin-14 by lin-4 mediates temporal pattern formation in *C. elegans*. *Cell.* 855-862.
33. **Bartel DP.** (2004) MicroRNAs: genomics, biogenesis, mechanism, and function. *Cell.* 281-297.
34. **Kim VN, Han J, Siomi MC.** (2009) Biogenesis of small RNAs in animals. *Nat Rev Mol Cell Biol.* 2009;10(2):126-139.
35. **Kim VN. (**2005) MicroRNA biogenesis: coordinated cropping and dicing. *Nat Rev Mol Cell Biol.* 376-385.
36. **Chendrimada TP, Gregory RI, Kumaraswamy E, et al.** (2005) TRBP recruits the Dicer complex to Ago2 for microRNA processing and gene silencing. *Nature.* 740-744.
37. **Borchert GM, Lanier W, Davidson BL.** (2006) RNA polymerase III transcribes human microRNAs. *Nat Struct Mol Biol.* 1097-1101.
38. **Lee Y, Ahn C, Han J, et al.** (2003) The nuclear RNase III Drosha initiates microRNA processing. *Nature.* 415-419.
39. **Denli AM, Tops BB, Plasterk RH, Ketting RF, Hannon GJ.** (2004) Processing of primary microRNAs by the Microprocessor complex. *Nature.* 231-235.

40. **Lund E, Güttinger S, Calado A, Dahlberg JE, Kutay U.** (2004) Nuclear export of microRNA precursors. *Science.* 95-98.
41. **Yi R, Qin Y, Macara IG, Cullen BR.** (2003) Exportin-5 mediates the nuclear export of pre-microRNAs and short hairpin RNAs. *Genes Dev.* 3011-3016.
42. **Tomari Y, Zamore PD.** (2005) Perspective: machines for RNAi. *Genes Dev.* 517-529.
43. **Matranga C, Tomari Y, Shin C, Bartel DP, Zamore PD.** (2005) Passenger-strand cleavage facilitates assembly of siRNA into Ago2-containing RNAi enzyme complexes. *Cell.* 607-620.
44. **Khvorova A, Reynolds A, Jayasena SD.** (2003) Functional siRNAs and miRNAs exhibit strand bias. *Cell.* 209-216.
45. **Schubert S, Grünweller A, Erdmann VA, Kurreck J.** (2005) Local RNA target structure influences siRNA efficacy: systematic analysis of intentionally designed binding regions. *J Mol Biol.* 883-893.
46. **Timmons L, Fire A.** (1998) Specific interference by ingested dsRNA. *Nature.* 854.
47. **Meister G, Tuschl T.** (2004) Mechanisms of gene silencing by double-stranded RNA. *Nature.* 343-349.
48. **Sijen T, Plasterk RH.** (2003) Transposon silencing in the *Caenorhabditis elegans* germ line by natural RNAi. *Nature.* 310-314.
49. **Zamore PD, Tuschl T, Sharp PA, Bartel DP.** (2000) RNAi: double-stranded RNA directs the ATP-dependent cleavage of mRNA at 21 to 23 nucleotide intervals. *Cell.* 25-33.
50. **Liu J, Carmell MA, Rivas FV, et al.** (2004) Argonaute2 is the catalytic engine of mammalian RNAi. *Science.* 1437-1441.
51. **Rand TA, Petersen S, Du F, Wang X.** (2005) Argonaute2 cleaves the anti-guide strand of siRNA during RISC activation. *Cell.* 621-629.
52. **Meister G.** (2013) Argonaute proteins: functional insights and emerging roles. *Nat Rev Genet.* 447-459.
53. **Tuschl T.** (2002) Expanding small RNA interference. *Nat Biotechnol.* 446-448.
54. **Fitzgerald K, Frank-Kamenetsky M, Shulga-Morskaya S, et al.** (2014) Effect of an RNA interference drug on the synthesis of proprotein convertase subtilisin/kexin type 9 (PCSK9) and the low-density lipoprotein receptor. *N Engl J Med.* 2229-2237.
55. **Juliano R.** (2007) Challenges to macromolecular drug delivery. *Biochem Soc Trans.* 41-43.
56. **Kanasty R, Dorkin JR, Vegas A, Anderson D.** (2013) Delivery materials for siRNA therapeutics. *Nat Mater.* 967-977.
57. **Davidson BL, McCray PB Jr.** (2011) Current prospects for RNA interference-based therapies. *Nat Rev Genet.* 329-340.
58. **Whitehead KA, Langer R, Anderson DG.** (2009) Knocking down barriers: advances in siRNA delivery. *Nat Rev Drug Discov.* 129-138.
59. **De Fougerolles A, Vornlocher HP, Maraganore J, Lieberman J.** (2007) Interfering with disease: a progress report on siRNA-based therapeutics. *Nat Rev Drug Discov.* 443-453.
60. **Corey DR.** (2007) Perspectives on In Vivo Delivery of siRNA. *IDrugs.* 521-524.
61. **Ozcan, G., Ozpolat, B., Coleman, R. L., Sood, A. K. & Lopez-Berestein, G.** (2015) Preclinical and clinical development of siRNA-based therapeutics. *Adv Drug Deliv Rev*, 108-119.

62. **Arraud N, Linares R, Tan S, Gounou C, Pasquet J-M, Mornet S, Brisson AR.** (2014)**.** Extracellular vesicles from blood plasma: deter-mination of their morphology, size, phenotype and concentration. *J Thromb Haemost*: 614–27
63. **Davidson BL, McCray PB Jr.** (2011) Current prospects for RNA interference-based therapies. *Nat Rev Genet.* 329-340.
64. **Akinc A, Maier M, Manoharan M, et al.** (2019) The Onpattro story and the clinical translation of nanomedicines containing nucleic acid-based drugs. *Nat Nanotechnol.* 1084-1087.
65. **Schroeder, A., Levins, C.G., Cortez, C., Langer, R. & Anderson,** (2010) D.G. Lipid-based nanotherapeutics for siRNA delivery. *J Intern Med*; 267, 9-21
66. **Semple SC, Akinc A, Chen J, et al.** (2010) Rational design of cationic lipids for siRNA delivery. *Nat Biotechnol.* 172-176.
67. **Walkey CD, Olsen JB, Guo H, et al.** (2012) Nanoparticle size and surface chemistry determine serum protein adsorption and macrophage uptake. *J Am Chem Soc.* 2139-2147.
68. **Torchilin VP.** (2005) Recent advances with liposomes as pharmaceutical carriers. *Nat Rev Drug Discov.* 145-160.
69. **Zelphati O, Wang Y, Kitada S, Reed JC, Felgner PL, Corbeil J.** (2001) Intracellular delivery of proteins with a new lipid-mediated delivery system. *J Biol Chem.* 35103-35110.
70. **Kowalski PS, Rudra A, Miao L, Anderson DG.** (2019) Delivering the messenger: advances in technologies for therapeutic mRNA delivery. *Mol Ther.* 710-728.
71. **Tagalakis AD, McAnulty RJ, Devaney J, et al.** (2018) Integrin-targeted nanocomplexes for siRNA delivery to the lungs. *Biomaterials.* 94-108.
72. **Sato Y, Murase K, Kato J, et al.** (2008) High-level expression of retinol binding protein and transthyretin in human stellate cells. *Hepatol Res.* 310-317.
73. **Belnoue E, Tougne C, Rochat AF, et al.** (2017) Targeting liver stellate cells using retinol-coupled liposomes improves prophylactic vaccine efficacy against malaria. *Front Immunol.*898.
74. **Whitehead KA, Langer R, Anderson DG.** (2009) Knocking down barriers: advances in siRNA delivery. *Nat Rev Drug Discov.* 129-138.
75. **Pozzi D, Caracciolo G, Digiacomo L, et al.** (2014) The biomolecular corona of lipid nanovectors alters the efficiency of in vivo DNA transfection. *ACS Nano.* 2788-2795.
76. **Estapé Senti, M. et al.** (2022) Anti-PEG antibodies compromise the integrity of PEGylated lipidbased nanoparticles via complement. *J Control Release*, 475-486 (2022).
77. **Kedmi, R., Ben-Arie, N. & Peer, D.** (2010) The systemic toxicity of positively charged lipid nanoparticles and the role of Toll-like receptor 4 in immune activation. *Biomaterials* 31, 6867-6875.
78. **Garber, K.** (2018)Alnylam launches era of RNAi drugs. *Nat Biotechnol*, 36, 777-778.
79. **Banks WA.** (2016) From blood-brain barrier to blood-brain interface: new opportunities for CNS drug delivery. *Nat Rev Drug Discov.* 275-292.
80. **Saraiva C, Praça C, Ferreira R, Santos T, Ferreira L, Bernardino L.** (2016) Nanoparticle-mediated brain drug delivery: overcoming blood-brain barrier to treat neurodegenerative diseases. *J Control Release*. 34-47.
81. **Deleavey GF, Damha MJ.** (2012) Designing chemically modified oligonucleotides for targeted gene silencing. *Chem Biol.* 937-954.

82. **Eckstein F.** (2014) Phosphorothioates, essential components of therapeutic oligonucleotides. *Nucleic Acid Ther.* 374-387.
83. **Shen X, Corey DR.** (2018) Chemistry, mechanism and clinical status of antisense oligonucleotides and duplex RNAs. *Nucleic Acids Res.* 1584-1600.
84. **Foster DJ, Brown CR, Shaikh S, et al.** (2019) Advanced siRNA designs further improve in vivo performance of GalNAc-siRNA conjugates. *Nucleic Acids Res.* 7340-7351..
85. **Nair JK, Willoughby JL, Chan A, et al.** (2014) Multivalent N-acetylgalactosamine-conjugated siRNA localizes in the liver and silences target genes after subcutaneous administration. *J Am Chem Soc.* 16958-16961.
86. **Springer, A.D. & Dowdy, S.F.** (2018) GalNAc-siRNA Conjugates: Leading the Way for Delivery of RNAi Therapeutics. *Nucleic Acid Ther*, 28, 109-118.
87. **Baenziger, J.U. & Fiete, D.** (2018) Galactose and N-acetylgalactosamine-specific endocytosis of glycopeptides by isolated rat hepatocytes. *Cell* 22, 611-620.
88. **Seymour, L.W. et al.** (2002) Hepatic drug targeting: phase I evaluation of polymer-bound doxorubicin. *J Clin Oncol;* 20, 1668-1676.
89. **Prakash, T.P. et al.** (2014) Targeted delivery of antisense oligonucleotides to hepatocytes using triantennary N-acetyl galactosamine improves potency 10-fold in mice. *Nucleic Acids Res*, 42, 8796-8807.
90. **Raposo G, Stoorvogel W.** (2013) Extracellular vesicles: exosomes, microvesicles, and friends. *J Cell Biol.* 373-383.
91. **Tkach M, Théry C.** (2016) Communication by extracellular vesicles: where we are and where we need to go. *Cell.* 1226-1232.
92. **Van Niel G, D'Angelo G, Raposo G.** (2018) Shedding light on the cell biology of extracellular vesicles. *Nat Rev Mol Cell Biol.* 213-228.
93. **Valadi H, Ekström K, Bossios A, Sjöstrand M, Lee JJ, Lötvall JO,** (2007) Exosome-mediated transfer of mRNAs and microRNAs is a novel mechanism of genetic exchange between cells. *Nat Cell Biol.* 654-659.
94. **Reshke, R., Taylor, J.A., Savard, A. *et al.*** (2020). Reduction of the therapeutic dose of silencing RNA by packaging it in extracellular vesicles via a pre-microRNA backbone. *Nat Biomed Eng* **4**, 52–68.
95. **Pan BT, Johnstone RM.** (1983) Fate of transferrin receptors during maturation of sheep reticulocytes in vitro: selective externalization of the receptor. *Cell.* 967-978.
96. **Harding C, Heuser J, Stahl P.** (1983) Receptor-mediated endocytosis of transferrin and recycling of the transferrin receptor in rat reticulocytes. *J Cell Biol.* 329-339.
97. **Théry C, Witwer KW, Aikawa E, et al.** (2018) Minimal information for studies of extracellular vesicles 2018 (MISEV2018): a position statement of the International Society for Extracellular Vesicles and update of the MISEV2014 guidelines. *J Extracell Vesicles.* 1535750.
98. **Kowal J, Tkach M, Théry C.** (2014) Biogenesis and secretion of exosomes. *Curr Opin Cell Biol.* 116-125.
99. **Wang, Q., Lu, Q.** (2017) Plasma membrane-derived extracellular microvesicles mediate non-canonical intercellular NOTCH signaling. *Nat Commun* 8, 709
100. **Cocucci E, Racchetti G, Meldolesi J.** (2009) Shedding microvesicles: artefacts no more. *Trends Cell Biol.* 43-51.

101. **Elmore S.** Apoptosis: a review of programmed cell death. *Toxicol Pathol.* 2007;35(4):495-516.
102. **Hugel B, Martínez MC, Kunzelmann C, Freyssinet JM.** (2005) Membrane microparticles: two sides of the coin. *Physiology (Bethesda)*.22-27.
103. **Kroemer G, Galluzzi L, Vandenabeele P, et al.** (2009) Classification of cell death: recommendations of the Nomenclature Committee on Cell Death *Cell Death Differ.* 3-11.
104. **Taylor RC, Cullen SP, Martin SJ.** (2008) Apoptosis: controlled demolition at the cellular level. *Nat Rev Mol Cell Biol.* 231-241.
105. **Henson PM, Bratton DL.** (2002) Antigenic changes on apoptotic cells: recognition, uptake, and the consequences to the host. *Autoimmunity.* 285-290.
106. **Jeppesen, D.K., Sanchez, Z.C., Kelley, N.M. *et al.*** (2025) Blebbisomes are large, organelle-rich extracellular vesicles with cell-like properties. *Nat Cell Biol* 27, 438–448
107. **Kalluri R, LeBleu VS.** (2020) The biology, function, and biomedical applications of exosomes. *Science.* 977.
108. **Raposo, G. and W. Stoorvogel.** (2013) Extracellular vesicles: Exosomes, microvesicles, and friends. The Journal of Cell Biology. **200**. 373-383
109. **Jiang, L., et al.** (2017)Determining the contents and cell origins of apoptotic bodies by flow cytometry. Scientific Reports. **7**, 14444.
110. **Gurung, S., Perocheau, D., Touramanidou, L. *et al.*** (2021) The exosome journey: from biogenesis to uptake and intracellular signaling. *Cell Commun Signal.* **19**, 47 .
111. **Hessvik, N.P. and A. Llorente.** (2018) Current knowledge on exosome biogenesis and release. *Cellular and molecular life sciences* : CMLS. **75**: 193-208. 98.
112. Stuffers, S., Sem Wegner, C., Stenmark, H. & Brech, A. Multivesicular endosome biogenesis in the absence of ESCRTs. Traffic 10, 925-937 (2009).
113. **Christ L, Raiborg C, Wenzel EM, Campsteijn C, Stenmark H.** (2017) Cellular functions and molecular mechanisms of the ESCRT membrane-scission machinery. *Trends Biochem Sci.* 42-56.
114. **Henne WM, Buchkovich NJ, Emr SD.** (2011) The ESCRT pathway. *Dev Cell.* 77-91.
115. **Colombo, M. et al.** (2013) Analysis of ESCRT functions in exosome biogenesis, composition and secretion highlights the heterogeneity of extracellular vesicles. *J Cell Sci* 126, 5553- 5565.
116. **ill DJ, Teo H, Sun J, Perisic O, Veprintsev DB, Williams RL.** (2007) Structural insight into the ESCRT-I/-II link and its role in MVB trafficking. *EMBO J.* 26 :600-612.
117. **Baietti MF, Zhang Z, Mortier E, et al.** (2007) Syndecan-syntenin-ALIX regulates the biogenesis of exosomes. *Nat Cell Biol.* 7 :677-685
118. **Im YJ, Kuo L, Ren X, Hurley JH.** (2007) Structure of the ESCRT-II endosomal trafficking complex. *Nature.* 449; 611-615.
119. **Ghossoub R, Lembo F, Rubio A, et al.** (2014) Syntenin-ALIX exosome biogenesis and budding into multivesicular bodies. *Nat Cell Biol.* 16 344-355.
120. **Fujii, K., Hurley, J. H. & Freed, E. O.** (2007) Beyond Tsg101: the role of Alix in 'ESCRTing' HIV-1. *Nat. Rev. Microbiol.* **5**, 912–916.
121. **Bari R., Guo Q., Xia B., Zhang Y.H., Giesert E.E., Levy S., Zheng J.J., Zhang X.A.** (2011). Tetraspanins regulate the protrusive activities of cell membrane. *Biochem. Biophys. Res. Commun.* **415**:619–626.

122. **Théry, C. et al.** (2001)Proteomic analysis of dendritic cell-derived exosomes: a secreted subcellular compartment distinct from apoptotic vesicles. *J Immunol* 166, 7309-7318.
123. **Skotland, T., Hessvik, N.P., Sandvig, K. & Llorente, A.** (2019) Exosomal lipid composition and the role of ether lipids and phosphoinositides in exosome biology. *J Lipid Res* 60, 9-18.
124. **Valadi, H. et al.** (2007) Exosome-mediated transfer of mRNAs and microRNAs is a novel mechanism of genetic exchange between cells. *Nat Cell Biol* 9, 654-659.
125. **Pegtel, D.M. et al.** (2010) Functional delivery of viral miRNAs via exosomes. *Proc Natl Acad Sci U S A*; 107, 6328-6333.
126. **Subra C, Laulagnier K, Perret B, Record M.** (2007), Exosome lipidomics unravels lipid sorting at the level of multivesicular bodies. *Biochimie.* 89, 205-212.
127. **Llorente A, Skotland T, Sylvänne T, Kauhanen D, Róg T, Orlowski A, et al.** (2013) Molecular lipidomics of exosomes released by PC-3 prostate cancer cells. *Biochim Biophys Acta.* 10; 1302-1309.
128. **Record M, Carayon K, Poirot M, Silvente-Poirot S.** (2014) Exosomes as new vesicular lipid transporters involved in cell-cell communication. *Biochim Biophys Acta.* 108-120.
129. **Lingwood D, Simons K.** (2010) Lipid rafts as a membrane-organizing principle. *Science.* 327; 46-50.
130. **Pfrieger FW, Vitale N.** (2018) Cholesterol and the journey of extracellular vesicles. *J Lipid Res*. Dec;59(12):2255-2261.
131. **Levental I, Veatch SL.** (2016) The continuing mystery of lipid rafts. *J Mol Biol.* 428; 4749-4764.
132. **Andreu Z, Yáñez-Mó M.** (2014) Tetraspanins in extracellular vesicle formation and function. *Front Immunol.* 442.
133. **Christ L, Raiborg C, Wenzel EM, Campsteijn C, Stenmark H.** (2017) Cellular functions and molecular mechanisms of the ESCRT membrane-scission machinery. *Trends Biochem Sci.* 42-56.
134. **Weyl A, Vanscheidt W, Weiss JM, Peschen M, Schopf E, Simon J.** (1996) Expression of the adhesion molecules ICAM-1, VCAM-1, and E-selectin and their ligands VLA-4 and LFA-1 in chronic venous leg ulcers. *J Am Acad Dermatol.* 418-23.
135. **Bache KG, Raiborg C, Mehlum A, Stenmark H.** (2003) STAM and Hrs are subunits of a multivalent ubiquitin-binding complex on early endosomes. *J Biol Chem.* 14: 12513-12521.
136. **Kahlert C, Melo SA, Protopopov A, et al.** (2014) Identification of double-stranded genomic DNA spanning all chromosomes with mutated KRAS and p53 DNA in exosomes from pancreatic cancer cells. *Cell.* 7:1549-1561.
137. **Sansone P, Savini C, Kurelac I, et al.** (2017) Packaging and transfer of mitochondrial DNA via exosomes regulate escape from dormancy in hormonal therapy-resistant breast cancer. *Proc Natl Acad Sci U S A.* 43 9066-9075.
138. **Cai J, Han Y, Ren H, et al.** (2013) Extracellular vesicle-mediated transfer of donor genomic DNA to recipient cells is a novel mechanism for genetic influence between cells. *J Mol Cell Biol.* 4, 227-238.

139. **Rodriguez-Muñoz M, Anglada T, Genescà A.** (2022) A matter of wrapper: Defects in the nuclear envelope of lagging and bridging chromatin threatens genome integrity. Semin Cell Dev Biol. 124-130.
140. **O'Grady, T. et al.** (2022) Sorting and packaging of RNA into extracellular vesicles shape intracellular transcript levels. *BMC Biol* 20, 72 .
141. **Bolukbasi MF, Mizrak A, Ozdener GB, et al.** (2012) miR-1289 and "Zipcode"-like sequences add to the complexity of post-transcriptional regulation in exosomes. *Cell Mol Life Sci.* 3569-3579.
142. **Santangelo L, Giurato G, Cicchini C, et al.** (2016) The RNA-binding protein SYNCRIP is a component of the hepatocyte exosomal machinery controlling microRNA sorting. *Cell Rep.* 3 :799-808.
143. **Wei Y, Niu B, Peng T, et al.** (2021) Exosomal long noncoding RNAs: emerging contributors to cancer progression and immunosuppressive microenvironment. *Front Immunol.* 12, 887-900.
144. **Yang L, Peng X, Li Y, et al.** (2017) Long non-coding RNAs involved in exosomal transmission of cancer. *Int J Biol Sci.* 7:852-863.
145. **Villarroya-Beltri C, Baixauli F, Gutiérrez-Vázquez C, et al.** (2014) Sorting it out: regulation of exosome loading. *Semin Cancer Biol.* 28:3-13.
146. **Squadrito ML, Baer C, Burdet F, et al.** (2014) Endogenous RNAs modulate microRNA sorting to exosomes and transfer to acceptor cells. *Cell Rep.* 8:1432-1446.
147. **Garcia-Martin R, Wang G, Brandão BB, Zanotto TM, Shah S, Kumar Patel S, Schilling B, Kahn CR.** (2021) MicroRNA sequence codes for small extracellular vesicle release and cellular retention. *Nature.* 7893: 446-451.
148. **Zearfoss NR, Deveau LM, Clingman CC, Schmidt E, Johnson ES, Massi F, Ryder SP.** (2014) A conserved three-nucleotide core motif defines Musashi RNA binding specificity. *J Biol Chem*. 51:35530-41.
149. **Bolukbasi MF, Mizrak A, Ozdener GB, Madlener S, Ströbel T, Erkan EP, Fan JB, Breakefield XO, Saydam O.** (2012) miR-1289 and "Zipcode"-like Sequence Enrich mRNAs in Microvesicles. *Mol Ther Nucleic Acids.* 2, e10.
150. **De Gaudenzi J, Frasch AC, Clayton C.** (2005) RNA-binding domain proteins in Kinetoplastids: a comparative analysis. Eukaryot Cell. **4** 2106-14.
151. **Nolte-'t Hoen, E.N. et al.** (2012) Deep sequencing of RNA from immune cell-derived vesicles uncovers the selective incorporation of small non-coding RNA biotypes with potential regulatory functions. *Nucleic Acids Res* 40, 9272-9285.
152. **Guduric-Fuchs, J. et al.** (2012) Selective extracellular vesicle-mediated export of an overlapping set of microRNAs from multiple cell types. *BMC Genomics* 13, 357
153. **Pigati, L. et al.** (2010) Selective release of microRNA species from normal and malignant mammary epithelial cells. *PLoS One* 5, e13515.
154. **Van Balkom, B.W., Eisele, A.S., Pegtel, D.M., Bervoets, S. & Verhaar, M.C.** (2015) Quantitative and qualitative analysis of small RNAs in human endothelial cells and exosomes provides insights into localized RNA processing, degradation and sorting. *J Extracell Vesicles 4,* 26760.
155. **Tian, T., et al.** (2014) Exosome uptake through clathrin-mediated endocytosis and macropinocytosis and mediating miR-21 delivery. *J Biol Chem.* **289**. 2258-67.
156. **Feng, D., et al.** (2010)**.** Cellular internalization of exosomes occurs through phagocytosis. *Traffic*. **11**. 675-87.

157. **Mattila P.K., and Lappalainen P.** (2008). Filopodia: molecular architecture and cellular functions. *Nat. Rev. Mol. Cell Biol.* **9**:446–454.
158. **Bornschlögl T.** (2013). How filopodia pull: what we know about the mechanics and dynamics of filopodia. *Cytoskeleton (Hoboken)*. **70,** 590–603.
159. **Heusermann, W., Hean, J., Trojer, D., Steib, E., Bueren, S. V., Graff-Meyer, A., Genoud, C., Martin, K., Pizzato, N., Voshol, J., Morrissey, D. V., Andaloussi, E. L., Wood, M. J., & Meisner-Kober, N. C.** (2016). Exosomes surf on filopodia to enter cells at endocytic hot spots, traffic within endosomes, and are targeted to the ER. *The Journal of Cell Biology*, **213**, 173-184
160. **Lehmann M.J., Sherer N.M., Marks C.B., Pypaert M., and Mothes W**. (2005). Actin- and myosin-driven movement of viruses along filopodia precedes their entry into cells. *J. Cell Biol.* **170**. 317–325.
161. **Yi-Zhi Wang, Charlotte C.M. Castillon, Kamil K. Gebis, Elizabeth T. Bartom, Alessandra d'Azzo, Anis Contractor, Jeffrey N. Savas,** (2024) Notch receptor-ligand binding facilitates extracellular vesicle-mediated neuron-to-neuron communication, *Cell Reports,* Volume 43, Issue 2, 113680, ISSN 2211-1247
162. **Han B, Zhang H, Tian R, Liu H, Wang Z, Wang Z, Tian J, Cui Y, Ren S, Zuo X, Tian R, Niu R, Zhang F.** (2022) Exosomal EPHA2 derived from highly metastatic breast cancer cells promotes angiogenesis by activating the AMPK signaling pathway through Ephrin A1-EPHA2 forward signaling. *Theranostics.* 4127-4146.
163. **Markin, V. S., & Albanesi, J. P.** (2002). Membrane fusion: stalk model revisited. *Biophysical Journal*, ***82***, 693-712.
164. **Chernomordik, L. V., & Kozlov, M. M.** (2008). Mechanics of membrane fusion. *Nature structural & molecular biology*, ***15***, 675.
165. **Kozlov MM, Chernomordik LV.** (1998) A mechanism of protein-mediated fusion: coupling between refolding of the influenza hemagglutinin and lipid rearrangements. *Biophys J*. **75**:1384-96.
166. **Epand RM, Epand RF.** Modulation of membrane curvature by peptides. (2009) *Biochem Biophys Res Commun.* 3:486-490.
167. **Kozlov MM, Chernomordik LV.** (1998) A mechanism of protein-mediated fusion: coupling between refolding of the influenza hemagglutinin and lipid rearrangements. *Biophys J.* 3; 1384-1396.
168. **Epand RM, Epand RF.** (2009) Modulation of membrane curvature by peptides. *Biochem Biophys Res Commun.* 3 :486-490.
169. **Cooper GM.** (2000)The Cell: A Molecular Approach. 2nd edition. Sunderland (MA): Sinauer Associates; 2000. Structure of the Plasma Membrane. Available from: https://www.ncbi.nlm.nih.gov/books/NBK9898/
170. **Markin VS, Kozlov MM, Borovjagin VL.** (1984) On the theory of membrane fusion. The stalk mechanism. *Gen Physiol Biophys.* 5 :361-377.
171. **McIntosh TJ, Simon SA.** (1992) Area per molecule and distribution of water in fully hydrated DLPE bilayers. *Biochemistry.* 36, 8374-8384.
172. **Schneider DJ, Feigenson GW.** (2013) Depletion of sphingomyelin in the plasma membrane alters receptor-mediated signal transduction. *Biophys J.* 6:1388-1398.
173. **Daniels DR, Smith DA.** (1999) Helix formation in localized shear flow: the role of entropy-enthalpy compensation. *Biophys J.* 6, 3363-3373.

174. **Devanandan H, Meredith SC, Freed KF.** (2013) Cholesterol-lipid interactions and the effect of single-body area constraints in bilayer membranes: potential impact on domain formation. *J Chem Phys.* 24, 244911.
175. **Daleke DL.** (2003) Regulation of transbilayer plasma membrane phospholipid asymmetry. *J Lipid Res.* 44, 233-242.
176. **Roux A, Cuvelier D, Nassoy P, et al.** (2005) Role of curvature and phase transition in lipid sorting and fission of membrane tubules. *EMBO J.* 8, 1537-1545.
177. **Immerberg J, Kozlov MM.** (2006) How proteins produce cellular membrane curvature. *Nat Rev Mol Cell Biol.* 7, 9-19.
178. **Shnyrova AV, Ayllón J, Mikhalyov II, et al.** (2013) Geometric catalysis of membrane fission driven by flexible dynamin rings. *Science.* 6126, 1433-1436.
179. **Campelo F, McMahon HT, Kozlov MM.** (2008) The hydrophobic insertion mechanism of membrane curvature generation by proteins. *Biophys J.* 5, 2325-2339.
180. **Rao Y, Ma L, Wang J, Zhang H.** (2010) Large F-BAR domain proteins form dimeric, polymeric or giant assemblies on lipid membranes. *Curr Opin Struct Biol.* 6, 817-823.
181. **Blumenthal R, Clague MJ, Durell SR, Epand RM.** (2003) Membrane fusion. *Chem Rev.* (1) 53-69.
182. **Hui SW, Viswanathan R, Zasadzinski JA, Israelachvili J.** (1984) The structure and stability of phospholipid bilayers by x-ray diffraction, electron microscopy, and calorimetry. *Biophys J.* 45, 637-648.
183. **Doms RW, Helenius A, White JM.** (1985) Membrane fusion activity of the influenza virus hemagglutinin. *J Biol Chem.* 5, 2973-2981.
184. **White JM, Delos SE, Brecher M, Schornberg K.** (2008) Structures and mechanisms of viral membrane fusion proteins: multiple variations on a common theme. *Crit Rev Biochem Mol Biol.* 3, 189-219.
185. **Lee J, Kim H, Yang J, Kim SC, Park ZY, Kim E.** (2021) Nexus of intramembrane protein-protein interactions and membrane curvature in the regulation of membrane remodeling. *Membranes (Basel).*8, 575.
186. **Mühlenbrock P, Herwig K, Vuong L, Mey I, Steinem C.** (2020) Fusion Pore Formation Observed during SNARE-Mediated Vesicle Fusion with Pore-Spanning Membranes. *Biophys J.* 1, 151-161.
187. **Kim JH, Ren Y, Ng WP, Li S, Son S, Kee YS, Zhang S, Zhang G, Fletcher DA, Robinson DN, Chen EH.** (2015) Mechanical tension drives cell membrane fusion. *Dev Cell.* 2015, 5, 561-73.
188. **Salzman NH, Maxfield FR.** (1988) Intracellular fusion of sequentially formed endocytic compartments. J Cell Biol. **106**. 1083-91.
189. **Huotari J, Helenius A** (2011). Endosome maturation. *EMBO J* **30**: 3481–3500
190. **Parolini I, Federici C, Raggi C, Lugini L, Palleschi S, De Milito A, et al.** (2009) Microenvironmental pH is a key factor for exosome traffic in tumor cells. J Biol Chem. **284**. 34211–22.
191. M**ellman I, Fuchs R, Helenius A.** (1986) Acidification of the endocytic and exocytic pathways. *Annu Rev Biochem.* **55**. 663–700.
192. **Fuchs R, Male P, Mellman I.** (1989) Acidification and ion permeabilities of highly purified rat liver endosomes. *J Biol Chem.* **264**. 2212–20.

193. **Di Paolo G, De Camilli P.** (2006) *P*hosphoinositides in cell regulation and membrane dynamics. *Nature.* **443.** 651–7.
194. **Bissig C, Gruenberg J.** (2013). Lipid sorting and multivesicular endosome biogenesis. *Cold Spring Harb Perspect Biol.* **5**
195. **Lemmon MA.** (2003) Phosphoinositide recognition domains. *Traffic.* **4**. 201–13.
196. **lumperman J, Raposo G.** (2014) The complex ultrastructure of the endolysosomal system. *Cold Spring Harb Perspect Biol* **6**
197. **Zerial M, McBride H.** (2001) Rab proteins as membrane organizers. *Nat Rev Mol Cell Biol.* **2**. 107–17.
198. **Tenmark H, et al.** (2009) *Rab GTPases as coordinators of vesicle traffic. Nat Rev Mol Cell* Biol. **10**. 513–25.
199. **Mellman I, et al.** (1996) Endocytosis and molecular sorting. Annu Rev Cell Dev Biol. **12**:575–625
200. **Novick P, Zerial M.** (1997) The diversity of Rab proteins in vesicle transport. Curr Opin Cell Biol. **9**: 496–504
201. H**su VW, Bai M, Li J.** (2012) Getting active: protein sorting in endocytic recycling. *Nat Rev Mol Cell Biol.* **13.** 323–8.
202. **van Weering JR, et al.** (2012) Molecular basis for SNX-BAR-mediated assembly of distinct endosomal sorting tubules. *EMBO J.* **31**. 4466–80
203. **Gillespie EJ, Ho CL, Balaji K, Clemens DL, et al.** (2013) Selective inhibitor of endosomal trafficking pathways exploited by multiple toxins and viruses. *Proc Natl Acad Sci*. **10**. 110
204. **Stechmann, B., Bai, S., Gobbo, E., et al.** (2010). Inhibition of Retrograde Transport Protects Mice from lethal Ricin Challenge. *Cell* **141,** 231-242
205. **Lindsay, A. J.** *(2020). The Endosomal Recycling Pathway—At the Crossroads of the Cell. International Journal of Molecular Sciences, **21**(17).*
206. **Kamerkar, S. et al.** (2017) Exosomes facilitate therapeutic targeting of oncogenic KRAS in pancreatic cancer. *Nature* 546, 498-503 (2017).
207. **Alvarez-Erviti, L. et al.** (2011) Delivery of siRNA to the mouse brain by systemic injection of targeted exosomes. *Nat Biotechnol* 29, 341-345
208. **Didiot, M.C. et al**. (2016) Exosome-mediated Delivery of Hydrophobically Modified siRNA for Huntingtin mRNA Silencing. *Mol Ther* 24, 1836-1847.
209. **McCann, J. et al.** (2022)Contaminating transfection complexes can masquerade as small extracellular vesicles and impair their delivery of RNA. *J Extracell Vesicles* 11, e12220).
210. **Carthew, R.W. & Sontheimer, E.J.** (2009) Origins and Mechanisms of miRNAs and siRNAs. *Cell* 136, 642-655.
211. **Yi, R., Qin, Y., Macara, I.G. & Cullen, B.R.** (2003) Exportin-5 mediates the nuclear export of pre-microRNAs and short hairpin RNAs. *Genes Dev* 17, 3011-3016.
212. **Kim, Y.K., Kim, B. & Kim, V.N.** (2016) Re-evaluation of the roles of DROSHA, Export in 5, and DICER in microRNA biogenesis. *Proc Natl Acad Sci U S A* 113, E 1881-1889.
213. **Cifuentes, D. et al.** (2010) A novel miRNA processing pathway independent of Dicer requires Argonaute2 catalytic activity. *Science* 328, 1694-1698.

214. **Cheloufi, S., Dos Santos, C.O., Chong, M.M. & Hannon, G.J.** (2010) A dicer-independent miRNA biogenesis pathway that requires Ago catalysis. *Nature* 465, 584-589.
215. **Yang, J.S. et al.** (2010) Conserved vertebrate mir-451 provides a platform for Dicer-independent, Ago2-mediated microRNA biogenesis. *Proc Natl Acad Sci U S A* 107, 15163-15168.
216. **Trinkle-Mulcahy, L.** (2018). Recent advances in proximity-based labeling methods for interactome mapping. *F1000Research*, **8.**
217. **Chen, L., & Perrimon, N.** (2017). Proximity-dependent labeling methods for proteomic profiling in living cells. *Wiley interdisciplinary reviews. Developmental biology*, *6*.
218. **C.L. Chen, Y. Hu, N.D. Udeshi, T.Y. Lau, F. Wirtz-Peitz, L. He, A.Y. Ting, S.A. Carr, N.** (2015) Perrimon Proteomic mapping in live Drosophila tissues using an engineered ascorbate peroxidase *Proc. Natl. Acad. Sci. U S A*, **112**, 12093-12098
219. **Lam, S. S., Martell, J. D., Kamer, K. J., Deerinck, T. J., Ellisman, M. H., Mootha, V. K., & Ting, A. Y.** (2015). Directed evolution of APEX2 for electron microscopy and proteomics. *Nature methods*, *12*(1), 51.
220. **Théry, C., Amigorena, S., Raposo, G. & Clayton, A.** (2006) Isolation and characterization of exosomes from cell culture supernatants and biological fluids. Curr Protoc Cell Biol Chapter 3, Unit 3.22.
221. **Dooley K, McConnell RE, Xu K, Lewis ND, Haupt S, Youniss MR, et al.** (2021) A versatile platform for generating engineered extracellular vesicles with defined therapeutic properties. *Mol Ther*. **29**. 1729-1743
222. **Ong, SE., Mann, M.** (2006) A practical recipe for stable isotope labeling by amino acids in cell culture (SILAC). *Nat Protoc 1,* 2650–2660
223. **Benedict Tan, Suat Peng, Siti Maryam J.M. Yatim, Jayantha Gunaratne, Walter Hunziker, Alexander Ludwig,** An Optimized Protocol for Proximity Biotinylation in Confluent Epithelial Cell Cultures Using the Peroxidase APEX2, (2020) *STAR Protocols,* Volume 1, Issue 2,m ISSN 2666-1667,
224. Cell profile example pipelines for Image analysis. https://cellprofiler.org/examples Accessed July 12, 2025.
225. **Arbuzova A, Korte T, Müller P, Herrmann A.** (1994) On the validity of lipid dequenching assays for estimating virus fusion kinetics. *Biochim Biophys Acta.*
226. **Röhrl C, Meisslitzer-Ruppitsch C, Bittman R, Li Z, Pabst G, Prassl R, Strobl W, Neumüller J, Ellinger A, Pavelka M, Stangl H.** (20212) Combined light and electron microscopy using diaminobenzidine photooxidation to monitor trafficking of lipids derived from lipoprotein particles. Curr Pharm Biotechnol.
227. **Patrick Walton, S.** (2010), Engineering active siRNA therapeutics. *The FEBS Journal*, 277: 4805-4805.
228. **Mackenzie, J. M., Jones, M. K., & Westaway, E. G.** (1999). Markers for trans-Golgi Membranes and the Intermediate Compartment Localize to Induced Membranes with Distinct Replication Functions in Flavivirus-Infected Cells. *Journal of Virology*, ***73***(11), 9555-9567.
229. **Alexa, A., and Rahnenfuhrer, J.** (2020). *topGO: Enrichment Analysis for Gene Ontology*.

230. **Damian Szklarczyk, Annika L Gable, Katerina C Nastou, David Lyon, Rebecca Kirsch, Sampo Pyysalo, Nadezhda T Doncheva, Marc Legeay, Tao Fang, Peer Bork, Lars J Jensen, Christian von Mering,** (2021) The STRING database in 2021: customizable protein–protein networks, and functional characterization of user-uploaded gene/measurement sets, *Nucleic Acids Research*, **49.** 605–612,
231. **Yuan R, Zhou Y, Arias GF, Dittmer DP.** (2023) Extracellular Vesicle Isolation by a Tangential-Flow Filtration-Based Large-Scale Purification Method. *Methods Mol Biol.* **6**.45-55
232. **Théry, C., Ostrowski, M. & Segura, E.** (2009) Membrane vesicles as conveyors of immune responses. *Nat Rev Immunol* 9, 581–593.
233. **Kowal J, Arras G, Colombo M, et al.** (2016) Proteomic comparison defines novel markers to characterize heterogeneous populations of extracellular vesicle subtypes. *Proc Natl Acad Sci U S A.*113 E968–E977.
234. **Marquez J, Dong J, Dong C, Tian C, Serrero G.** (2021) Identification of Prostaglandin F2 Receptor Negative Regulator (PTGFRN) as an internalizable target in cancer cells for antibody-drug conjugate development. *PLoS One.* **16**
235. **Stéphanie Charrin, François le Naour, Olivier Silvia et al.** (2009) Lateral organization of membrane proteins: tetraspanins spin their web. *Biochem J* **420** 133–154.
236. **Driscoll TP, Bidone TC, Ahn SJ, Yu A, Groisman A, Voth GA,** (2021) Integrin-based mechanosensing through conformational deformation. *Biophys J.* 120 4349-4359.
237. **Lee, HJ., Zheng, J.J. (2010)** PDZ domains and their binding partners: structure, specificity, and modification. *Cell Commun Signal* **8**, 8.
238. **Kanca O, Bellen HJ, Schnorrer F.** (2017) Gene Tagging Strategies To Assess Protein Expression, Localization, and Function in *Drosophila*. *Genetics.* **2**. 389-412.
239. **Zoonens M, Miroux B.** (2010) Expression of membrane proteins at the Escherichia coli membrane for structural studies. *Methods Mol Biol.* **601** 49-66.
240. **Ullrich O, Reinsch S, Urbé S, Zerial M, Parton RG.** (1996) Rab11 regulates recycling through the pericentriolar recycling endosome. *J Cell Biol.* **4** 913-24.
241. **Leventis PA, Grinstein S.** (2010) The distribution and function of phosphatidylserine in cellular membranes. *Annu Rev Biophys.* **39** 407-27.
242. **Nagata S, Suzuki J, Segawa K, Fujii T.** (2016) Exposure of phosphatidylserine on the cell surface. *Cell Death Differ*. **6** 952-61.
243. **Farquhar MG, Palade GE.** (2002) The Golgi apparatus from artifact to center stage. *J Cell Biol.* **3** 77s-103s.
244. **Wear MA, Yamashita A, Kim K, Maéda Y, Cooper JA.** (2003) How capping protein binds the barbed end of the actin filament. *Curr Biol.* **17**. 1531-7.
245. **Edwards M, Zwolak A, Schafer DA, Sept D, Dominguez R, Cooper JA.** (2014) Capping protein regulators fine-tune actin assembly dynamics. *Nat Rev Mol Cell Biol.* **10** 677-89.
246. **Vicente-Manzanares, M., Ma, X., Adelstein, R.** ***et al.*** (2009) Non-muscle myosin II takes centre stage in cell adhesion and migration. *Nat Rev Mol Cell Biol* **10**, 778–790
247. **Sellers JR.** (2000) Myosins: a diverse superfamily. *Biochim Biophys Acta.* **17** 3-22.
248. **Hofer, A., Brown, E.** (2003) Extracellular calcium sensing and signalling. *Nat Rev Mol Cell Biol* **4**, 530–538

249. **Gerke V, Moss SE.** (2002) Annexins: from structure to function. *Physiol Rev.* **2** 331-71
250. **Babiychuk EB, Draeger A.** (2000) Annexins in cell membrane dynamics. Ca(2+)-regulated association of lipid microdomains. *J Cell Biol.* **5** 1113-24.
251. **Hofer, A., Brown, E.** (2003) Extracellular calcium sensing and signalling. *Nat Rev Mol Cell Biol* **4**, 530–538
252. **Duleh SN, Welch MD.** (2010) WASH and the Arp2/3 complex regulate endosome shape and trafficking. *Cytoskeleton (Hoboken)*. **3** 193-206.
253. **Pollard TD, Cooper JA.** (2009) Actin, a central player in cell shape and movement. Science. **326** 1208-12.
254. **Mullins RD, Heuser JA, Pollard TD.** (1998) The interaction of Arp2/3 complex with actin: nucleation, high affinity pointed end capping, and formation of branching networks of filaments. *Proc Natl Acad Sci U S A.* **11** 6181-6.
255. **Campellone KG, Welch MD.** (2010) A nucleator arms race: cellular control of actin assembly. *Nat Rev Mol Cell Biol.* **4** 237-51.
256. **Theriot JA.** (2000) The polymerization motor. Traffic. **1** 19-28.
257. **Derivery E, Sousa C, Gautier JJ, Lombard B, Loew D, Gautreau A.** (2009) The Arp2/3 activator WASH controls the fission of endosomes through a large multiprotein complex. *Dev Cell.* **5** 712-23.
258. **Kozlov MM, Campelo F, Liska N, Chernomordik LV, Marrink SJ, McMahon HT.** (2014) Mechanisms shaping cell membranes. Curr Opin Cell Biol. **29** 53-60.
259. **Seaman MNj, Freeman CL.** (2014) Analysis of the Retromer complex-WASH complex interaction illuminates new avenues to explore in Parkinson disease. *Commun Integr Biol.* **13** e29483.
260. **Gomez TS, Billadeau DD.** (2009) A FAM21-containing WASH complex regulates retromer-dependent sorting. *Dev Cell.* **5** 699-711.
261. **Cullen PJ, Korswagen HC.** (2011) Sorting nexins provide diversity for retromer-dependent trafficking events. *Nat Cell Biol.* **14** 29-37.
262. **Cullen PJ.** (2008) Endosomal sorting and signalling: an emerging role for sorting nexins. *Nat Rev Mol Cell Biol.* **7** 574-82.
263. **Clairfeuille T, Mas C, Chan AS, Yang Z, Tello-Lafoz M, Chandra M, et al. (**2016) A molecular code for endosomal recycling of phosphorylated cargos by the SNX27-retromer complex. *Nat Struct Mol Biol.* **10** 921-932.
264. **Harding C, Heuser J, Stahl P.** (1983) Receptor-mediated endocytosis of transferrin and recycling of the transferrin receptor in rat reticulocytes. *J Cell Biol.* **2** 329-39.
265. **Cullen PJ, Steinberg F.** (2018) To degrade or not to degrade: mechanisms and significance of endocytic recycling. Nat Rev Mol Cell Biol. **11** 679-696.
266. **Jiang, Y., Zhang, X., Nie, H. *et al.*** (2024)Dissecting diazirine photo-reaction mechanism for protein residue-specific cross-linking and distance mapping. *Nat Commun* 15, 6060
267. **Morgens DW, Wainberg M, Boyle EA, Ursu O, Araya CL, Tsui CK, Haney MS, Hess GT, Han K, Jeng EE, Li A, Snyder MP, Greenleaf WJ, Kundaje A, Bassik MC.** (2017) Genome-scale measurement of off-target activity using Cas9 toxicity in high-throughput screens. *Nat Commun*

268. **Zavodszky, E., Seaman, M., Moreau, K. et al**. (2014) Mutation in VPS35 associated with Parkinson's disease impairs WASH complex association and inhibits autophagy. *Nat Commun*